Virtual photon polarization and dilepton anisotropy in pion-nucleon and heavy-ion collisions

Polarisation virtueller Photonen und Dileptonanisotropie in Pion-Nukleon- und Schwerionenkollisionen

Zur Erlangung des Grades eines Doktors der Naturwissenschaften (Dr. rer. nat.)
genehmigte Dissertation von M. Sc. Enrico Speranza aus Foligno (Italien)
Tag der Einreichung: 16.05.2017, Tag der Prüfung: 26.06.2017
Darmstadt 2018 — D 17

1. Gutachten: Prof. Dr. Bengt Friman
2. Gutachten: Prof. Dr. Tetyana Galatyuk

TECHNISCHE UNIVERSITÄT DARMSTADT

Fachbereich Physik
Institut für Kernphysik

Virtual photon polarization and dilepton anisotropy in pion-nucleon and heavy-ion collisions
Polarisation virtueller Photonen und Dileptonanisotropie in Pion-Nukleon- und Schwerionenkollisionen

Genehmigte Dissertation von M. Sc. Enrico Speranza aus Foligno (Italien)

1. Gutachten: Prof. Dr. Bengt Friman
2. Gutachten: Prof. Dr. Tetyana Galatyuk

Tag der Einreichung: 16.05.2017
Tag der Prüfung: 26.06.2017

Darmstadt 2018 — D 17

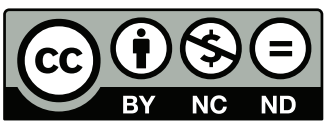

Erklärung zur Dissertation

Hiermit versichere ich, die vorliegende Dissertation ohne Hilfe Dritter nur mit den angegebenen Quellen und Hilfsmitteln angefertigt zu haben. Alle Stellen, die aus Quellen entnommen wurden, sind als solche kenntlich gemacht. Diese Arbeit hat in gleicher oder ähnlicher Form noch keiner Prüfungsbehörde vorgelegen.

Darmstadt, den 16 Mai 2017

_____

(Enrico Speranza)

Abstract

The goal of this Thesis is to study photon polarization and dilepton anisotropies as a tool to understand hadronic and heavy-ion collisions. First, the anisotropies of the dilepton angular distribution for the reaction $\pi N \to N e^+ e^-$ are studied. We employ consistent effective interactions for baryon resonances up to spin-5/2, where non-physical degrees of freedom are eliminated, to compute the anisotropy coefficients for isolated intermediate baryon resonances. It is shown that the spin and parity of the intermediate baryon resonance is reflected in the angular dependence of the anisotropy coefficient. We then compute the anisotropy coefficient including the $N(1520)$ and $N(1440)$ resonances, which are essential at the collision energy of the recent data obtained by the HADES collaboration on this reaction. We conclude that the anisotropy coefficient provides useful constraints for unravelling the resonance contributions to this process.

In order to study the medium effects on the dilepton polarization observables, we present a general framework for studying the angular anisotropy of dileptons produced from polarized virtual photons in relativistic heavy-ion collisions. The connection between the anisotropy coefficients and the medium evolution via flow velocity and temperature profile is obtained. We consider the dilepton production from quark-antiquark annihilation in the quark-gluon plasma phase and pion annihilation in the hadronic phase through electromagnetic interactions. The thermal and flow effects on the anisotropy coefficients are studied in the case of a static uniform medium, and a system with an expansion longitudinal and transverse to the beam axis. It is shown that the anisotropy coefficients are non-zero in a thermalized medium, and depend on the flow of the medium as well as on the transverse momentum and invariant mass of the virtual photon. The present framework can be implemented in a realistic hydrodynamic simulation of relativistic heavy-ion collisions in order to study the effect of non-trivial medium properties on dilepton anisotropy.

Zusammenfassung

Das Ziel dieser Doktorarbeit ist die Untersuchung von Photonenpolarisation und Dileptonanisotropie als Mittel zum Verständnis hadronischer und Schwerionenkollisionen. Zunächst werden die Anisotropien in der Winkelverteilung von Dileptonen aus der Reaktion $\pi N \to N e^+ e^-$ untersucht. Wir benutzen konsistente effektive Wechselwirkungen für Baryon-Resonanzen bis Spin-5/2, wo nicht-physikalische Freiheitsgrade eliminiert werden, um die Anisotropiekoeffizienten für isolierte intermediäre baryonische Resonanzen zu berechnen. Es wird gezeigt, dass sich Spin und Parität der intermediären baryonischen Resonanz in der Winkelverteilung des Anisotropiekoeffizienten widerspiegeln. Im Anschluss berechnen wir den Anisotropiekoeffizienten, wobei wir die Resonanzen $N(1520)$ und $N(1440)$ berücksichtigen, die bei der Kollisionsenergie der neuesten Daten, die von der HADES Kollaboration für diese Reaktion gewonnen wurden, essentiell sind. Wir schlussfolgern, dass der Anisotropiekoeffizient nützliche Beschränkungen liefern kann, um die Anteile der Resonanzen zu diesem Prozess zu entschlüsseln.

Um Mediumeffekte auf die Dileptonpolarisationsobservablen zu untersuchen, stellen wir ein allgemeines Framework zur Untersuchung von Winkelanisotropien von Dileptonen, die von polarisierten virtuellen Photonen in relativistischen Schwerionenkollisionen erzeugt wurden, vor. Es wird der Zusammenhang zwischen den Anisotropiekoeffizienten und der Entwicklung des Mediums via Flussgeschwindigkeit und Temperaturprofil gewonnen. Wir ziehen Dileptonproduktion aus Quark-Antiquark-Annihilation in der Quark-Gluon-Plasmaphase, sowie aus Pion-Annihilation in der hadronischen Phase via elektromagnetischer Wechselwirkungen in Betracht. Die thermischen und die Flusseffekte auf die Anisotropiekoeffizienten werden untersucht für den Fall eines statischen, gleichförmigen Mediums, sowie eines Systems mit Expansion in longitudinaler und transversaler Richtung zur Strahlachse. Es wird gezeigt, dass die Anisotropiekoeffizienten in einem thermalisierten Medium verschieden von Null sind und sowohl vom Fluss des Mediums, als auch vom transversalen Impuls und der invarianten Masse des virtuellen Photons abhängen. Das vorgestellte Framework kann in einer realistischen hydrodynamischen Simulation relativistischer Schwerionenkollisionen zur Untersuchung des Effekts nichttrivialer Eigenschaften des Mediums auf die Dileptonanisotropie implementiert werden.

Contents

Introduction

The study of how processes depend on the spin of the particles can reveal crucial aspects of the underlying theory that governs nuclear and particle physics. By means of spin studies, it is possible to extract important information about the nature of particles and their fundamental interactions. Therefore, spin physics has a broad range of applications in many different fields. In hadron physics, polarization observables are a crucial tool for a detailed understanding of elementary processes [1–3]. In high-energy particle physics, spin studies of reactions can play an important role for searches of new physics beyond the Standard Model [4]. In heavy-ion collisions, It has been recently shown that the polarization of Lambda baryons created in noncentral collisions is deeply connected with fluid properties, like vorticity, of strongly-interacting matter [5–7].

Among the zoo of particles present in nature, there is one that plays a special role in heavy-ion and hadronic physics: the photon. In a relativistic quantum field theory, photons can, for a brief moment, have a rest mass different from zero and hence they can decay in a dilepton (e.g. electron and positron) according to Quantum-Electrodynamics. We will refer to *real photons* to those photons with vanishing rest mass and to *virtual photons* to those with non-vanishing rest mass. This Thesis is devoted to the study of the polarization of virtual photons as a tool for understanding elementary hadronic reactions and many-body processes such as thermalization of the hot and dense matter created in heavy-ion collisions. More specifically, this Thesis aims at building a framework for studying how observables that carry information on the polarization state of photons change from the case where the photon is emitted from an elementary reaction occurring in vacuum, to the case where it is emitted from a medium.

One of the most exciting challenges of contemporary nuclear physics is understanding the features of strongly-interacting matter, i.e., the matter obeying Quantum-Chromodynamics (QCD). Figure 1 schematically shows the QCD phase diagram as a function of temperature and net baryon density.

In the Large Hadron Collider (LHC) and the Relativistic Heavy Ion Collider (RHIC), high-energy heavy-ion collisions experiments create strongly-interacting matter by colliding atomic nuclei at energies much higher than the nuclear rest masses. The matter formed is characterized by an extremely high temperature, greater than 200 MeV ($\sim 10^{12}$ K), and almost vanishing net baryon density. It is believed that these conditions existed in the very early universe about 10^{-5} s after the big bang [8, 9]. Under such extreme conditions, quarks and gluons are deconfined and form a new phase of QCD called the quark-gluon plasma (QGP). Thus, relativistic heavy-ion collisions provide a unique opportunity to study and characterize different phases of QCD. Another important feature of QCD matter formed in high-energy heavy-ion collisions is that it shows strong collective behavior and its space-time evolution can be described quite accurately using relativistic hydrodynamics [10–15].

The region of the phase diagram at moderate temperatures and high net baryon densities is studied in intermediate-energy heavy-ion collisions, where the center of mass

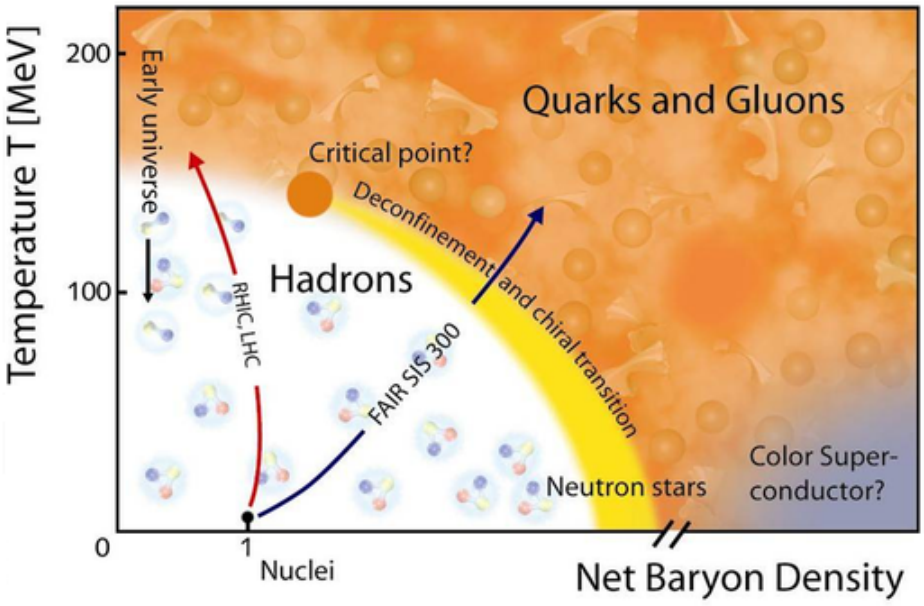

Figure 1.: The phase diagram of strongly-interacting matter.

energy of the collisions is of the order of a few GeV per nucleon. The facility SIS18 at GSI and, in the future, FAIR SIS100 at GSI aim at exploring the region with temperatures up to 200 MeV and net baryon densities up to six times the nuclear matter density.

QCD matter under extreme conditions exists also in other astrophysical contexts. In the interior of neutron stars, strongly-interacting matter reaches extremely high net baryon density which is of the order of 10^{15} g/cm^3, i.e., four times bigger than the central density of nuclei. At even higher densities, exotic states of matter like a color superconducting phase are hypothesized [16].

From the experimental point of view, extracting signals for the various phases explored in heavy-ion collisions is not an easy task and one of the biggest challenge is to find proper ways to probe QCD matter. Since, in heavy-ion collisions experiments, one can only observe and analyze the spectra of emitted particles, it is important to investigate their production mechanisms and interactions. Hadronic observables interact strongly and do not probe the entire space-time volume of the QCD matter because they depend only on the final state of the medium. Electromagnetic radiation (both real and virtual photons), instead, has been proposed to be an important probe for the study of QCD matter [17–25]. Photons are emitted throughout all stages of the collision and, since they do not feel the strong force, they escape the reaction volume undisturbed. This means that photons carry direct information on the properties of the strongly-interacting matter and on its space-time evolution. Moreover, the study of photon polarization and dilepton angular distributions has been proposed to be an important tool for understanding the early pre-equilibrium dynamics of the QCD matter and the onset of thermalization [26–28]. Recently, real and virtual photon polarization has been proposed to study the momentum anisotropy distribution of quarks and gluons in the collisions [29, 30]. The best way to explore the polarization of virtual photons is by analyzing the anisotropy coefficients of the angular distribution of the dilepton produced from its decay. Although

promising from a theoretical point of view, the study of photon polarization is a big challenge for experiments because photons are a rare probe and angular distributions require multiple-differential analyses and, hence, high statistics. However, in the last years some measurements of the anisotropy coefficients of dileptons have been carried out by the NA60 Collaboration at LHC [31] and the HADES Collaboration at GSI [32]. Theoretical analyses of the results necessitate further investigations [30].

Dileptons are also crucial for the study of the in-medium properties of hadrons. Vacuum properties like mass and lifetime of hadrons can significantly change due to the interaction of the hadron with the constituents of the medium. In-medium modifications of vector mesons is of special importance for the interpretation of dilepton spectra in heavy-ion collisions at LHC, RHIC and SIS18 energies. Dileptons invariant mass spectra have been recognized to be a unique tool for accessing the in-medium spectral functions of the vector mesons. In particular the ρ meson plays a crucial role in the search for signals for chiral symmetry restoration [33–36]. The in-medium modification of the ρ meson is believed to be dominated by its strong interaction with nucleons and baryon resonances, i.e., short-lived excited states of nucleons. Thus, a detailed understanding of elementary reactions is an essential prerequisite for a systematic analysis of heavy-ion data.

Pion-nucleon scattering provides a unique way to study the coupling between the ρ, the nucleon and baryon resonances. In pion-nucleon scattering, in fact, baryon resonances are excited and can subsequently decay into a nucleon and a ρ meson; the ρ converts into a virtual photon which, in turn, decays into a lepton pair. Pion-nucleon scattering is also a powerful tool to study electromagnetic interactions of baryons in the *time-like region*, i.e., the region where the photon four-momentum squared is larger than zero. The determination of the quantum numbers of the baryon resonances produced in pion-nucleon collisions is important for gaining a deeper understanding of hadron-hadron interactions in general and dilepton production in hadronic collisions in particular. The study of the angular distribution of dileptons can provide valuable information on the spin and parity of the intermediate resonances. In principle, by comparing measured angular distributions of the dileptons with theoretical predictions for different resonance states, it should be possible to set constraints on the quantum numbers of the resonance. The same idea has been used e.g. to determine the quantum numbers of the $X(3872)$ meson [37].

While a lot of effort has been invested in the study of dilepton production in nucleon-nucleon collisions both in experiment and theory, pion-nucleon collisions are less explored and, unfortunately, the worldwide data is rather poor. Recently, the HADES Collaboration has started a dedicated pion-nucleon programme and, for the first time, a combined study of dilepton and hadronic final state has been performed [38–42] by means of the High Acceptance Di-Electron Spectrometer [43]. More precisely reactions for four different pion beam momenta have been studied, namely 0.656, 0.69, 0.748 and 0.8 GeV. The beam at 0.69 GeV allows for a higher statistics and, therefore, it is more suitable for dilepton analyses.

At the intermediate energies explored in the HADES experiment, the task is facilitated by the small number of baryon resonances that contribute significantly. However, in practice the situation is often more complex than the ideal case of an isolated resonance which dominates the cross section. Thus, in general there is interference with nearby resonances and with a non-resonant background which must be accounted for.

In this Thesis we propose a novel way to disentangle contributions of baryon resonances with different spin and parity in elementary pion-nucleon reactions by studying

the anisotropy coefficients of the dilepton angular distribution. These coefficients reflect the polarization state of the virtual photon and, in turn, that of the resonance. Moreover, we present a formalism that generalizes the calculation of dilepton anisotropies from the case where the virtual photon is emitted in vacuum to the case where it is emitted from a thermalized medium. In particular, we study virtual photons originating in heavy-ion collisions and we show the connection between the dilepton anistropies and the medium evolution. We consider two basic electromagnetic processes: quark-antiquark annihilation in the QGP phase and pion annihilation in the confined phase. In order to describe the medium evolution, we study the case of a static uniform medium and a longitudinal Bjorken expansion plus an expansion transverse to the beam axis. We will show that, in general, a thermalized medium does produce polarized photons.

The Thesis is organized as follows. In Chapter 1, we will review the spin density matrix formalism. The photon produced in a reaction, in fact, is in general in a mixed state. We will see that a convenient way to describe the polarization state of the photon is by means of the spin density matrix. We will also discuss the angular distribution of dileptons originating from the decay of a spin-1 particle in a model-independent way and show the connection between the spin density matrix elements and the anisotropy coefficients. In Chapter 2, we will calculate the anisotropy coefficients for dileptons in pion-nucleon scattering and discuss how these observables can help disentangle different baryon resonance states. In order to move our discussion to reactions occurring in the medium, in Chapter 3 we briefly outline the basic concepts of thermal field theory needed to calculate dilepton production from a thermalized medium. In Chapter 4 we briefly discuss relativistic hydrodynamics which is needed to model the space-time evolution in heavy-ion collisions. In Chapter 5, we present a formalism for calculating the anisotropy coefficients for thermal dileptons and we will illustrate their connection with the medium evolution described via flow velocity and temperature profile. In the end, a summary and outlook are given. In Appendix A, we will summarize the notations and conventions used in the Thesis. In Appendix B, we report the Feynman rules for the Lagrangians describing the hadronic models used in Chapter 2. In Appendix C, we will give the explicit expressions for the Lorentz transformations used in the calculation carried out in Chapter 5.

Chapter 1

The spin density matrix formalism

In this Chapter we will discuss the spin density matrix formalism [2, 44], which will be extensively used in the Thesis. In Section 1.1 and 1.2, we briefly discuss the main features of spin-1/2 and spin-1 particles, respectively. In Section 1.3, the notion of spin density matrix is presented and the main properties are outlined. In a general process where a spin-1 particle is created and then decays, one can define a production and decay spin density matrix. This will be treated in Section 1.4. The connection between the spin density matrix and the anisotropy coefficients of the angular distribution is given in Section 1.5 for the decay of a virtual photon into dilepton, and in Section 1.6 for the decay of a ρ meson into pions. A general expression for the angular distribution for the decay of a spin-1 particle in presence of parity violating processes is derived in Section 1.7. Finally, the effect of the frame transformations on the anisotropy coefficients is discussed in Section 1.8.

1.1 Spin-1/2 particles and the spin polarization vector

Consider a beam composed of spin-1/2 particles. Imagine that we send the beam through a Stern-Gerlach apparatus having the magnetic field gradient aligned with the direction z. In general, the beam will be split into two different parts corresponding to two different states with eigenvalues $m = +1/2$ and $m = -1/2$ of the z—component S_z of the spin operator $\mathbf{S}$, each with lower intensity than the original beam. Now imagine that one of the two final beams, say the lower one, is blocked. This implies that the particles of the emerging beam will all be in the state corresponding to $m = +1/2$. If we rotate the apparatus such that the magnetic field gradient is now aligned along the direction z' and we again block the lower beam, then the emerging particles will be in the state $m' = +1/2$, where m' is the eigenvalue of the operator $S_{z'}$.

Let us in general consider a Stern-Gerlach apparatus where one of the final beams is blocked. if we can find an orientation of the apparatus such that the emerging beam has the same intensity as the initial one, then we will say that the beam is in a *pure state*, meaning that all the particles of the beam are in the same state. A pure state is described by only one state vector in the Hilbert space $|\chi\rangle$. The pure state can be always written as a linear combination of eigenstates. In the case of spin-1/2 particle the spin state in general is given by

$$|\chi\rangle = a_1|+\rangle + a_2|-\rangle, \tag{1.1}$$

where $|+\rangle$ and $|-\rangle$ are the eigenstates of S_z with eigenvalues $m = +1/2$ and $-1/2$, respectively, a_1 and a_2 being two complex number. Therefore the general state is characterized by four real parameters. The eigenstates can be represented by

$$|+\rangle = \begin{pmatrix} 1 \\ 0 \end{pmatrix}, \qquad |-\rangle = \begin{pmatrix} 0 \\ 1 \end{pmatrix}. \tag{1.2}$$

The most general spinor is therefore given by

$$|\chi\rangle = \begin{pmatrix} a_1 \\ a_2 \end{pmatrix}, \tag{1.3}$$

One of the four real parameters is just an overall phase which is irrelevant, and we can assume for example that the first coefficient a_1 is real. Furthermore, we want the state vector to be normalized

$$\langle\chi|\chi\rangle = |a_1|^2 + |a_2|^2 = 1. \tag{1.4}$$

This condition restricts the number of independent parameters to two. We introduce the two independent parameters θ and ϕ and, without loss of generality, we can write the spinor as

$$|\chi\rangle = \begin{pmatrix} \cos\frac{\theta}{2} \\ e^{i\phi}\sin\frac{\theta}{2} \end{pmatrix}. \tag{1.5}$$

For spin 1/2, the spin operator is proportional to the Pauli matrices as $\mathbf{S} = \frac{1}{2}\boldsymbol{\sigma}$. We now want to introduce the spin polarization vector $\mathbf{P}$, whose components are defined as the expectation value of the Pauli matrices, i.e.

$$P_i = \langle\sigma_i\rangle, \tag{1.6}$$

with $i = x, y, z$. For a pure state $|\chi\rangle$, the expectation values is given by

$$\langle\sigma_i\rangle = \langle\chi|\sigma_i|\chi\rangle, \tag{1.7}$$

where σ_i are the Pauli matrices

$$\sigma_x = \begin{pmatrix} 0 & 1 \\ 1 & 0 \end{pmatrix}, \quad \sigma_y = \begin{pmatrix} 0 & -i \\ i & 0 \end{pmatrix}, \quad \sigma_z = \begin{pmatrix} 1 & 0 \\ 0 & -1 \end{pmatrix}, \tag{1.8}$$

Using the general state (1.5), the components of the spin polarization vector are given by

$$P_x = \sin\theta\cos\phi, \tag{1.9}$$
$$P_y = \sin\theta\sin\phi, \tag{1.10}$$
$$P_z = \cos\theta. \tag{1.11}$$

Note that the spin polarization vector has unit magnitude

$$|\mathbf{P}| = \sqrt{P_x^2 + P_y^2 + P_z^2} = 1. \tag{1.12}$$

The two parameters θ and ϕ have a specific physical meaning. θ can be interpreted as the polar angle of the spin polarization vector, namely the angle between the spin polarization vector and the axis z, ϕ is the azimuthal angle of the spin polarization vector. Note that for an eigenstates $|\pm\rangle$, the components of the spin polarization vector are $P_x = 0$, $P_y = 0$ and $P_z = \pm 1$. So, the spin polarization vector specifies the direction where the spins of all the particles in the beam are pointing.

Now consider the case of two beams. The first one is made of N_a particles prepared in the pure state $|\chi_a\rangle$ and the second one made of N_b particles prepared in the pure state $|\chi_b\rangle$. We assume that the two beams are prepared independently, meaning that there is no definite phase between the states of the two beams. The joint beam will not be a pure state anymore, meaning that we cannot express it in terms of a state vector. This state is called a *mixed state*. The only thing we can say about the joint beam is that we will have a certain probability $\mathcal{P}_a = N_a/N$ that a particle in the beam will be in the state $|\chi_a\rangle$ and a probability $\mathcal{P}_b = N_b/N$ that it will be in the state $|\chi_b\rangle$. The total spin polarization vector will be given by the statistical average of the polarization of the particles of the first beam and the polarization of the particles in the second beam, i.e.

$$P_i = \mathcal{P}_a \langle \chi_a | \sigma_i | \chi_a \rangle + \mathcal{P}_b \langle \chi_b | \sigma_i | \chi_b \rangle. \tag{1.13}$$

We can then write

$$\mathbf{P} = \mathcal{P}_a \mathbf{P}^{(a)} + \mathcal{P}_b \mathbf{P}^{(b)}, \tag{1.14}$$

where $\mathbf{P}^{(a)}$ and $\mathbf{P}^{(b)}$ are the spin polarization vector of the first and second beam, respectively. Using the fact that $|\mathbf{P}^{(a)}| = |\mathbf{P}^{(b)}| = 1$, the magnitude of the total spin polarization vector is given by

$$|\mathbf{P}| = \sqrt{|\mathcal{P}_a \mathbf{P}^{(a)} + \mathcal{P}_b \mathbf{P}^{(a)}|^2} = \sqrt{\mathcal{P}_a^2 + \mathcal{P}_b^2 + 2\mathcal{P}_a \mathcal{P}_b \mathbf{P}^{(a)} \cdot \mathbf{P}^{(b)}} \leq 1, \tag{1.15}$$

the equal holds only in the case in which $\mathbf{P}^{(a)}$ and $\mathbf{P}^{(a)}$ are parallel and point in the same direction, meaning that the two beams are in the same state. Thus, in general $0 \leq |\mathbf{P}| \leq 1$. Specifically, the condition for having a pure state is only $|\mathbf{P}| = 1$. The condition $|\mathbf{P}| = 0$ corresponds to a spin-1/2 mixed state that is completely unpolarized.

The concepts of a pure and a mixed state can obviously be extended to any kind of state. A pure state is a state that can be specified by only one state vector or, in other words, as a linear combination of a certain basis. Contrary, a mixed state cannot be written as only one state vector. One can only specify the states in which the mixture can be with a relative statistical weight. We will see in Section 1.3 an alternative way to treat pure and mixed states by using the density matrix.

1.2 Spin-1 particles

The study of the polarization states of spin-1 particles will be a central topic of this Thesis. A massive spin-1 particle has three polarization states. We define the helicity λ of the particle as the projection of the spin $\mathbf{S}$ onto the direction of motion $\mathbf{q}$

$$\lambda = \frac{\mathbf{S} \cdot \mathbf{q}}{|\mathbf{q}|}. \tag{1.16}$$

For spin-1 particles the helicity has the three eigenvalues $+1$, -1, 0. The eigenvalue $\lambda = +1$ corresponds to the right-handed circularly polarized state, $\lambda = -1$ to left-handed circularly polarized state and $\lambda = 0$ to longitudinal polarization state. We denote with $|\lambda\rangle$ and $\epsilon^\mu(q,\lambda)$ the state and the polarization vector describing a spin-1 particle with 4-momentum q^μ and helicity λ, respectively. In the frame where the spin-1 particle is at rest, $\mathbf{q} = 0$, the polarization vectors can be written as

$$\epsilon^\mu(q,-1) = \frac{1}{\sqrt{2}}(0,1,-i,0), \tag{1.17a}$$

$$\epsilon^\mu(q,0) = (0,0,0,1), \tag{1.17b}$$

$$\epsilon^\mu(q,+1) = -\frac{1}{\sqrt{2}}(0,1,i,0), \tag{1.17c}$$

where we fixed the coordinate system such that the the fourth component of the vectors is oriented along the direction $\mathbf{q}$ as seen before boosted to the spin-1 rest frame. The polarization vectors are normalized such that

$$\epsilon^\mu(q,\lambda)(\epsilon_\mu(q,\lambda'))^* = -\delta_{\lambda\lambda'}, \tag{1.18}$$

and they are transverse to q^μ, i.e.,

$$\epsilon^\mu(q,\lambda)\, q_\mu = 0. \tag{1.19}$$

The sum over all polarization yields

$$\sum_{\lambda=\pm1,0} \epsilon^\mu(q,\lambda)(\epsilon^\mu(q,\lambda'))^* = -g^{\mu\nu} + \frac{q^\mu q^\nu}{q^2}. \tag{1.20}$$

The polarization vectors describing a circularly polarized particles lie in the plane transverse to the particle momentum. We will call the basis describing state of definite helicity, the circular basis.

A spin-1 particle can also be linearly polarized, meaning that the polarization vectors for a particle at rest are simply given by

$$\epsilon^\mu(q,1) = (0,1,0,0), \tag{1.21a}$$

$$\epsilon^\mu(q,2) = (0,0,1,0), \tag{1.21b}$$

$$\epsilon^\mu(q,0) = (0,0,0,1), \tag{1.21c}$$

where here 1 and 2 denote the two linearly polarized states. We will call the set of the polarization vectors above the linear basis. The relation between the linear and circular basis is

$$\epsilon^\mu(q,1) = -\frac{1}{\sqrt{2}}[\epsilon^\mu(q,+1) - \epsilon^\mu(q,-1)], \tag{1.22a}$$

$$\epsilon^\mu(q,2) = -\frac{i}{\sqrt{2}}[\epsilon^\mu(q,+1) + \epsilon^\mu(q,-1)]. \tag{1.22b}$$

We note that the state describing linearly polarized particles do not have definite angular momentum. In the case of massless spin-1 particles, there are only two polarizations, the two transverse spin states.

1.3 Spin density matrix

As already discussed in Section 1.1, a pure state can be always written as a state vector. This implies that pure states have maximal information [45]. By "maximal information" we mean that a pure state is characterized by the existence of an experiment that can predict the result with certainty. If we for example have completely linearly polarized light, we can properly orient a polarizing filter such that each photon is transmitted. Therefore we know that we can predict with certainty that the beam is in that specific state. In general we can have more experiments that determine uniquely a state. This is equal to saying that the state can be a linear superposition of other states which we call basis. In this case we only have uncertainty in the quantum-mechanical sense: each coefficient of the linear combination represents the probability amplitude that the initial state is measured to be in the corresponding state of the basis. In principle we can define a complete set of operators that specify the state uniquely.

A mixed state, on the other hand, does not have maximal information. For instance, in the case of partially polarized light, we cannot find an orientation of the polarization analyzer such that all photons are transmitted. A mixed state cannot be specified by only a single state vector. In other words a mixed state is an incoherent superposition of pure states. In this case we have uncertainty not only in the quantum-mechanical sense, but also in the statistical sense. The probability of finding a certain experimental result is given by the statistical average: first one calculates the expectation value of each pure state composing the mixture then takes the average.

In order to treat mixed states properly, we introduce the spin density matrix formalism [2, 44, 45]. Consider a mixed spin state formed by independently prepared pure spin states $|\psi_i\rangle$ each one with a certain statistical weight (probability) $\mathcal{P}_i$, such that $\sum_i \mathcal{P}_i = 1$. We define the operator spin density matrix as

$$\rho = \sum_i \mathcal{P}_i |\psi_i\rangle\langle\psi_i|, \tag{1.23}$$

where the index i runs over the total number of states. Clearly, the spin density matrix in Eq. (1.23) is diagonal in the state vectors $|\psi_i\rangle$. In general each pure state can be decomposed into a basis of orthonormal states $|\phi_m\rangle$ as

$$|\psi_i\rangle = \sum_m c_m^{(i)} |\phi_m\rangle, \tag{1.24}$$

where $c_m^{(i)}$ are complex coefficients and m runs over the number of states forming the basis. By substituting Eq. (1.24) into (1.23) we obtain

$$\rho = \sum_{i,m,m'} \mathcal{P}_i c_m^{(i)} c_{m'}^{(i)*} |\phi_m\rangle\langle\phi_{m'}| \tag{1.25}$$

The equation above is the spin density matrix in the basis $|\phi_m\rangle$. The elements of the density matrix are given by

$$\rho_{mm'} = \sum_i \mathcal{P}_i c_m^{(i)} c_{m'}^{(i)*}. \tag{1.26}$$

Consider an operator O. Its expectation value $\langle O \rangle$ for the mixed state described by the spin density matrix, (1.25) is given by

$$\langle O \rangle = \mathrm{Tr}(\rho O). \tag{1.27}$$

In the case we want to calculate the spin polarization vector as in Eq. (1.13), the spin density matrix is given by

$$\rho = \mathcal{P}_a |\chi_a\rangle\langle\chi_a| + \mathcal{P}_b |\chi_b\rangle\langle\chi_b| \tag{1.28}$$

and the spin polarization vector by

$$P_i = \langle \sigma_i \rangle = \mathrm{Tr}(\rho \sigma_i). \tag{1.29}$$

In this Section we considered mixed spin states. Clearly the concept of density matrix can be extended to any kind of state and also to the case where the set of states is not discrete.

1.3.1 Properties of the spin density matrix

The expression (1.25) for the density matrix refers to the particular basis $|\phi_n\rangle$. We can calculate the expression for the spin density matrix in another basis by applying a unitary transformation T to $|\phi_m\rangle$, i.e.

$$|\phi'_r\rangle = \sum_m T_{rm} |\phi_m\rangle. \tag{1.30}$$

The transformed spin density matrix takes the form

$$\rho' = T \rho T^{-1}. \tag{1.31}$$

Due to the cyclic property of the trace, we note that

$$\mathrm{Tr}\,\rho' = \mathrm{Tr}\,\rho. \tag{1.32}$$

We list here some important properties of the spin density matrix.

1. The trace of the spin density matrix is unity, i.e.

$$\mathrm{Tr}\,\rho = 1. \tag{1.33}$$

   This simply follow from the condition $\sum_i \mathcal{P}_i = 1$. More generally, there might be situations in which the spin density matrix is not normalized ($\mathrm{Tr}\,\rho \neq 1$) and the mean value of any operator O is then given by[1]

$$\langle O \rangle = \frac{\mathrm{Tr}(\rho O)}{\mathrm{Tr}\,\rho}. \tag{1.34}$$

[1] For example, this will be the case when we will define the spin density matrix for virtual photons in scattering processes in the next Sections. We will prefer not to normalize the spin density matrix. However, we will give the next properties considering a normalized spin density matrix.

2. The spin density matrix is by construction a hermitian matrix

$$\rho_{mm'} = \rho^*_{m'm} \tag{1.35}$$

3. The diagonal elements are real and non negative, i.e.

$$\rho_{mm} \geq 0, \tag{1.36}$$

this comes from the fact that the diagonal elements are probabilities and thus can not be negative.

4. Since ρ is an hermitian matrix, there exist a unitary matrix U that diagonalizes ρ, i.e.

$$\rho^D = U^{-1}\rho U, \tag{1.37}$$

where ρ^D is diagonal, i.e.

$$\rho_{mm'} = c_m \delta_{mm'}, \tag{1.38}$$

with $c_m \geq 0$.

5. If we calculate the trace of the spin density matrix squared, we obtain

$$\mathrm{Tr}\,\rho^2 = \mathrm{Tr}\,(\rho^D)^2 = \sum_m c_m^2 \leq \left(\sum_m c_m\right)^2 = (\mathrm{Tr}\,\rho)^2 = 1, \tag{1.39}$$

where we used the properties 1-4. We conclude that

$$\mathrm{Tr}\,\rho^2 \leq 1. \tag{1.40}$$

The equality in Eq. (1.40) holds only if the spin density matrix describes a pure state. In fact, if the system is characterized by only a pure state, say $|\psi\rangle$, the spin density matrix takes the simple form

$$\rho = |\psi\rangle\langle\psi|, \tag{1.41}$$

meaning that, in this basis, ρ is diagonal with one eigenvalue being equal to unity and all the others to zero. Hence $\mathrm{Tr}\,\rho^2 = 1$, and this, as already discussed, holds in any basis.

1.3.2 Number of independent parameters of the spin density matrix and the tensor polarization

Consider a pure state for a particle of spin S. We can write the state as a vector with $2S+1$ complex components, therefore we have $2(2S+1)$ real parameters. We can eliminate one real parameter by imposing the normalization of the state. In addition, we can eliminate an overall phase. Therefore, the total number of independent real parameters is $2(2S+1)-2 = 4S$.

Consider now a mixed state described by the spin density matrix ρ. Since ρ is a hermitian matrix of dimension $2S+1$, the total number of real parameters that specify it fully is

$(2S+1)^2$ (there are $2S+1$ real diagonal elements plus $2(2S+1)(2S)/2$ real parameters in the off-diagonal elements). If we assume the normalization condition (1.33), the number of parameters is clearly $(2S+1)^2-1$.

Let us first consider a mixed state of spin-1/2 particles. According to the discussion above, ρ is a 2×2 matrix with four independent real parameters. Any 2×2 hermitian matrix can always be written in terms of the unity matrix I and the Pauli matrices $\boldsymbol{\sigma} = (\sigma_x, \sigma_y, \sigma_z)$ as

$$\rho = \frac{1}{2}(aI + \mathbf{b}\cdot\boldsymbol{\sigma}), \tag{1.42}$$

where a and $\mathbf{b}$ are the four real parameters such that

$$a = \mathrm{Tr}\,\rho, \qquad b_i = \mathrm{Tr}\,(\rho\sigma_i). \tag{1.43}$$

If the spin density matrix is normalized, Eq. (1.33), then the total number of real parameters is three, and we have

$$\rho = \frac{1}{2}(I + \mathbf{P}\cdot\boldsymbol{\sigma}), \tag{1.44}$$

where $\mathbf{P}$ is the spin polarization vector defined in Eq. (1.6). This means that the three components of the spin polarization vector are the three real parameters that fully specify the spin density matrix for the case of spin-1/2 particles. We can write Eq. (1.44) explicitly by using the Puali matrices, i.e.

$$\rho = \frac{1}{2}\begin{pmatrix} 1+P_z & P_x - iP_y \\ P_x + iP_y & 1-P_z \end{pmatrix} \tag{1.45}$$

We note that the case of spin-1/2 particles is special. In this case the Pauli matrices play two roles: they are a basis for expressing any 2×2 hermitian matrix and they are also the operators that define the spin.

If we want to generalize the previous discussion for spin greater than 1/2, it is not sufficient just to substitute the Pauli matrices with proper spin operators because the spin matrices do not form a complete basis. Consider now the case of spin-1 particles. The number of real parameters that specify the corresponding normalized spin density matrix is eight. The spin density matrix in the spin-1 particle rest frame can be written as [1, 2, 46]

$$\rho = \frac{1}{3}\left[1 + \frac{3}{2}\mathbf{P}\cdot\mathbf{S} + \sqrt{\frac{3}{2}}\sum_{i,j} T_{ij}(S_iS_j + S_jS_i)\right], \tag{1.46}$$

with T_{ij} real, symmetric and traceless ($\sum_i T_{ii} = 0$). In the above equation $\mathbf{S} = (S_x, S_y, S_z)$ denote the 3×3 traceless matrices representing the spin-1 operators, i.e.,

$$S_x = \frac{1}{\sqrt{2}}\begin{pmatrix} 0 & 1 & 0 \\ 1 & 0 & 1 \\ 0 & 1 & 0 \end{pmatrix}, \quad S_y = \frac{i}{\sqrt{2}}\begin{pmatrix} 0 & -1 & 0 \\ 1 & 0 & -1 \\ 0 & 1 & 0 \end{pmatrix}, \quad S_z = \begin{pmatrix} 1 & 0 & 0 \\ 0 & 0 & 0 \\ 0 & 0 & -1 \end{pmatrix}. \tag{1.47}$$

The vector **P** in Eq. (1.46) is the spin polarization vector for spin-1 particle defined analogously with the spin-1/2 case, i.e.

$$\mathbf{P} = \langle \mathbf{S} \rangle. \tag{1.48}$$

Therefore the number of real parameters are the three components of spin polarization vector and the five components of T_{ij}. Note that Eq. (1.46) shows that, even in absence of a net spin-polarization ($\mathbf{P} = \mathbf{0}$), the system can still be polarized due to T_{ij}. The tensor T_{ij} is called *tensor polarization* and its explicit expression is given by

$$T_{ij} = \frac{1}{2}\sqrt{\frac{3}{2}}\left(\langle S_i S_j + S_j S_i \rangle - \frac{4}{3}\delta_{ij}\right). \tag{1.49}$$

The spin density matrix can be diagonalized in the form

$$\rho = \frac{1}{3}\begin{pmatrix} 1 + \frac{3}{2}P_z + \sqrt{\frac{3}{2}}T_{zz} & 0 & 0 \\ 0 & 1 - \sqrt{6}T_{zz} & 0 \\ 0 & 0 & 1 - \frac{3}{2}P_z + \sqrt{\frac{3}{2}T_{zz}} \end{pmatrix}. \tag{1.50}$$

The spin density matrix for spin-1 particles in Eq. (1.46) and (1.50) is given in the photon rest frame. For a covariant generalization see e.g. [2, 47]. All the properties discussed above still hold for in a covariant treatment.

1.4 Spin density matrix for production and decay of spin-1 particles

The spin density matrix discussed in the previous Sections is also a very useful tool to describe spin-1 particle polarization state in a process where there is a formation of a spin-1 particle and then its decay. In this Section we want to discuss the spin density formalism approach to calculate decay of spin-1 particles. Consider the process in which a spin-1 particle is created together with some other particles denoted with A. The spin-1 particle then decays into two particles X_1 and X_2, i.e.

$$\text{initial state} \to \text{spin-1 particle} + A \to X_1 + X_2 + A. \tag{1.51}$$

If we assume that, once produced, the spin-1 particle does not interact with A, we can factorize the problem into two parts: the matrix element of the production mechanism $\mathcal{M}^{\text{prod}}(\lambda)$ which takes into account the production of the spin-1 particle and the final state excluding X_1 and X_2, and the matrix element of the decay $\mathcal{M}^{\text{dec}}(\lambda)$, which only takes into account the decay of the spin-1 particle into X_1, X_2. This kind of factorization will be extensively discussed in Chapter 2 for vacuum processes, and in Chapter 3 in medium. In the matrix element we made the dependence on the spin-1 particle helicity λ explicit. Thus, we have

$$\mathcal{M}^{\text{prod}}(\lambda) = (\epsilon^{\mu}(\lambda))^* W_{\mu} \tag{1.52}$$

$$\mathcal{M}^{\text{dec}}(\lambda) = L_{\mu}\epsilon^{\mu}(\lambda), \tag{1.53}$$

where W_μ describes the production of the spin-1 particle and L_μ its decay. Moreover, $\epsilon^\mu(\lambda)$ is the polarization vector of the spin-1 particle corresponding to helicity λ (the dependence on the momentum is not shown explicitly). The matrix element for the full reaction is given by

$$\mathcal{M} = \sum_\lambda \mathcal{M}^{\text{dec}}(\lambda)\mathcal{M}^{\text{prod}}(\lambda) \tag{1.54}$$

$$= \sum_\lambda L_\mu \epsilon^\mu(\lambda)(\epsilon^\nu(\lambda))^* W_\nu \tag{1.55}$$

The cross section is given by the squared matrix element summed over all the polarization of the initial and final state

$$\sum_{\text{pol}} |\mathcal{M}|^2 = \sum_{\text{pol}} \sum_{\lambda,\lambda'} L_\mu \epsilon^\mu(\lambda)(\epsilon^\nu(\lambda))^* W_\nu W^*_{\nu'} \epsilon^{\nu'}(\lambda')(\epsilon^{\mu'}(\lambda'))^* L^*_{\mu'} \tag{1.56}$$

We then find

$$W_{\mu\nu} = \sum_{\text{pol}} W_\mu W^*_\nu, \tag{1.57}$$

$$L_{\mu\nu} = \sum_{\text{pol}} L_\mu L^*_\nu, \tag{1.58}$$

where in the definition of $W_{\mu\nu}$ the sum is meant over all the polarization of the initial states and the final states except the spin-1 particle and X_1 and X_2, while in the definition of $L_{\mu\nu}$ the sum is meant over the polarization of X_1 and X_2 only. We can rewrite Eq. (1.56) as

$$\sum_{\text{pol}} |\mathcal{M}|^2 = \sum_{\lambda,\lambda'} \rho^{\text{prod}}_{\lambda\lambda'} \rho^{\text{dec}}_{\lambda'\lambda} = \sum_{\lambda,\lambda'} \rho^{\text{dec}}_{\lambda'\lambda} \rho^{\text{prod}}_{\lambda\lambda'}, \tag{1.59}$$

where we have introduced the *production spin density matrix* describing the creation of the spin-1 particle

$$\rho^{\text{prod}}_{\lambda\lambda'} = (\epsilon^\mu(\lambda))^* W_{\mu\nu} \epsilon^\nu(\lambda'), \tag{1.60}$$

and the *decay spin density matrix* describing the decay of the spin-1 particle

$$\rho^{\text{dec}}_{\lambda'\lambda} = (\epsilon^\mu(\lambda'))^* L_{\nu\mu} \epsilon^\mu(\lambda). \tag{1.61}$$

Note that Eq. (1.56) can also be written as

$$\sum_{\text{pol}} |\mathcal{M}|^2 = W_{\mu\nu} L^{\mu\nu}, \tag{1.62}$$

where we used the polarization sum Eq. (1.20) and current conservation, which implies $q_\mu W^{\mu\nu} = q_\mu L^{\mu\nu} = 0$. Note that the spin density matrices defined in Eq. (1.60) and Eq. (1.61) are in general not normalized, i.e. $\text{Tr}\,\rho \neq 1$.

As a final remark, we want to point out that the spin density matrices defined in Eqs. (1.60)-(1.61) do not in general describe a pure spin-1 particle state. This is due

to the fact that the tensors Eqs. (1.57)-(1.58) contains the incoherent sum over the polarizations of the initial and final states required for the definition of a cross section. This implies that the photon is not in a pure a state. Only when there is no sum, namely if we fix the polarizations of all the initial particles, the spin-1 particle will be in a pure state. Once we perform the statistical average, the photon state looses "information" in the sense discussed in Sections 1.1 and 1.3. In order to understand this, consider an hypothetical case in which we can fix the polarization of the initial and final state of a reaction. A virtual photon formed in such a polarized reaction will be also in a pure state, say with helicity -1, $|-1\rangle$. Now we repeat the experiment with different polarization states for the initial and final particles and we see that, for example, the photon is in the state with helicity $+1$, $|+1\rangle$. If we assume that these two polarization states have the same probability to be realized, like in a reaction of unpolarized particles, the photon state cannot be described by a pure state, but rather by the spin density matrix (that here we assumed normalized)

$$\rho^{\text{prod}} = \frac{1}{2}|-1\rangle\langle -1| + \frac{1}{2}|+1\rangle\langle +1| \tag{1.63}$$

which is clearly a spin density matrix describing a mixed state since

$$\text{Tr}\,(\rho^{\text{prod}})^2 = 0.5 < 1, \tag{1.64}$$

as discussed in Subsection 1.3.1. The spin density matrix is a very important tool for describing the polarization state of particles and will be extensively discussed and used in this Thesis. In the following Sections we will give explicit expressions of the decay spin density matrix of particular processes, in particular the decay of virtual photons into dileptons.

1.5 Angular distribution for $\gamma \to e^+e^-$

The decay process considered in this Thesis is the decay of a virtual photon into dilepton. Such a decay is described by quantum electrodynamics. The amplitude is given by

$$L_\mu = e\,\bar{u}_s(p_-)\gamma_\mu v_{s'}(p_+), \tag{1.65}$$

where $\bar{u}_s(p_-)$ is the spinor describing an electron with polarization s and momentum p_- while $v_{s'}(p_+)$ a positron with polarization s' and momentum p_+, and e is the electric charge. Squaring the amplitudes and summing over the polarization of the electron and positron yields the lepton tensor (from now on we drop the common factor e, the electric charge)

$$L_{\mu\nu} = 4[p_{+\mu}p_{-\nu} + p_{+\nu}p_{-\mu} - (p_+ \cdot p_- + m_e^2)g_{\mu\nu}]. \tag{1.66}$$

In the rest frame of the photon, the momentum of the electron is

$$p_-^\mu = (\sqrt{m_e^2 + |\mathbf{p}|^2}, |\mathbf{p}|\sin\theta_e\cos\phi_e, |\mathbf{p}|\sin\theta_e\sin\phi_e, |\mathbf{p}|\cos\theta_e), \tag{1.67}$$

where θ_e and ϕ_e are the polar and azimuthal angle between the electron three-momentum and the quantization axis, $|\mathbf{p}|$ being the modulus of the electron momentum in the photon rest frame. The momentum of the positron is then

$$p_+^\mu = (\sqrt{m_e^2 + |\mathbf{p}|^2}, -|\mathbf{p}|\sin\theta_e\cos\phi_e, -|\mathbf{p}|\sin\theta_e\sin\phi_e, -|\mathbf{p}|\cos\theta_e). \tag{1.68}$$

In order to derive the explicit expression for the decay spin density matrix from Eq. (1.61), we use the polarization vectors in Eqs. (1.17). This implies that the quantization axis chosen is along the virtual photon momentum. We use the convention for the order of the helicities in the spin density matrix in which the labels of the rows and columns run from helicity -1 to $+1$. Thus, we have

$$\rho^{\rm dec}_{\lambda',\lambda} = \begin{pmatrix} \frac{1}{2}(L_{xx}+L_{yy}) & \frac{1}{\sqrt{2}}(L_{xz}+iL_{yz}) & \frac{1}{2}(-L_{xx}-2iL_{xy}+L_{yy}) \\ \frac{1}{\sqrt{2}}(L_{xz}-iL_{yz}) & L_{zz} & -\frac{1}{\sqrt{2}}(L_{xz}+iL_{yz}) \\ \frac{1}{2}(-L_{xx}+2iL_{xy}+L_{yy}) & -\frac{1}{\sqrt{2}}(L_{xz}-iL_{yz}) & \frac{1}{2}(L_{xx}+L_{yy}) \end{pmatrix}. \tag{1.69}$$

We recall that the spin density matrix is by definition hermitian. Substituting the explicit expression for the lepton tensor, we obtain

$$\rho^{\rm dec}_{\lambda',\lambda} = 4|\mathbf{p}|^2 \begin{pmatrix} 1+\cos^2\theta_e+\alpha & -\frac{\sqrt{2}}{2}\sin 2\theta_e e^{i\phi_e} & \sin^2\theta_e e^{2i\phi_e} \\ -\frac{\sqrt{2}}{2}\sin 2\theta_e e^{-i\phi_e} & 2(1-\cos^2\theta_e)+\alpha & \frac{\sqrt{2}}{2}\sin 2\theta_e e^{i\phi_e} \\ \sin^2\theta_e e^{-2i\phi_e} & \frac{\sqrt{2}}{2}\sin 2\theta_e e^{-i\phi_e} & 1+\cos^2\theta_e+\alpha \end{pmatrix}, \tag{1.70}$$

where $\alpha = 2m_e^2/|\mathbf{p}|^2$. The angular distribution is proportional to the square of the matrix element. Thus, using Eq. (1.59), we find

$$\begin{aligned} \frac{d\sigma}{d\Omega_e} \propto \sum_{\rm pol}|\mathcal{M}|^2 \propto{}& (1+\cos^2\theta_e+\alpha)(\rho^{\rm prod}_{-1,-1}+\rho^{\rm prod}_{+1,+1}) + [2(1-\cos^2\theta_e)+\alpha]\rho^{\rm prod}_{0,0} \\ &+ \frac{\sqrt{2}}{2}\sin 2\theta_e\left[e^{-i\phi_e}(\rho^{\rm prod}_{0,+1}-\rho^{\rm prod}_{-1,0}) + e^{i\phi_e}((\rho^{\rm prod}_{0,+1})^*-(\rho^{\rm prod}_{-1,0})^*)\right] \\ &+ \sin^2\theta_e(e^{-2i\phi_e}\rho^{\rm prod}_{-1,+1} + e^{2i\phi_e}(\rho^{\rm prod}_{-1,+1})^*), \end{aligned} \tag{1.71}$$

where Ω_e denotes the lepton solid angle. The above equation can be rearranged in the form

$$\begin{aligned} \frac{d\sigma}{d\Omega_e} \propto{}& 4|\mathbf{p}|^2\mathcal{N}_e(1+\lambda_\theta\cos^2\theta_e + \lambda_e\sin^2\theta_e\cos 2\phi_e + \lambda_{\theta\phi}\sin 2\theta_e\cos\phi_e \\ &+ \lambda^\perp_\phi\sin^2\theta_e\sin 2\phi_e + \lambda^\perp_{\theta\phi}\sin 2\theta_e\sin\phi_e). \end{aligned} \tag{1.72}$$

The anisotropy coefficients are given by

$$\lambda_\theta = \frac{1}{\mathcal{N}_e}(\rho^{\rm prod}_{-1,-1}+\rho^{\rm prod}_{+1,+1}-2\rho^{\rm prod}_{0,0}), \tag{1.73a}$$

$$\lambda_\phi = \frac{1}{\mathcal{N}_e}2{\rm Re}\,(\rho^{\rm prod}_{-1,+1}), \tag{1.73b}$$

$$\lambda_{\theta\phi} = \frac{1}{\mathcal{N}_e}\sqrt{2}{\rm Re}\,(\rho^{\rm prod}_{0,+1}-\rho^{\rm prod}_{-1,0}), \tag{1.73c}$$

$$\lambda^\perp_\phi = \frac{1}{\mathcal{N}_e}2{\rm Im}\,(\rho^{\rm prod}_{-1,+1}), \tag{1.73d}$$

$$\lambda^\perp_{\theta\phi} = \frac{1}{\mathcal{N}_e}\sqrt{2}{\rm Im}\,(\rho^{\rm prod}_{0,+1}-\rho^{\rm prod}_{-1,0}), \tag{1.73e}$$

the normalization factor being

$$\mathcal{N}_e = \rho^{\text{prod}}_{-1,-1} + \rho^{\text{prod}}_{+1,+1} + 2\rho^{\text{prod}}_{0,0} + \alpha(\rho^{\text{prod}}_{-1,-1} + \rho^{\text{prod}}_{+1,+1} + \rho^{\text{prod}}_{0,0}). \tag{1.74}$$

We note that the terms proportional to the coefficients $\lambda^{\perp}_{\phi}$ and $\lambda^{\perp}_{\theta\phi}$ in Eq. (1.72) violate reflection symmetry $\phi_e \to -\phi_e$, but not parity. The general expression for the total cross section is given by integrating (1.72) over the solid angle

$$\sigma \propto \frac{4\pi}{3} 4|\mathbf{p}|^2 \mathcal{N}_e (3 + \lambda_\theta). \tag{1.75}$$

Thus, for dilepton final state we have

$$\sigma \propto \frac{4\pi}{3} 4|\mathbf{p}|^2 (4 + 3\alpha)(\rho^{\text{prod}}_{-1,-1} + \rho^{\text{prod}}_{+1,+1} + \rho^{\text{prod}}_{0,0}). \tag{1.76}$$

The interpretation of the λ_θ coefficient becomes clear if we integrate over the azimuthal angle of the electron momentum ϕ_e. In this case only the angle independent term and the term proportional to λ_θ of Eq. (1.72) do not vanish, and hence the diagonal elements of $\rho^{\text{prod}}_{\lambda,\lambda'}$ contribute to the total cross section. Moreover, if we consider the massless case, i.e. $m_e = 0$, the angular distribution can be cast in the form

$$\frac{d\sigma}{d\cos\theta_e} \propto \Sigma_\perp (1 + \cos^2\theta_e) + \Sigma_\parallel (1 - \cos^2\theta_e), \tag{1.77}$$

where $\Sigma_\perp = \rho^{\text{had}}_{-1,-1} + \rho^{\text{had}}_{1,1}$ and $\Sigma_\parallel = 2\rho^{\text{had}}_{0,0}$ are the contributions of the transverse and parallel polarizations of the intermediate photon to the differential cross section. Equation (1.77) can be rearranged in the following way:

$$\frac{d\sigma}{d\cos\theta_e} \propto C(1 + \lambda_\theta \cos^2\theta_e), \tag{1.78}$$

where the anisotropy coefficient λ_θ is given by

$$\lambda_\theta = \frac{\Sigma_\perp - \Sigma_\parallel}{\Sigma_\perp + \Sigma_\parallel}. \tag{1.79}$$

Thus, the anisotropy coefficients provides information on the polarization of the virtual photon. If the virtual photon is created via the decay of an intermediate resonance, as we will see in Chapter 2, then λ_θ in general depends on the quantum numbers of the resonance, and on the emission angle.

Predictions for the λ_θ coefficient for some dilepton sources are given in Ref. [27]. In particular, for the Drell-Yan process (quark-antiquark annihilation) $\lambda_\theta = +1$ (the virtual photon is completely transversely polarized), while for the pion annihilation process $\lambda_\theta = -1$ (the virtual photon is completely longitudinally polarized). In the latter two examples we assumed that the polar angle is measured with respect to the axis defined from the initial particle momenta in the center of mass frame. We will see in Section 1.8 that the anisotropy coefficients will depend on the choice of the quantization axis.

1.6 Angular distribution for $\rho \to \pi^+\pi^-$

It is also interesting to study the decay of the ρ meson into two pions. The matrix element for this decay process is given by the difference between the positive and negative pion momenta,

$$L_\mu = g\,(p_{+\mu} - p_{-\mu}) \tag{1.80}$$

where g is the coupling constant $\rho\pi\pi$ and the four-momenta are analog to those in the dilepton case, i.e.

$$p_-^\mu = (\sqrt{m_\pi^2 + |\mathbf{p}|^2}, |\mathbf{p}|\sin\theta_\pi\cos\phi_\pi, |\mathbf{p}|\sin\theta_\pi\sin\phi_\pi, |\mathbf{p}|\cos\theta_\pi), \tag{1.81}$$

where we changed the subscript of the polar and azimuthal angle. After we square the matrix element, we find (we again drop the common factor g)

$$L_{\mu\nu} = (p_{+\mu} - p_{-\mu})(p_{+\nu} - p_{-\nu}). \tag{1.82}$$

We note that $L_{\mu\nu}$ is symmetric, as in the dilepton case. The decay spin density matrix is again given by Eq. (1.69), which in this case yields

$$\rho^{\mathrm{dec}}_{\lambda',\lambda} = 2|\mathbf{p}|^2 \begin{pmatrix} 1-\cos^2\theta_\pi & \frac{\sqrt{2}}{2}\sin 2\theta_\pi e^{i\phi_\pi} & -\sin^2\theta_\pi e^{2i\phi_\pi} \\ \frac{\sqrt{2}}{2}\sin 2\theta_\pi e^{-i\phi_\pi} & 2\cos^2\theta_\pi & -\frac{\sqrt{2}}{2}\sin 2\theta_\pi e^{i\phi_\pi} \\ -\sin^2\theta_\pi e^{-2i\phi_\pi} & -\frac{\sqrt{2}}{2}\sin 2\theta_\pi e^{-i\phi_\pi} & 1-\cos^2\theta_\pi \end{pmatrix}, \tag{1.83}$$

the order of the labels of the rows and column is the same as in Eq. (1.69). Thus, the angular distribution is given by Eq. (1.59) and it has the same general form as for the dilepton final state Eq. (1.72). However, the anisotropy coefficients differ by a factor -1:

$$\lambda_\theta = -\frac{1}{\mathcal{N}_\pi}(\rho^{\mathrm{prod}}_{-1,-1} + \rho^{\mathrm{prod}}_{+1,+1} - 2\rho^{\mathrm{prod}}_{0,0}), \tag{1.84a}$$

$$\lambda_\phi = -\frac{1}{\mathcal{N}_\pi} 2\mathrm{Re}\,(\rho^{\mathrm{prod}}_{-1,+1}), \tag{1.84b}$$

$$\lambda_{\theta\phi} = -\frac{1}{\mathcal{N}_\pi}\sqrt{2}\mathrm{Re}\,(\rho^{\mathrm{prod}}_{0,+1} - \rho^{\mathrm{prod}}_{-1,0}), \tag{1.84c}$$

$$\lambda^\perp_\phi = -\frac{1}{\mathcal{N}_\pi} 2\mathrm{Im}\,(\rho^{\mathrm{prod}}_{-1,+1}), \tag{1.84d}$$

$$\lambda^\perp_{\theta\phi} = -\frac{1}{\mathcal{N}_\pi}\sqrt{2}\mathrm{Im}\,(\rho^{\mathrm{prod}}_{0,+1} - \rho^{\mathrm{prod}}_{-1,0}). \tag{1.84e}$$

Moreover, the normalization factor is

$$\mathcal{N}_\pi = \rho^{\mathrm{prod}}_{-1,-1} + \rho^{\mathrm{prod}}_{+1,+1}, \tag{1.85}$$

while the total cross section is given by

$$\sigma = \frac{8\pi}{3} 2|\mathbf{p}|^2(\rho^{\mathrm{prod}}_{-1,-1} + \rho^{\mathrm{prod}}_{+1,+1} + \rho^{\mathrm{prod}}_{0,0}). \tag{1.86}$$

By comparing the anisotropy coefficients Eqs. (1.84a)-(1.84e) with the those for the decay of virtual photon into dilepton Eqs. (1.73a)-(1.73e), one sees that, apart from the different normalization factor, there is just a change in sign. We note that the λ_θ coefficients of Eqs. (1.73a) and (1.84a) have the same physical meaning, but this is reflected differently in the angular distribution. For example, Eq. (1.73a) can take on values between -1 and $+1$, with -1 for a completely longitudinal photon ($\rho^{\text{prod}}_{-1,-1} = \rho^{\text{prod}}_{+1,+1} = 0$) and $+1$ for a completely transverse one ($\rho^{\text{prod}}_{0,0} = 0$). On the other hand, the coefficient in Eq. (1.84a) is not bounded and can, due to the different normalization factor, take on values between -1 and $+\infty$, with -1 describing a completely transversely polarized photon and $+\infty$ a completely longitudinally polarized photon.

1.7 Angular distribution for parity violating processes

In this Section we want to give a general expression for the decay spin density matrix valid for any kind of decay for the spin-1 particle into two particles, allowing also for parity violation. As in the previous Sections, we finally want to give the expression for the angular distribution of the final state particles in the rest frame. Consider a state $|J,M\rangle$ describing a particle at rest with total spin J and spin projection M along a direction, say z. If we apply a general rotation

$$R(\alpha,\beta,\gamma) = e^{-i\alpha J_z} e^{-i\beta J_y} e^{-i\gamma J_z} \tag{1.87}$$

on the state $|J,M\rangle$ of angles α, β and γ around the axes x, y and z, respectively, we find

$$R(\alpha,\beta,\gamma)|J,M\rangle = \sum_{M'=-J}^{J} D^J_{M',M}(\alpha,\beta,\gamma)|J,M'\rangle, \tag{1.88}$$

where M' is the spin projection on the old quantization axis z, obtained after the rotation R. Equation (1.88) expresses the rotated state in terms of the states with spin projection M'. Therefore the Wigner matrices are defined as

$$D^J_{M',M}(\alpha,\beta,\gamma) = \langle J,M'|R(\alpha,\beta,\gamma)|J,M\rangle, \tag{1.89}$$

hence

$$D^J_{M',M}(\alpha,\beta,\gamma) = e^{-i\alpha M'} d^J_{M',M}(\beta) e^{-i\gamma M}, \tag{1.90}$$

with

$$d^J_{M',M}(\beta) = \langle J,M'|e^{-i\beta J_y}|J,M\rangle, \tag{1.91}$$

the reduced real matrices.

Consider now a spin-1 particle with helicity λ and polarization vectors given by Eq. (1.17) decaying into two particles X_1, X_2 with helicities λ_1 and λ_2, respectively. We have

$$\text{spin-1 particle } (\lambda) \;\rightarrow\; X_1(\lambda_1) + X_2(\lambda_2). \tag{1.92}$$

We now define the amplitude for such a process as

$$\mathcal{M}^{\text{dec}}(\lambda, \lambda_1, \lambda_2) = W_\mu(\lambda_1, \lambda_2)\, \epsilon^\mu(\lambda). \tag{1.93}$$

The terms of the above equation depend also on the solid polar and azimuthal angle respectively θ_X and ϕ_X of one of the two particles in the final state in the spin-1 rest frame. This dependence is not explicit in the notation. The decay spin density matrix defined in (1.61) is given by

$$\rho^{\text{dec}}_{\lambda'\lambda} = \sum_{\lambda_1,\lambda_2} (\mathcal{M}^{\text{dec}}(\lambda', \lambda_1, \lambda_2))^*\, \mathcal{M}^{\text{dec}}(\lambda, \lambda_1, \lambda_2), \tag{1.94}$$

where the sum runs over all the possible values for the helicities of the decay products. In the total matrix element squared Eq. (1.56), the sum over the final spin states are done incoherently, while that over photon helicities is done coherently. That is why in Eq. (1.94) we need to allow for $\lambda \neq \lambda'$. It is convenient to write the general decay amplitude (1.93) in terms of helicity amplitudes. At this point, we want to make use of the helicity formalism to decompose the decay amplitude [48–50]. In this Thesis we will not go through the derivations of the helicity formalism, but we will only use its results. Equation Eq. (1.93) can be expressed as

$$\mathcal{M}^{\text{dec}}(\lambda, \lambda_1, \lambda_2) = \sqrt{\frac{3}{4\pi}} A_{\lambda_1\lambda_2} \left(D^1_{\lambda,\, \lambda_1-\lambda_2}(\phi_X, \theta_X, -\phi_X)\right)^*. \tag{1.95}$$

Here $A_{\lambda_1\lambda_2}$ is the so-called helicity amplitude which describes the strength of the particular configuration of helicities for the two-particle final state. Note that the helicity amplitudes do not depend on the angles. In Eq. (1.95) all the dependence on the angles is in the Wigner functions. By substituting Eq. (1.95) into Eq. (1.94), we obtain the general expression for the decay of spin density matrix in terms of the helicity amplitudes, i.e.

$$\rho^{\text{dec}}_{\lambda'\lambda} = \frac{3}{4\pi} \sum_{\lambda_1,\lambda_2} |A_{\lambda_1\lambda_2}|^2 D^1_{\lambda',\, \lambda_1-\lambda_2}(\phi_X, \theta_X, -\phi_X) \left(D^1_{\lambda,\, \lambda_1-\lambda_2}(\phi_X, \theta_X, -\phi_X)\right)^*. \tag{1.96}$$

We can now calculate the components of the decay spin density matrix, by using the explicit expression of the Wigner matrices Eq. (1.90). We will give an expression in the case in which there are two spin-1/2 particles in the final states. Hence the sum over λ_1 and λ_2 runs over the values $-1/2$ and $1/2$ We use the conventions given in [51], i.e.

$$D^1_{0,0} = \cos\theta_X, \tag{1.97a}$$

$$D^1_{-1,-1} = D^1_{+1,+1} = \frac{1+\cos\theta_X}{2}, \tag{1.97b}$$

$$D^1_{0,+1} = -(D^1_{+1,0})^* = D^1_{-1,0} = -(D^1_{0,-1})^* = \frac{e^{i\phi_X}\sin\theta_X}{\sqrt{2}}, \tag{1.97c}$$

$$D^1_{-1,+1} = (D^1_{+1,-1})^* = \frac{e^{2i\phi_X}(1-\cos\theta_X)}{2}, \tag{1.97d}$$

where we dropped the explicit dependence of the angles of the Wigner matrices. The components of the spin density matrix are thus given by

$$4\frac{4\pi}{3}\rho^{\text{dec}}_{-1-1} = \Big[|A_{+\frac{1}{2}-\frac{1}{2}}|^2 + |A_{-\frac{1}{2}+\frac{1}{2}}|^2 + 2\Big(|A_{+\frac{1}{2}+\frac{1}{2}}|^2 + |A_{-\frac{1}{2}-\frac{1}{2}}|^2\Big)\Big] + \Big[|A_{+\frac{1}{2}-\frac{1}{2}}|^2 + |A_{-\frac{1}{2}+\frac{1}{2}}|^2 - 2\Big(|A_{+\frac{1}{2}+\frac{1}{2}}|^2 + |A_{-\frac{1}{2}-\frac{1}{2}}|^2\Big)\Big]\cos^2\theta_X - 2\Big(|A_{+\frac{1}{2}-\frac{1}{2}}|^2 - |A_{-\frac{1}{2}+\frac{1}{2}}|^2\Big)\cos\theta_X, \tag{1.98}$$

$$4\frac{4\pi}{3}\rho^{\text{dec}}_{+1+1} = \Big[|A_{+\frac{1}{2}-\frac{1}{2}}|^2 + |A_{-\frac{1}{2}+\frac{1}{2}}|^2 + 2\Big(|A_{+\frac{1}{2}+\frac{1}{2}}|^2 + |A_{-\frac{1}{2}-\frac{1}{2}}|^2\Big)\Big] + \Big[|A_{+\frac{1}{2}-\frac{1}{2}}|^2 + |A_{-\frac{1}{2}+\frac{1}{2}}|^2 - 2\Big(|A_{+\frac{1}{2}+\frac{1}{2}}|^2 + |A_{-\frac{1}{2}-\frac{1}{2}}|^2\Big)\Big]\cos^2\theta_X + 2\Big(|A_{+\frac{1}{2}-\frac{1}{2}}|^2 - |A_{-\frac{1}{2}+\frac{1}{2}}|^2\Big)\cos\theta_X, \tag{1.99}$$

$$4\frac{4\pi}{3}\rho^{\text{dec}}_{00} = 2\Big(|A_{+\frac{1}{2}-\frac{1}{2}}|^2 + |A_{-\frac{1}{2}+\frac{1}{2}}|^2\Big) - \Big[2\Big(|A_{+\frac{1}{2}-\frac{1}{2}}|^2 + |A_{-\frac{1}{2}+\frac{1}{2}}|^2\Big) - 4\Big(|A_{+\frac{1}{2}+\frac{1}{2}}|^2 + |A_{-\frac{1}{2}-\frac{1}{2}}|^2\Big)\Big]\cos^2\theta_X, \tag{1.100}$$

$$4\frac{4\pi}{3}\rho^{\text{dec}}_{-10} = -\frac{1}{\sqrt{2}}\Big[|A_{+\frac{1}{2}-\frac{1}{2}}|^2 + |A_{-\frac{1}{2}+\frac{1}{2}}|^2 - 2\Big(|A_{+\frac{1}{2}+\frac{1}{2}}|^2 + |A_{-\frac{1}{2}-\frac{1}{2}}|^2\Big)\Big]e^{i\phi_X}\sin 2\theta_X + \frac{2}{\sqrt{2}}\Big(|A_{+\frac{1}{2}-\frac{1}{2}}|^2 - |A_{-\frac{1}{2}+\frac{1}{2}}|^2\Big)e^{i\phi_X}\sin\theta_X, \tag{1.101}$$

$$4\frac{4\pi}{3}\rho^{\text{dec}}_{0+1} = \frac{1}{\sqrt{2}}\Big[|A_{+\frac{1}{2}-\frac{1}{2}}|^2 + |A_{-\frac{1}{2}+\frac{1}{2}}|^2 - 2\Big(|A_{+\frac{1}{2}+\frac{1}{2}}|^2 + |A_{-\frac{1}{2}-\frac{1}{2}}|^2\Big)\Big]e^{i\phi_X}\sin 2\theta_X + \frac{2}{\sqrt{2}}\Big(|A_{+\frac{1}{2}-\frac{1}{2}}|^2 - |A_{-\frac{1}{2}+\frac{1}{2}}|^2\Big)e^{i\phi_X}\sin\theta_X, \tag{1.102}$$

$$4\frac{4\pi}{3}\rho^{\text{dec}}_{-1+1} = \Big[|A_{+\frac{1}{2}-\frac{1}{2}}|^2 + |A_{-\frac{1}{2}+\frac{1}{2}}|^2 - 2\Big(|A_{+\frac{1}{2}+\frac{1}{2}}|^2 + |A_{-\frac{1}{2}-\frac{1}{2}}|^2\Big)\Big]e^{2i\phi_X}\sin^2\theta_X. \tag{1.103}$$

The angular distribution is obtained from Eq. (1.59). We obtain a general expression of the form (we use the same notation as in [52, 53]):

$$\frac{d\sigma}{d\Omega_X} \propto \frac{1}{4}\frac{3}{4\pi}\mathcal{N}(1 + \lambda_\theta\cos^2\theta_X + \lambda_\phi\sin^2\theta_X\cos 2\phi_X + \lambda_{\theta\phi}\sin 2\theta_X\cos\phi_X + \lambda^\perp_\phi\sin^2\theta_X\sin 2\phi_X + \lambda^\perp_{\theta\phi}\sin 2\theta_X\sin\phi_X + 2A_\theta\cos\theta_X + 2A_\phi\sin\theta_X\cos\phi_X + 2A^\perp_\phi\sin\theta_X\sin\phi_X). \tag{1.104}$$

Note that in the general expression above for the angular distribution there are three additional terms proportional to A_θ, A_ϕ and $A_\phi^\perp$. These terms are those which allow for parity violation. The anisotropy coefficients are given by

$$\lambda_\theta = \frac{a}{\mathcal{N}}(\rho^{\text{prod}}_{-1,-1} + \rho^{\text{prod}}_{+1,+1} - 2\rho^{\text{prod}}_{0,0}), \tag{1.105a}$$

$$\lambda_\phi = \frac{a}{\mathcal{N}} 2\text{Re}\,(\rho^{\text{prod}}_{-1,+1}), \tag{1.105b}$$

$$\lambda_{\theta\phi} = \frac{a}{\mathcal{N}}\sqrt{2}\text{Re}\,(\rho^{\text{prod}}_{0,+1} - \rho^{\text{prod}}_{-1,0}), \tag{1.105c}$$

$$\lambda^\perp_\phi = \frac{a}{\mathcal{N}} 2\text{Im}\,(\rho^{\text{prod}}_{-1,+1}), \tag{1.105d}$$

$$\lambda^\perp_{\theta\phi} = \frac{a}{\mathcal{N}}\sqrt{2}\text{Im}\,(\rho^{\text{prod}}_{0,+1} - \rho^{\text{prod}}_{-1,0}), \tag{1.105e}$$

$$A_\theta = \frac{b}{\mathcal{N}}(\rho^{\text{prod}}_{+1,+1} - \rho^{\text{prod}}_{-1,-1}), \tag{1.105f}$$

$$A_\phi = \frac{b}{\mathcal{N}}\sqrt{2}\text{Re}\,(\rho^{\text{prod}}_{0,+1} + \rho^{\text{prod}}_{-1,0}), \tag{1.105g}$$

$$A^\perp_\phi = \frac{b}{\mathcal{N}}\sqrt{2}\text{Im}\,(\rho^{\text{prod}}_{0,+1} + \rho^{\text{prod}}_{-1,0}), \tag{1.105h}$$

where we defined

$$a = |A_{+\frac{1}{2}-\frac{1}{2}}|^2 + |A_{-\frac{1}{2}+\frac{1}{2}}|^2 - 2\left(|A_{+\frac{1}{2}+\frac{1}{2}}|^2 + |A_{-\frac{1}{2}-\frac{1}{2}}|^2\right), \tag{1.106a}$$

$$b = |A_{+\frac{1}{2}-\frac{1}{2}}|^2 - |A_{-\frac{1}{2}+\frac{1}{2}}|^2, \tag{1.106b}$$

$$\begin{aligned}\mathcal{N} = &\left(|A_{+\frac{1}{2}-\frac{1}{2}}|^2 + |A_{-\frac{1}{2}+\frac{1}{2}}|^2\right)(\rho^{\text{prod}}_{-1,-1} + \rho^{\text{prod}}_{+1,+1} + 2\rho^{\text{prod}}_{0,0}) \\ &+ 2\left(|A_{+\frac{1}{2}+\frac{1}{2}}|^2 + |A_{-\frac{1}{2}-\frac{1}{2}}|^2\right)(\rho^{\text{prod}}_{-1,-1} + \rho^{\text{prod}}_{+1,+1}).\end{aligned} \tag{1.106c}$$

In the case of parity conserving decay processes, $|A_{+\frac{1}{2}-\frac{1}{2}}|^2 = |A_{-\frac{1}{2}+\frac{1}{2}}|^2$, hence $b = 0$, and the coefficients A_θ, A_ϕ and $A_\phi^\perp$ vanish.

1.8 Frame transformations

The angular distribution is not a Lorentz invariant. We recall that the angular distribution in Eq. (1.104) is expressed in the spin-1 particle rest frame. In order to define a set of polar coordinates in the spin-1 particle rest frame, one needs to choose a quantization axis. The polar and azimuthal angle are then measured with respect to that quantization axis. More precisely, we define a plane in the spin-1 particle rest frame containing the momenta of the colliding beams and the momentum of the spin-1 particle. We will call this plane the *production plane*. In this plane we define an axis with respect to which the polar angle θ_X is measured. The azimuthal angle ϕ_X is measured with respect to the production plane, where X refers to the final particle, as in the previous Section. Clearly, the number of quantization axes one can choose is infinite and the anisotropy coefficients Eqs. (1.105) will assume different values according to different choices of quantization axes. In the literature there are three commonly used definitions for the quantization axes defining three different frames: the helicity frame, the Collins-Soper frame and the

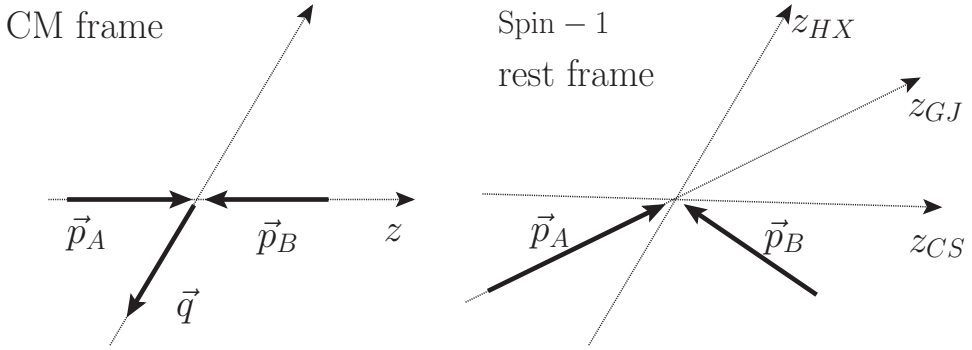

Figure 1.1.: Left panel: center of momentum frame of the initial particles. The vectors $\vec{p}_A$, $\vec{p}_B$ and $\vec{q}$ are the momenta of the two initial particles and the spin-1 particle, respectively. Right panel: spin-1 particle rest frame. Different choices for the quantization axis are shown.

Gottfried-Jackson frame. In the helicity frame, the quantization axis is chosen to be parallel to the spin-1 particle momentum frame. The Collins-Soper frame quantization axis is defined as the bisector of the angle between the two beams [54]. Finally, in the Gottfried-Jackson frame the quantization axis is the direction of the momentum of one of the two colliding beams [55]. The different choices for the quantization axes are depicted in Figure 1.1.

Consider the unit vector specifying the direction of the final particle in the spin-1 rest frame

$$\hat{r} = (\sin\theta_X \cos\phi_X, \sin\theta_X \sin\phi_X, \cos\theta_X), \tag{1.107}$$

where the polar and azimuthal angle are measured with respect to a given quantization axis. The quantization axes defining the different frames discussed in the previous paragraph all lie in the production plane which we denote by the plane xz. Therefore, in order to find the transformation between different frames, we can consider a rotation about the y axis by an angle δ [53, 56]

$$R_y(\delta) = \begin{pmatrix} \cos\delta & 0 & -\sin\delta \\ 0 & 1 & 0 \\ \sin\delta & 1 & \cos\delta \end{pmatrix}. \tag{1.108}$$

Let us denote by $\hat{r}'$ the unit vector expressed in the new frame

$$\hat{r}' = (\sin\theta'_X \cos\phi'_X, \sin\theta'_X \sin\phi'_X, \cos\theta'_X), \tag{1.109}$$

where the primed angles denote that they are measured with respect to the new quantization axis. In order to find the relation between the old and the new angles, we compute $R_y^{-1}(\delta)\hat{r}'$,

$$\sin\theta_X \cos\phi_X = \cos\delta \sin\theta'_X \cos\phi'_X + \sin\delta \cos\theta'_X, \tag{1.110a}$$
$$\sin\theta_X \sin\phi_X = \sin\theta'_X \sin\phi'_X, \tag{1.110b}$$

$$\cos\theta_X = \cos\delta\cos\theta'_X - \sin\delta\sin\theta'_X\cos\phi'_X. \tag{1.110c}$$

By substituting Eqs. (1.110) into the general expression for the angular distribution Eq. (1.104), one obtains

$$\begin{aligned}\frac{d\sigma}{d\Omega'_X} \propto \mathcal{N}(1 &+ \lambda'_\theta\cos^2\theta'_X + \lambda'_\phi\sin^2\theta'_X\cos 2\phi'_X + \lambda'_{\theta\phi}\sin 2\theta'_X\cos\phi'_X \\ &+ \lambda^{\perp\prime}_\phi\sin^2\theta'_X\sin 2\phi'_X + \lambda^{\perp\prime}_{\theta\phi}\sin 2\theta'_X\sin\phi'_X \\ &+ 2A'_\theta\cos\theta'_X + 2A'_\phi\sin\theta'_X\cos\phi'_X + 2A'^{\perp}_\phi\sin\theta'_X\sin\phi'_X),\end{aligned} \tag{1.111}$$

where the primed anisotropy coefficients are given by [53, 56]

$$\lambda'_\theta = \frac{\lambda_\theta - 3\Lambda}{1+\Lambda}, \tag{1.112a}$$

$$\lambda'_\phi = \frac{\lambda_\phi + \Lambda}{1+\Lambda}, \tag{1.112b}$$

$$\lambda'_{\theta\varphi} = \frac{\lambda_{\theta\phi}\cos 2\delta - \frac{1}{2}(\lambda_\theta - \lambda_\phi)\sin 2\delta}{1+\Lambda}, \tag{1.112c}$$

$$\lambda^{\perp\prime}_\phi = \frac{\lambda^\perp_\phi\cos\delta - \lambda^\perp_{\theta\phi}\sin\delta}{1+\Lambda}, \tag{1.112d}$$

$$\lambda^{\perp\prime}_{\theta\phi} = \frac{\lambda^\perp_\phi\sin\delta + \lambda^\perp_{\theta\phi}\cos\delta}{1+\Lambda}, \tag{1.112e}$$

$$A'_\theta = \frac{A_\theta\cos\delta + A_\phi\sin\delta}{1+\Lambda}, \tag{1.112f}$$

$$A'_\phi = \frac{-A_\theta\sin\delta + A_\phi\cos\delta}{1+\Lambda}, \tag{1.112g}$$

$$A^{\perp\prime}_\phi = \frac{A^\perp_\phi}{1+\Lambda}, \tag{1.112h}$$

with

$$\Lambda = \frac{1}{2}(\lambda_\theta - \lambda_\phi)\sin^2\delta - \frac{1}{2}\lambda_{\theta\phi}\sin 2\delta. \tag{1.113}$$

In order to understand the relevance of the choice of quantization axis, let us consider the case of a fully transverse polarized spin-1 particle, i.e. $\lambda_\theta = 1$ and $\lambda_\phi = \lambda_{\theta\phi} = 0$. If we now look at the anisotropy coefficients in a frame where the new quantization axis is perpendicular to the old one ($\delta = \pi/2$), according to Eqs. (1.112), we get $\lambda'_\theta = -1/3$, $\lambda'_\phi = 1/3$ and $\lambda'_{\theta\phi} = 0$. Therefore, in the new frame, the spin-1 particle is partially longitudinally polarized and it has also a considerable azimuthal anisotropy. Consider now the case in which we start with a fully longitudinally polarized particle ($\lambda_\theta = -1$ and $\lambda_\phi = \lambda_{\theta\phi} = 0$). In the new frame rotated again by a $\pi/2$ angle, we find $\lambda'_\theta = +1$, $\lambda'_\phi = -1$ and $\lambda'_{\theta\phi} = 0$, meaning that the particle is fully transverse polarized and it has also a strong azimuthal anisotropy. These examples show that, in order to fully determine the polarization state of a spin-1 particle, it is not sufficient to study only the polar anisotropy λ_θ, but it is crucial to study all azimuthal anisotropies, as well.

1.8.1 Transformation between the helicity and the Collins-Soper frame

The example analyzed in the end of the last Section concerning two frames related by a rotation of $\delta = \pi/2$ is the case of the helicity and Collins-Soper frame when the transverse momentum of the spin-1 particle is much greater than its longitudinal momentum ($q_T \gg q_L$), where transverse and longitudinal refers to the beam axis. In the following we will give the explicit expression for the transformation angle δ between the helicity and Collins-Soper frame. We consider the case in which we can ignore the masses of the particles in the initial state [56]. Let us denote by p_A^μ and p_B^μ the 4-momenta of the two initial particles which, in the center of momentum frame, are given by

$$p_A^\mu = \begin{pmatrix} |\mathbf{p}| \\ 0 \\ 0 \\ |\mathbf{p}| \end{pmatrix}, \qquad p_B^\mu = \begin{pmatrix} |\mathbf{p}| \\ 0 \\ 0 \\ -|\mathbf{p}| \end{pmatrix}, \tag{1.114}$$

where $|\mathbf{p}|$ is the magnitude of the 3-momentum of the initial particles. We choose to orient our reference frame with the z axis along the beam direction. Let us assume that the spin-1 particle is emitted with a certain angle θ with respect to the beam axis so that its 4-momentum reads

$$q^\mu = \begin{pmatrix} q^0 \\ |\mathbf{q}|\sin\theta \\ 0 \\ |\mathbf{q}|\cos\theta) \end{pmatrix}. \tag{1.115}$$

If we want to go to the helicity frame, we can perform two Lorentz transformations: one rotation to align the z axis with the momentum of the spin-1 particle and one boost along the momentum, i.e.

$$R_\nu^\mu = \begin{pmatrix} 1 & 0 & 0 & 0 \\ 0 & \cos\theta & 0 & -\sin\theta \\ 0 & 0 & 1 & 0 \\ 0 & \sin\theta & 0 & \cos\theta \end{pmatrix}, \qquad B_\nu^\mu = \begin{pmatrix} \gamma & 0 & 0 & -\gamma v \\ 0 & 1 & 0 & 0 \\ 0 & 0 & 1 & 0 \\ -\gamma v & 0 & 0 & \gamma \end{pmatrix}, \tag{1.116}$$

where $v = |\mathbf{q}|/q^0$ is the velocity of the particle and $\gamma = 1/\sqrt{1-v^2}$ the Lorentz factor. If we apply the previous transformation to q^μ we clearly get

$$q'^\mu = B_\nu^\mu R_\alpha^\nu q^\alpha = \begin{pmatrix} M \\ 0 \\ 0 \\ 0 \end{pmatrix}, \tag{1.117}$$

where M is the mass of the spin-1 particle. The two initial particles are transformed as

$$p_A'^\mu = B_\nu^\mu R_\alpha^\nu p_A^\alpha = \begin{pmatrix} |\mathbf{p}|\gamma(1 - v\cos\theta) \\ -|\mathbf{p}|\sin\theta \\ 0 \\ |\mathbf{p}|\gamma(-v + \cos\theta)) \end{pmatrix}, \qquad p_B'^\mu = B_\nu^\mu R_\alpha^\nu p_B^\alpha = \begin{pmatrix} |\mathbf{p}|\gamma(1 + v\cos\theta) \\ |\mathbf{p}|\sin\theta \\ 0 \\ -|\mathbf{p}|\gamma(v + \cos\theta) \end{pmatrix}. \tag{1.118}$$

The Collins-Soper frame is defined as the frame where the quantization axis is taken as the bisector of one beam and the opposite of the other beam in the spin-1 rest frame, therefore it is defined by the unit vector

$$\hat{z}_{CS} = \frac{|\mathbf{p}'_B|\mathbf{p}'_A - |\mathbf{p}'_A|\mathbf{p}'_B}{||\mathbf{p}'_B|\mathbf{p}'_A - |\mathbf{p}'_A|\mathbf{p}'_B|}. \tag{1.119}$$

where $\mathbf{p}'_A$ and $\mathbf{p}'_B$ are the 3-momenta of the two initial beams in the helicity frame. By construction $\hat{z}_{CS}$ is given by

$$\hat{z}_{CS} = \begin{pmatrix} \sin\delta_{HX\to CS} \\ 0 \\ \cos\delta_{HX\to CS} \end{pmatrix}, \tag{1.120}$$

where $\delta_{HX\to CS}$ is the angle to use in the counterclockwise rotation in Eq. (1.108) to go from the helicity to the Collins-Soper frame. By substituting the spatial components of Eq. (1.118) into Eq. (1.119), one finds

$$\cos\delta_{HX\to CS} = \frac{1}{\gamma}\frac{\cos\theta}{\sqrt{\frac{1}{\gamma^2}\cos^2\theta + \sin^2\theta}} = \frac{Mq_L}{M_T|\mathbf{q}|} \tag{1.121a}$$

$$\sin\delta_{HX\to CS} = \frac{\sin\theta}{\sqrt{\frac{1}{\gamma^2}\cos^2\theta + \sin^2\theta}} = \frac{q^0 q_T}{M_T|\mathbf{q}|}. \tag{1.121b}$$

where we defined the longitudinal and transverse momentum of the spin-1 particle to the beam axis in the lab frame as $q_L = |\mathbf{q}|\cos\theta$ and $q_T = |\mathbf{q}|\sin\theta$, and $M_T = \sqrt{M^2 + q_T^2}$ being the transverse mass. From Eqs. (1.121) we note that if $q_T \gg q_L$, the helicity and Collins-Soper frame are separated by an angle of $\pi/2$, while in the opposite case in which $q_T \ll q_L$, the two frames coincide. The derivation of the rotation angle in the case in which we can not ignore the masses of the initial particles is more complicated from the computational point of view, but no more instructive and the considerations above still hold. As discussed in the previous Section, there are also other frames which are commonly used for expressing the angular distribution and the rotation angles between different frames in terms of kinematic variables can be found in [57].

1.8.2 Frame-invariant quantities

Although the anisotropy coefficients in Eqs. (1.105) are frame dependent, it is possible to define a combination of the coefficients that is frame invariant [56, 58], i.e.

$$\tilde{\lambda} \equiv \frac{\lambda_\theta + 3\lambda_\phi}{1 - \lambda_\phi}. \tag{1.122}$$

One can show that $\tilde{\lambda}$ is invariant by using the frame transformations for the anisotropy coefficients Eqs. (1.112). We can study $\tilde{\lambda}$ for a simple case. Consider the Drell-Yan process [59] in hadronic collisions, where quark and antiqaurk in the hadrons annihilate into a virtual photon that decays into a lepton pair. The "naive" Drell-Yan process where the

transverse momenta of the quarks are ignored is such that $\lambda_\theta = 1$ and the other coefficients are all vanishing in the Collin-Soper frame. This implies that the frame-invariant quantity is $\tilde{\lambda} = 1$. Hence, Eq. (1.122) reduces to that so-called Lam-Tung relation [60]

$$\lambda_\theta + 4\lambda_\phi = 1. \tag{1.123}$$

This relation is a result due to the spin-1/2 nature of the quarks and it is shown to be insensitive to perturbative QCD corrections [61]. Since the Lam-Tung relation is a solid prediction of perturbative QCD, its violation may manifest non-perturbative effects and the fact that, in the dilepton rest frame, the plane containing the momenta of the initial hadrons and the plane containing the annihilating quarks do not coincide [62]. Experimental violations of the Lam-Tung relation were found by many experiments [63–69] and the theoretical interpretation of results is an active research field.

Chapter 2

Virtual photon polarization and dilepton anisotropy in pion-nucleon collisions

The aim of this Chapter is to explore the reaction $\pi N \to R \to N e^+ e^-$, where R is the intermediate baryon resonance (see Figure 2.1), in terms of effective Lagrangian models at the center-of-momentum (CM) energy of the HADES experiment, i.e. $\sqrt{s} = 1.49$ GeV. In particular we study the angular distribution of the produced dileptons using the spin density matrix formalism presented in the previous Chapter.

The general expression for the angular distribution of dileptons originating from the decay of a virtual photon was discussed in Chapter 1 and it is given by Eq. (1.72):

$$\frac{d\sigma}{d\Omega_e} \propto \mathcal{N}(1 + \lambda_\theta \cos^2\theta_e + \lambda_e \sin^2\theta_e \cos 2\phi_e + \lambda_{\theta\phi} \sin 2\theta_e \cos\phi_e + \lambda_\phi^\perp \sin^2\theta_e \sin 2\phi_e + \lambda_{\theta\phi}^\perp \sin 2\theta_e \sin\phi_e). \tag{2.1}$$

where θ_e and ϕ_e are the polar and azimuthal angles of one of the two leptons in the rest frame of the photon. As already mentioned in Chapter 1, the anisotropy coefficients depend on the choice of the quantization axis. In this Chapter, we use the helicity frame. As we discuss in Section 2.1, in the reaction $\pi N \to R \to N e^+ e^-$, the anisotropy coefficients depend on the quantum numbers of the intermediate baryon resonance and on the scattering angle θ_{γ^*} of the virtual photon.

In pion-nucleon scattering, it is expected that a major part of the dilepton production cross section is due to s-channel baryon resonances with a mass close to the CM energy $\sqrt{s}$. The emergence of a dilepton anisotropy in these processes can be understood as follows. The initial state, which in the CM frame contains a pion with momentum $\mathbf{p}$ and a nucleon with momentum $-\mathbf{p}$, can be expanded in terms of eigenstates of orbital angular momentum

$$|\pi(\mathbf{p}); N(-\mathbf{p})\rangle \propto \sum_{lm} Y_{lm}^*(\theta, \phi)\, |lm\rangle\,, \tag{2.2}$$

where θ and ϕ specify the direction of $\mathbf{p}$ with respect to the quantization axis. Here spin quantum numbers as well as the normalization are omitted for simplicity. We choose the quantization axis z parallel to the momentum of the incident pion, implying that $\theta = 0$. Since $Y_{lm}(\theta = 0, \phi) \neq 0$ only for $m = 0$, the z-component of the orbital angular momentum vanishes in the initial state. Hence, the projection of the total spin of the intermediate baryon resonance on the beam axis is given by the z-component of the nucleon spin. This means that only the $J_z = +1/2$ and $-1/2$ states of the resonance are populated.

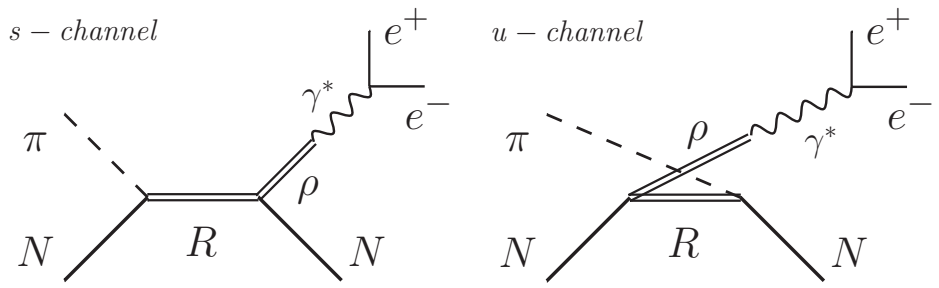

Figure 2.1.: Feynman diagrams for pion-nucleon scattering with an intermediate baryon resonance R. In this we Chapter we both consider the s-channel and the u-channel process.

As a result, in case of an unpolarized nucleon target, spin-1/2 intermediate resonances are unpolarized, and consequently there is no preferred direction in the CM frame. Accordingly, in this case all observables are independent of the scattering angle, i.e., the angle θ_{γ^*} of the virtual photon in the CM frame. On the other hand, intermediate resonances of spin$\geq 3/2$ have a nontrivial polarization, implying an angular anisotropy in the CM frame. Consequently, in this case, observables show a nontrivial dependence on the scattering angle θ_{γ^*}, which reflects the quantum numbers of the resonance.

This Chapter is based on [70] and it is structured in the following way. In Section 2.1 we give the expressions of the differential cross section and the anisotropy coefficient. In Section 2.2 we briefly review the effective Lagrangian of our model. This is followed by a presentation of the numerical results for the anisotropy coefficient for an isolated resonance in Section 2.3, where we also briefly explore the effect of nearby resonances.

2.1 Cross section and anisotropy coefficient

The differential cross section of the process $\pi N \to N e^+ e^-$ can be written in the form

$$\frac{d\sigma}{dM\, d\cos\theta_{\gamma^*} d\Omega_e} = \frac{M}{64(2\pi)^4 s} \frac{|\mathbf{p}_f|}{|\mathbf{p}_i|} \frac{1}{n_{\text{pol}}} \sum_{\text{pol}} |\mathcal{M}|^2 , \tag{2.3}$$

where $\mathcal{M}$ is the matrix element. The process considered has three particles in the final state, hence in general the CM frame does not coincide with the rest frame of the lepton pair. The scattering angle θ_{γ^*} is the polar angle of the momentum of the virtual photon in the CM frame measured from the beam axis (see Figure 2.2), and $d\Omega_e$ is the solid angle of the electron in the rest frame of the lepton pair [71]. Moreover, M is the invariant mass of the lepton pair, s is the square of the CM energy, $\mathbf{p}_i$ and $\mathbf{p}_f$ are the CM three-momenta of the initial and final nucleons, respectively. The sum is over all spin states of the initial and final state particles and n_{pol} is the spin degeneracy in the initial state.

The square of the matrix element can be written in the form of Eq. (1.62)

$$\sum_{\text{pol}} |\mathcal{M}|^2 = \frac{e^2}{q^4} W_{\mu\nu} L^{\mu\nu}, \tag{2.4}$$

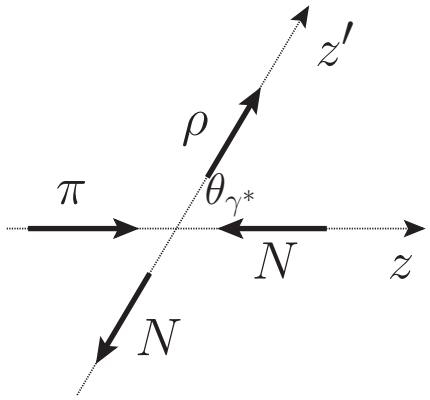

Figure 2.2.: Pion-nucleon scattering in the CM frame. The beam axis is denoted by z.

where $L^{\mu\nu}$ is the lepton tensor Eq. (1.66). The quantity

$$W_{\mu\nu} = \sum_{\text{pol}} W_\mu W_\nu^* \tag{2.5}$$

is the hadronic tensor, where W_μ is the hadronic part of the matrix element $\mathcal{M} = W_\mu L^\mu$ (L^μ is defined in Eq. (1.65)). The tensor $W^{\mu\nu}$ contains all the information about the hadronic interaction that originates the photon. We note that the factorization in Eq. (2.4) between the hadronic and leptonic part is due to the fact that we are considering the leading order contribution of the electromagnetic interaction. In order to calculate the angular distribution of the lepton pair, we use the spin density matrix formalism discussed in Section 1.5. The nontrivial angular distribution of the dilepton is connected with the polarization state of the decaying virtual photon through the anisotropy coefficients. In this Chapter we will focus on the coefficient λ_θ Eq. (1.73a). In general it is a function of the photon invariant mass M and the scattering angle θ_γ.

2.2 The model

In order to calculate the hadronic tensor $W^{\mu\nu}$, we need models to describe strong and electromagnetic interactions of the hadrons in our process. In this Section we outline the different models used.

2.2.1 Vector Meson Dominance

One important aspect of hadron physics is the study of electromagnetic interaction of hadrons. Vector Meson Dominance (VMD) is the most commonly used model to describe the interaction between hadrons and photons. The idea of VMD is that the photon couples to hadrons through the exchange of vector mesons. Here we will discuss the two main versions of VMD, one proposed by Sakurai [72, 73] based on the field-current identity and the second proposed by Kroll, Lee and Zumino [74] which preserves gauge invariance. In [75] one can find an exhaustive discussion about VMD.

Sakurai was the first who proposed a theory of strong interactions mediated by vector mesons [72] based on the Yang-Mills theory [76]. Consider a theory describing ρ mesons and pions. The Lagrangian is given by

$$\mathcal{L} = -\frac{1}{4}\vec{\rho}_{\mu\nu}\cdot\vec{\rho}^{\,\mu\nu} + \frac{1}{2}m_\rho^2\vec{\rho}_\mu\cdot\vec{\rho}^{\mu} + \frac{1}{2}D_\mu\vec{\pi}\cdot D^\mu\vec{\pi} - \frac{1}{2}m_\pi^2\vec{\pi}\cdot\vec{\pi}, \tag{2.6}$$

where $\vec{\rho}_\mu$ and $\vec{\pi}$ are the isovector field of the ρ meson and pion, respectively, and m_ρ and m_π their mass. Neglecting ρ self interactions, the field tensor $\vec{\rho}_{\mu\nu}$ is given by

$$\vec{\rho}_{\mu\nu} = \partial_\mu\vec{\rho}_\nu - \partial_\nu\vec{\rho}_\mu. \tag{2.7}$$

The interaction are generated by the covariant derivative D_μ through

$$D_\mu\vec{\pi} = \partial_\mu\vec{\pi} - g_{\rho\pi\pi}\vec{\rho}\times\vec{\pi}. \tag{2.8}$$

For the neutral ρ meson, ρ^0, the interaction with pions reads

$$\mathcal{L}_{\rho\pi} = -g_{\rho\pi\pi}\rho_\mu J_\pi^\mu, \tag{2.9}$$

where the current is given by

$$J_{\pi\mu} = i(\pi^-\partial_\mu\pi^+ - \pi^+\partial_\mu\pi^-), \tag{2.10}$$

π^+ and π^- being the charge pion fields.

At this point we would like to include the interaction between the photon and the ρ. The basic assumption of the VMD version proposed by Sakurai [72, 73] is that the hadronic electromagnetic current operator is proportional to the vector meson field, i.e.

$$J_{EM\,\mu} = \frac{m_\rho^2}{g_\rho}\rho_\mu^0, \tag{2.11}$$

where g_ρ is a coupling constant to be discussed below. Equation (2.11) is called the field-current identity, meaning that we identify the electromagnetic current with the ρ^0 field times a constant factor. The electromagnetic interaction Lagrangian is thus given by

$$\mathcal{L}_{\rho\gamma}^1 = -\frac{em_\rho^2}{g_\rho}\rho_\mu^0 A^\mu, \tag{2.12}$$

where A^μ is the photon field. We refer to Eq. (2.12) as the first version of VMD. Note that the interaction Lagrangian Eq. (2.12) is not gauge invariant and, therefore, we can not simply add it to Eq. (2.6) along with the photon kinetic term. In order to preserve gauge invariance, we can instead consider the following interaction Lagrangian following Kroll, Lee and Zumino [74]

$$\mathcal{L}_{\rho\gamma}^2 = -\frac{e}{2g_\rho}F^{\mu\nu}\rho_{\mu\nu}^0, \tag{2.13}$$

where $F^{\mu\nu} = \partial_\mu A_\nu - \partial_\nu A_\mu$ is the electromagnetic field strength tensor. Note that the interaction between neutral ρ and photon in Eq. (2.13) is gauge invariant by construction,

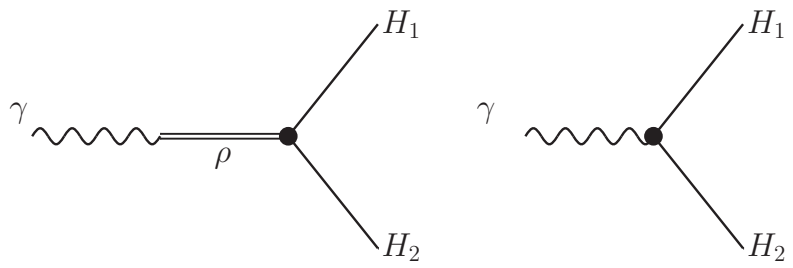

Figure 2.3.: Feynman diagrams for the vector meson dominance (H_1 and H_2 are two generic hadrons). The Lagrangian (2.14) allwos only for processes corresponding to the Feynman diagram in the left panel, while the Lagrangian (2.15) allows for processes corresponding to both Feynman diagrams.

since $F^{\mu\nu}$ is gauge invariant. We refer to Eq. (2.13) as the second version of VMD. It is important to realize that Eq. (2.13) can be written in momentum space as $2q^2\rho_\mu A^\mu$, where we used the fact that the ρ meson is divergenceless. This means that for momentum $q^2 = 0$, the photon will decouple from the ρ meson and hence from hadronic matter. Therefore, in the second version of VMD, we need another term in the Lagrangian that directly couples photons to hadronic matter of the form $-eJ_\mu A^\mu$ in which J_μ is the hadronic current that, for instance, is given by Eq. (2.10) for the interaction between the photon and pions. To summarize, one has the following interactions for the first and second version of the VMD, respectively:

$$\mathcal{L}_1 = -\frac{em_\rho^2}{g_\rho}\rho_\mu A^\mu - g_{\rho\pi\pi}\rho_\mu J^\mu, \tag{2.14}$$

$$\mathcal{L}_2 = -\frac{e}{2g_\rho}F_{\mu\nu}\rho^{\mu\nu} - eJ_\mu A^\mu - g_{\rho\pi\pi}\rho_\mu J^\mu. \tag{2.15}$$

We can now use the Lagrangians (2.14)-(2.15) to calculate the pion form factor. Consider the transition $\gamma \to \pi^+\pi^-$. Using the current (2.10), the matrix element is given by

$$\mathcal{M}^\mu_{\gamma\to\pi^+\pi^-} = -e(p^+ - p^-)^\mu F_\pi(q^2), \tag{2.16}$$

where $F_\pi(q^2)$ is the pion form factor which is a quantity that measures the deviation from a pointlike behaviour of the coupling between photon and pions. From Eq. (2.14) and (2.15), one finds for the pion form factor

$$F_\pi(q^2) = -\frac{m_\rho^2}{q^2 - m_\rho^2}\frac{g_{\rho\pi\pi}}{g_\rho}, \tag{2.17}$$

$$F_\pi(q^2) = 1 - \frac{q^2}{q^2 - m_\rho^2}\frac{g_{\rho\pi\pi}}{g_\rho}, \tag{2.18}$$

respectively. For zero momentum transfer we should have $F_\pi(0) = 1$ because the photon sees the pion as pointlike. One can see that Eq. (2.18) automatically satisfies the condition $F_\pi(0) = 1$, while in Eq. (2.17) we must demand $g_{\rho\pi\pi} = g_\rho$. This leads to the argument

of universality of the couplings, namely that the couplings of the ρ with all particles is the same. The primary motivation for this is that the interactions are produced by the minimal substitution through the covariant derivative as in gauge theory. Note that without universality, only the second version of VMD would satisfy the condition $F_\pi(0) = 1$. In this Thesis, we will use the second version of VMD for describing the coupling between ρ and photon.

2.2.2 Spin-1/2 resonances

The interaction of spin-1/2 baryons with pions and ρ mesons is described by the Lagrangian densities of Ref. [71],

$$\mathcal{L}_{R_{1/2}N\pi} = -\frac{g_{RN\pi}}{m_\pi}\bar{\psi}_R\Gamma\gamma^\mu\vec{\tau}\psi_N\cdot\partial_\mu\vec{\pi} + \text{h.c.}, \tag{2.19}$$

$$\mathcal{L}_{R_{1/2}N\rho} = \frac{g_{RN\rho}}{2m_\rho}\bar{\psi}_R\vec{\tau}\sigma^{\mu\nu}\tilde{\Gamma}\psi_N\cdot\vec{\rho}_{\mu\nu} + \text{h.c.}. \tag{2.20}$$

Here, and also in the Lagrangians involving higher spin resonances given below, $\Gamma = \gamma_5$ for $J^P = 1/2^+$, $3/2^-$ and $5/2^+$ resonances and $\Gamma = 1$ otherwise, and $\tilde{\Gamma} = \gamma_5\Gamma$.

2.2.3 Higher spin resonances

The most important problem concerning the covariant treatment of higher-spin fields is the presence of unphysical lower-spin degrees of freedom. For fields describing particles with spin s greater than $1/2$, there will be not only the physical components relative to s, but also those corresponding to the lower spin sector $s-1, s-2, \ldots$ So, in practice, one implicitly considers also the effect due to the lower-spin background. The reason for this is the following. Higher spin fermions are represented by Rarita-Schwinger spinor fields [77] in effective Lagrangian models. These fields transform according to a product of a spin-1/2 and one or more spin-1 representations of the Lorentz group. Therefore they contain some contributions describing the propagation of lower-spin states. For example, in the case of spin-3/2 fields, the components defining the vector-spinor field ψ_μ are 16, while one would expect that only 4 are the components describing the physical degrees of freedom. As a consequence one implicitly considers also spin-1/2 background. In a consistent Lagrangian involving higher-spin baryons, the lower-spin components of the Rarita-Schwinger fields should not contribute to observable quantities.

Such a consistent interaction scheme for spin-3/2 fermions was developed by Pascalutsa [78–80] and generalized for spin-5/2 fermions by Vrancx et al. [81]. In this Thesis we specify the Lagrangian describing the interaction of higher-spin baryon resonances based on the scheme of Ref. [81]. In this scheme, the lower-spin degrees of freedom are eliminated from observables by requiring that the Lagrangian is invariant under the gauge transformation

$$\psi_\mu \to \psi_\mu + i\partial_\mu\chi, \tag{2.21}$$

$$\psi_{\mu\nu} \to \psi_{\mu\nu} + \frac{i}{2}(\partial_\mu\chi_\nu + \partial_\nu\chi_\mu), \tag{2.22}$$

for spin-3/2 (ψ_μ) and spin-5/2 ($\psi_{\mu\nu}$) Rarita-Schwinger fields, respectively. In the above equations, χ and χ_μ are arbitrary spinor and spinor-vector fields, respectively. The gauge

Table 2.1.: Parameters of the 9 baryon resonances included in the model.

Resonance	J^P	Mass	Width	BR (%)		Coupling constants	
		[GeV]	[GeV]	$N\pi$	$N\rho$	$g_{RN\pi}$	$g_{RN\rho}$
$N(1440)$	$1/2^+$	1.44	0.35	65	4	0.385	21.303
$N(1520)$	$3/2^-$	1.520	0.115	60	20	0.148	17.166
$N(1535)$	$1/2^-$	1.535	0.15	45	2	0.160	1.480
$N(1650)$	$1/2^-$	1.655	0.165	77	8	0.174	0.896
$N(1675)$	$5/2^-$	1.675	0.15	40	1	0.0007	18.989
$N(1680)$	$5/2^+$	1.68	0.13	67.5	9	0.003	21.694
$\Delta(1232)$	$3/2^+$	1.232	0.117	100	0	0.248	0
$\Delta(1600)$	$3/2^+$	1.6	0.35	17.5	12.5	0.045	44.4
$\Delta(1620)$	$1/2^-$	1.63	0.145	25	16	0.168	2.683

invariance of Eqs. (2.21) and (2.22) is ensured if only the gauge invariant combination of the fields

$$G_{\mu,\nu} = i(\partial_\mu \psi_\nu - \partial_\nu \psi_\mu), \tag{2.23}$$

$$G_{\mu\nu,\lambda\rho} = -\partial_\mu \partial_\nu \psi_{\lambda\rho} - \partial_\lambda \partial_\rho \psi_{\mu\nu} + \frac{1}{2}(\partial_\mu \partial_\lambda \psi_{\nu\rho} + \partial_\mu \partial_\rho \psi_{\nu\lambda} + \partial_\nu \partial_\lambda \psi_{\mu\rho} + \partial_\nu \partial_\rho \psi_{\mu\lambda}) \tag{2.24}$$

appear in the Lagrangian. Furthermore, by defining the fields

$$\begin{aligned} \Psi_\mu &= \gamma^\nu G_{\mu,\nu}, \\ \Psi_{\mu\nu} &= \gamma^\lambda \gamma^\rho G_{\mu\nu,\lambda\rho}, \end{aligned} \tag{2.25}$$

and making the replacements

$$\psi_\mu \to \frac{1}{m}\Psi_\mu, \quad \text{and} \quad \psi_{\mu\nu} \to \frac{1}{m^2}\Psi_{\mu\nu} \tag{2.26}$$

in a “traditional" Lagrangian containing Rarita-Schwinger fields one obtains a gauge invariant and hence consistent Lagrangian. The mass parameter m in Eq. (2.26) is introduced for dimensional reasons.

Starting from the Lagrangians of Ref. [81] and taking the isospin structure into account, we obtain the expressions

$$\mathcal{L}_{R_{3/2}N\pi} = \frac{i g_{RN\pi}}{m_\pi^2} \bar{\Psi}_R^\mu \Gamma \vec{\tau} \psi_N \cdot \partial_\mu \vec{\pi} + \text{h.c.}, \tag{2.27}$$

$$\mathcal{L}_{R_{5/2}N\pi} = -\frac{g_{RN\pi}}{m_\pi^4} \bar{\Psi}_R^{\mu\nu} \Gamma \vec{\tau} \psi_N \cdot \partial_\mu \partial_\nu \vec{\pi} + \text{h.c.}, \tag{2.28}$$

for the Lagrangians describing the resonance-nucleon-pion interaction. In the case of Δ resonances, the Pauli matrices $\vec{\tau}$ appearing in the above and the following Lagrangians have to be replaced by the isospin-$3/2 \to 1/2$ transition matrices.

The resonance-nucleon-ρ interaction Lagrangian is analogous to the electromagnetic resonance-nucleon transition Lagrangian. Out of the three Lagrangians given in Ref. [81]

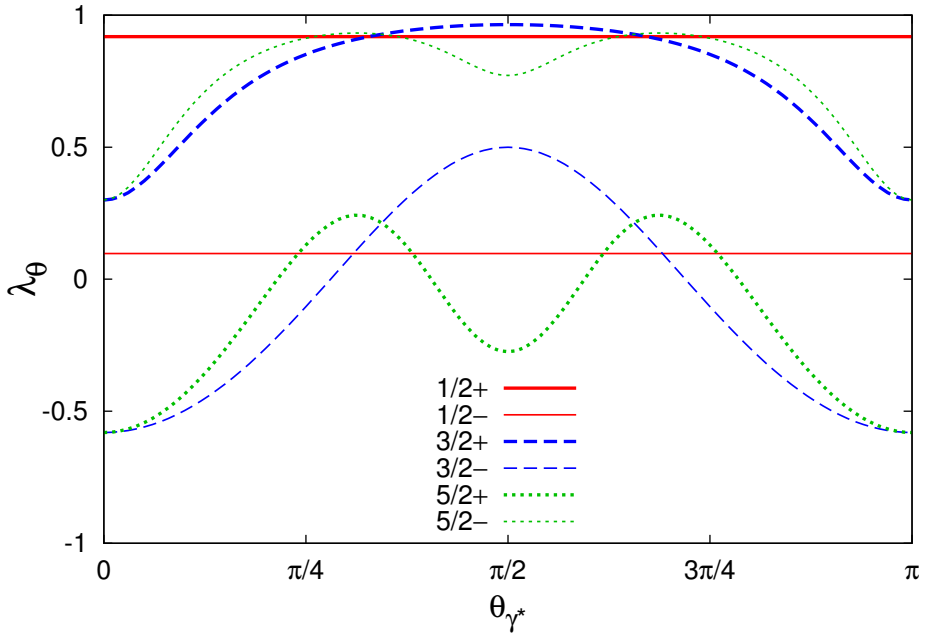

Figure 2.4.: The anisotropy coefficient λ_θ as a function of the virtual photon polar angle θ_{γ^*} for hypothetical resonance states with different spins and parities in the s-channel at a dilepton mass $M = 0.5$ GeV. The resonance masses coincide with $\sqrt{s} = 1.49$ GeV, the resonance widths are $\Gamma_R = 0.15$ GeV.

we choose the one with the lowest number of derivatives. After including the isospin structure of the interaction, the Lagrangians are given by

$$\mathcal{L}_{R_{3/2}N\rho} = \frac{ig_{RN\rho}}{4m_\rho^2}\bar{\Psi}_R^\mu \vec{\tau}\gamma^\nu\tilde{\Gamma}\psi_N\cdot\vec{\rho}_{\nu\mu} + \text{h.c.}, \tag{2.29}$$

$$\mathcal{L}_{R_{5/2}N\rho} = -\frac{g_{RN\rho}}{(2m_\rho)^4}\bar{\Psi}_R^{\mu\nu}\vec{\tau}\tilde{\Gamma}\gamma^\rho(\partial_\mu\psi_N)\cdot\vec{\rho}_{\rho\nu} + \text{h.c.}. \tag{2.30}$$

For the Feynman rules corresponding to the Lagrangians just discussed, see Appendix B.

We explore the relevance of the different spins and parities by computing the anisotropy coefficient with a hypothetical resonance for each spin-parity combination, all with the same mass and width, $m_R = 1.49$ GeV and $\Gamma_R = 0.15$ GeV. The mass was chosen to coincide with the CM energy $\sqrt{s}$ used in our calculations, thus assuming that in the s-channel the resonance is on the mass shell.

We also made calculations including all well established resonance states in the relevant energy domain. These states are the nucleon resonances $N(1440)\ 1/2^+$, $N(1520)\ 3/2^-$, $N(1535)\ 1/2^-$, $N(1650)\ 1/2^-$, $N(1675)\ 5/2^-$, $N(1680)\ 5/2^+$, and the Δ resonances $\Delta(1600)\ 3/2^+$, and $\Delta(1620)\ 1/2^-$. The coupling constants $g_{RN\pi}$ and $g_{RN\rho}$ were determined from the widths of the $R \to N\pi$ and $R \to N\rho \to N\pi\pi$ decays. The empirical values for these partial widths were obtained as a product of the total width and the appropriate branching ratio as given by the Particle Data Group [82]. Masses of the resonances are also taken from Ref. [82]. The parameters of the baryon resonances included in the model are given in Table 2.1.

We stress that the present model is intended to be valid for virtual photon masses not far from the ρ meson mass. The gauge invariant version of the vector meson dominance (2.13) does not contribute to processes with real photons and, therefore, the model has to be supplemented by a separate coupling of baryon resonances to the nucleon and photon, if we want to describe processes with low mass virtual or real photons. On the other hand, using the original (not gauge invariant) version of the vector meson dominance by Sakurai [72], the photonic branching ratios of $N(1710)$ and $\Delta(1905)$ are overpredicted [83]. The $\Delta(1232)$ resonance is not included, since there is no direct information available on the coupling strengths to the $N\rho$ channel and its mass is far below the CM energy considered.

We use a simplifying approximation for the momentum dependence of the resonance width $\Gamma(p^2)$, where p_R is resonance momentum. We assumed that it is given by that of the $N\pi$ channel, and employ the parametrization of Ref. [71], i.e.

$$\Gamma(p_R^2) = \Gamma(m_R^2)\frac{m_R}{\sqrt{p_R^2}}\left(\frac{p_\pi}{p_{\pi R}}\right)^{2l+1}\left(\frac{p_{\pi R}^2+\delta^2}{p_\pi^2+\delta^2}\right)^{l+1}, \tag{2.31}$$

where l is the angular momentum of the pion, p_π is the magnitude of the outgoing 3-momentum in the resonance rest frame and $p_{\pi R}$ is the same for an on-shell resonance ($p_R^2 = m_R^2$). The parameter δ is given by

$$\delta^2 = (m_R - m_N - m_\pi)^2 + \frac{\left[\Gamma(m_R^2)\right]^2}{4}, \tag{2.32}$$

where m_N is the nucleon mass.

2.3 Results

We employ the model described above to compute the anisotropy coefficient λ_θ of Eq. (1.79) for the reaction $\pi N \to N e^+ e^-$. In the following we discuss the dependence of the anisotropy coefficient on the polar angle of the virtual photon θ_{γ^*}. In all the calculations, the CM energy is set to $\sqrt{s} = 1.49$ GeV, corresponding to the HADES data.

In order to demonstrate the effect of different spin-parity baryon resonance states on the λ_θ coefficient, we first use the model with the hypothetical resonances discussed above, including only the s-channel Feynman diagram. In Fig. 2.4 we show the anisotropy coefficient for dileptons of invariant mass $M = 0.5$ GeV. In this case the resonance in the intermediate state is on-shell and, therefore, the results should correspond to standard angular momentum coupling. Figure 2.4 shows that the spin and parity of the intermediate resonance is reflected in a characteristic angular dependence of the anisotropy coefficient. In particular, in the spin-1/2 channels the λ_θ coefficient is independent of θ_{γ^*}, in accordance with the arguments given in the introduction. Based on the same arguments, the z-component of the total spin coincides with the z-component of the initial nucleon spin. Since the nucleon target is unpolarized, the $J_z = +1/2$ and $-1/2$ polarization states of each resonance are equally populated. This means that there is no preferred direction and, consequently, that the λ_θ coefficient is isotropic.

The dependence of the anisotropy coefficient on the quantum numbers of the intermediate baryon resonance can be interpreted in terms of angular momentum coupling,

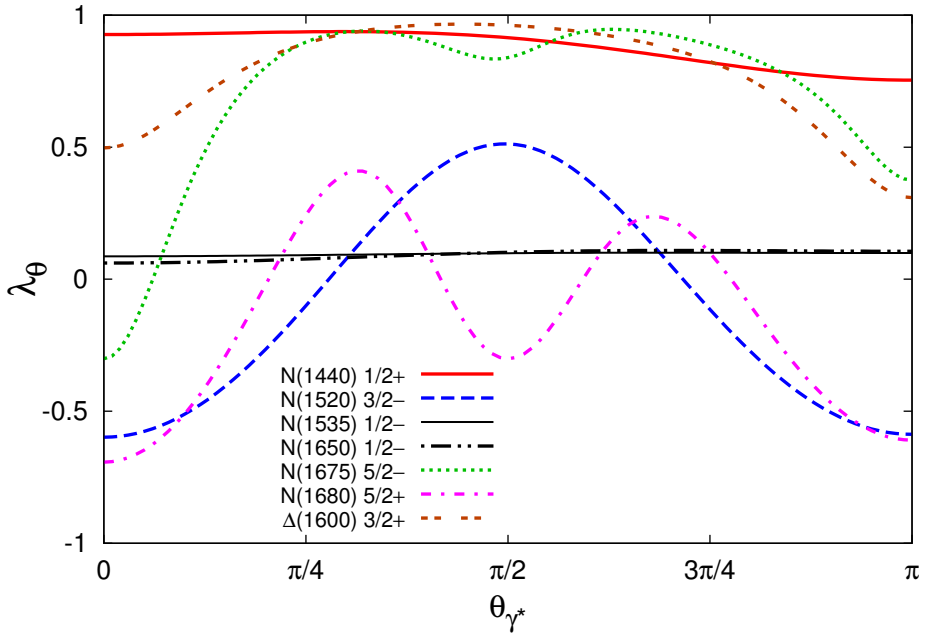

Figure 2.5.: The anisotropy coefficient λ_θ as a function of the virtual photon polar angle at a dilepton mass $M = 0.5$ GeV including s- and u-channel diagrams. The CM energy is $\sqrt{s} = 1.49$ GeV. For further details, see the text.

once one accounts for the fact that, in the non-relativistic limit, the off-diagonal coupling Eq. (2.20) is purely transverse. We note that for all channels considered, except $J^P = 1/2^+$, two values of the final state orbital angular momentum are possible. The strengths of these channels and their relative phase depend on the structure of the interaction vertices Eqs. (2.20), (2.29), and (2.30). Thus, a different choice for the interaction Lagrangians [81] may lead to a somewhat different angular dependence of the anisotropy coefficient. This indicates a certain model dependence of the results. However, as long as the lowest angular momentum states dominate, we expect the results presented here to remain valid, at least on a qualitative level.

In Fig. 2.5 we show the λ_θ coefficient obtained from the s- and u-channel diagrams of seven of the physical resonance states considered. (The contribution of the $\Delta(1620)$, which has a shape very similar to the other spin-$1/2^-$ states, is left out for the sake of clarity). Here, the characteristic shapes presented in Fig. 2.4 are modified mainly by the interference with the u-channel resonance contributions.

In order to assess which of the resonances are important for the dilepton production process at the CM energy of the HADES experiment, we compute the differential cross section $d\sigma/dM$ by first integrating Eq. (2.3) over the electron solid angle Ω_e. Figure 2.6 shows the dependence of the differential cross section on the scattering angle of the virtual photon at $\sqrt{s} = 1.49$ GeV and a dilepton invariant mass of $M = 0.5$ GeV. For the coupling constants we used our fitted values given in Table 2.1. Figure 2.6 shows that the two dominant contributions are given by the $N(1520)$ and the $N(1440)$. Moreover, we integrated the cross section over the scattering angle θ_{γ^*}. We find that at $\sqrt{s} = 1.49$ GeV and $M = 0.5$ GeV, the $N(1520)$ has a cross section $d\sigma/dM = 0.44$ μb/GeV, and the $N(1440)$

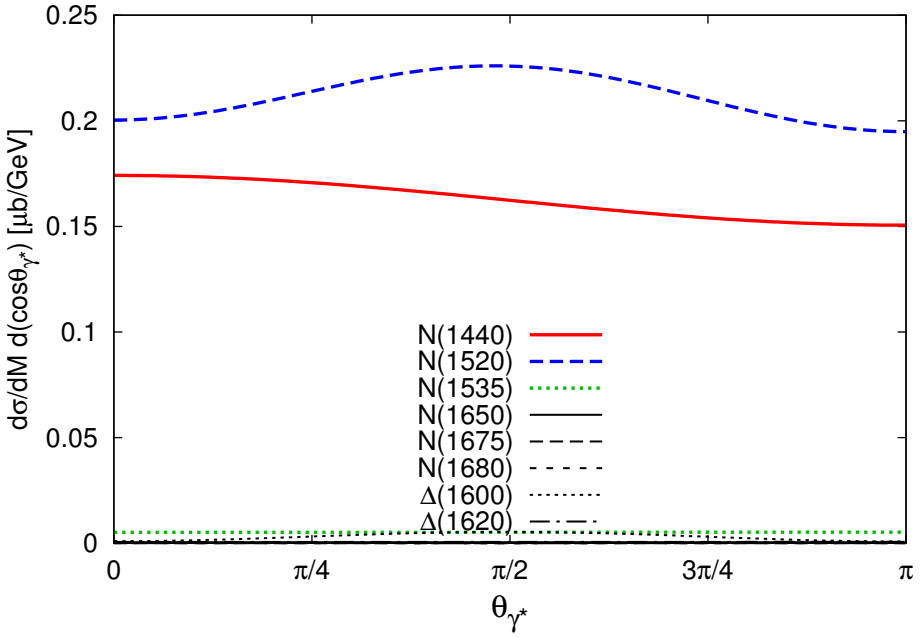

Figure 2.6.: The differential cross section as a function of the virtual photon polar angle for the baryon resonances included in the model at $\sqrt{s} = 1.49$ GeV CM energy and dilepton invariant mass $M = 0.5$ GeV.

has a cross section $d\sigma/dM = 0.33$ μb/GeV. These results contain both s- and u-channel diagrams. The combined cross section taking into account both $N(1520)$ and $N(1440)$ and their interference is $d\sigma/dM = 0.84$ μb/GeV when all coupling constants are assumed to have the same phase and $d\sigma/dM = 0.70$ μb/GeV if we assume that the matrix elements involving the two resonances have the opposite phase. The range of baryon resonance widths and branching ratios given by the Particle Data Group [82] induce uncertainties in the differential cross sections. In particular, the $N(1520)$ contribution may vary by about 40%. For the $N\rho$ branching ratio of the $N(1440)$ resonance, only an upper limit is given. As a result, the combined total cross section including both the $N(1440)$ and $N(1520)$ can be up to a factor of 2 larger than the values given above. On the other extreme, the $N(1440)$ branching ratio into the ρN channel may vanish, implying that corresponding contribution to dilepton production is negligible. Nevertheless, the average values of the branching ratios used here yield reasonable agreement with experiment, as discussed below.

The largest sub-leading contributions to the cross section are due to the $N(1535)$ and $\Delta(1600)$ resonances, which yield 0.011 μb/GeV and 0.0078 μb/GeV, respectively. Although these are negligible compared to the dominant contributions, the interference of these resonances with the dominant ones could contribute at most about $\pm 20\%$ in the ideal case, where the interference is either constructive or destructive throughout the whole phase space. We computed these interference terms numerically, and found that they are negligible compared to the $N(1520)$ and $N(1440)$ contributions. This remains true also when the uncertainties of the sub-leading contributions are taken into account.

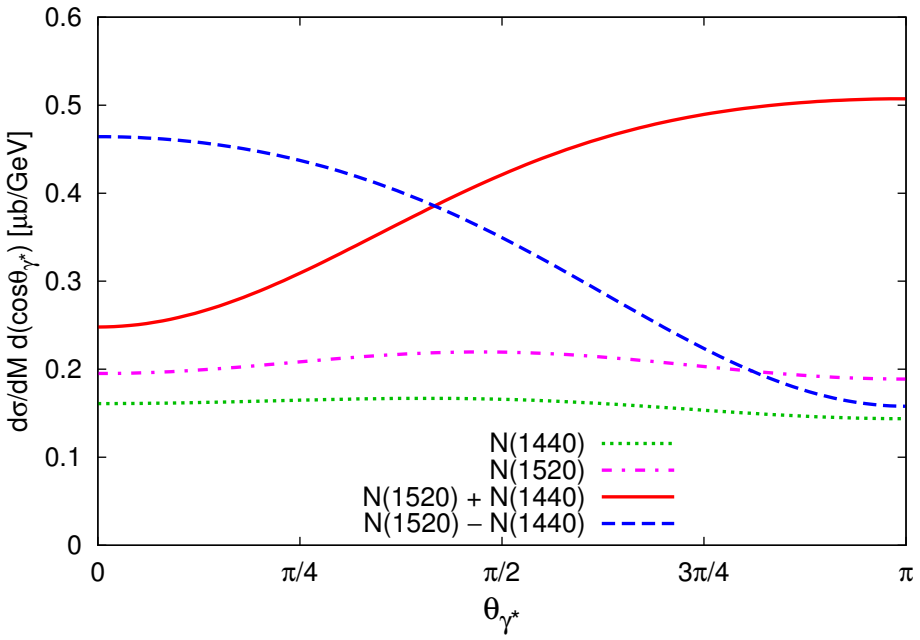

Figure 2.7.: The contribution of the two dominant resonances, $N(1440)$ and $N(1520)$, to the differential cross section of dilepton production at $\sqrt{s} = 1.49$ GeV CM energy. Two of the curves show the result obtained from s- and u-channel diagrams of each resonance. The other two curves are obtained from the sum of all four diagrams (s- and u-channel diagrams of both resonances), assuming a positive and negative relative sign between the amplitudes of the two resonances.

Our calculation of $d\sigma/dM$ is consistent with the results of [71] at $M = 0.5$ GeV within the uncertainties discussed above. Moreover, the cross section in [71] has been compared with preliminary HADES data and found to be in a reasonable agreement at $\sqrt{s} = 1.49$ GeV and $M = 0.5$ GeV [39]. An alternative check of the reliability of the model is obtained by studying the process $\pi N \to N\pi\pi$. We thus computed the neutral ρ contribution of the differential cross section at 0.5 GeV invariant mass of the pion pair, including the $N(1520)$ resonance in both the s- and u-channels. Taking the uncertainties discussed above into account, we obtain a value for $d\sigma/dM$ between 5 and 10 mb/GeV, which is consistent with the result of the partial wave analysis of the Bonn-Gatchina group, presented in [40].

The double-differential cross section, $d\sigma/dMd\cos\theta_{\gamma^*}$ obtained from the s- and u-channel diagrams with the $N(1520)$ and $N(1440)$ resonances is shown in Fig. 2.7 as a function of the polar angle of the virtual photon, θ_{γ^*}. Here two of the curves correspond to the contributions of the two resonances without interference. In the other two, the interference terms are included, assuming either a positive or negative relative sign between the two resonance amplitudes. In general, the interaction vertices of the resonances with pions and ρ mesons can be complex, as a result of their microscopic structure [84]. This can result in an energy dependent relative phase of two resonance amplitudes between 0

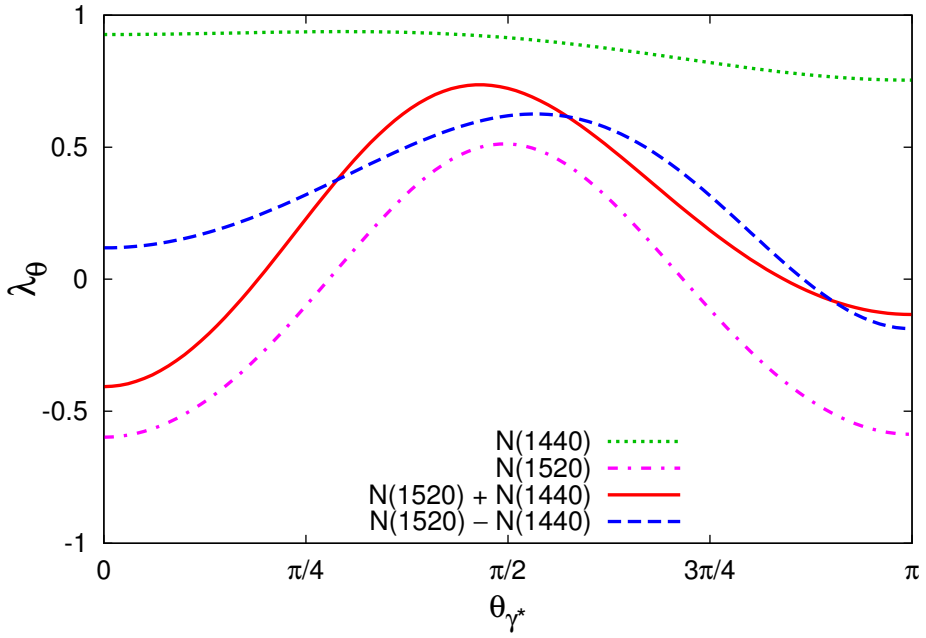

Figure 2.8.: The contribution of the two dominant resonances, $N(1440)$ and $N(1520)$, to the anisotropy coefficient, λ_θ at $\sqrt{s} = 1.49$ GeV CM energy. The various curves correspond to the same assumptions as in Fig. 2.7.

and π. Since this phase is unknown, we give the results for two limiting cases, assuming a positive or negative relative sign between the $N(1520)$ and $N(1440)$ amplitudes.

From Fig. 2.7 it is clear that the relative phase has a strong influence on the shape of the θ_{γ^*} dependence of the differential cross section. Moreover, as discussed above the magnitude of the $N(1440)$ contribution is uncertain, which in turn affects the shape of the differential cross section. This suggests that the unknown phase and the coupling strength of the $N(1440)$ to the $N\rho$ channel can be constrained by data on the angular distribution.

In Fig. 2.8 we show the dominant contributions to the anisotropy coefficient λ_θ as a function of θ_{γ^*}. As in Fig. 2.7, we show results for the two limiting assumptions for the relative phase of the two resonance amplitudes. In both cases, the shape of the curve approximately follows that of the $N(1520)$ contribution, which implies that it is only weakly affected by the uncertainties of the $N(1440)$ parameters. The anisotropy parameter λ_θ has a maximum around $\theta_{\gamma^*} = \pi/2$. Thus, virtual photons emitted perpendicular to the beam axis in the CM frame tend to be transversely polarized, while virtual photons emitted along the beam direction are almost unpolarized or, in the case of a positive relative phase between the two resonances, photons travelling in the forward direction tend to be longitudinally polarized.

For the sake of completeness, we also studied the effect on the anisotropy coefficient of the inclusion of the two largest sub-leading contributions, namely the $N(1535)$ and the $\Delta(1600)$. In Figs 2.10 and 2.11 the anisotropy coefficient resulting from the inclusion of the $N(1535)$ is shown. We computed the two limiting cases for the phase between the $N(1535)$, the $N(1520)$ and the $N(1440)$. In Fig 2.10 we added the $N(1535)$ amplitude

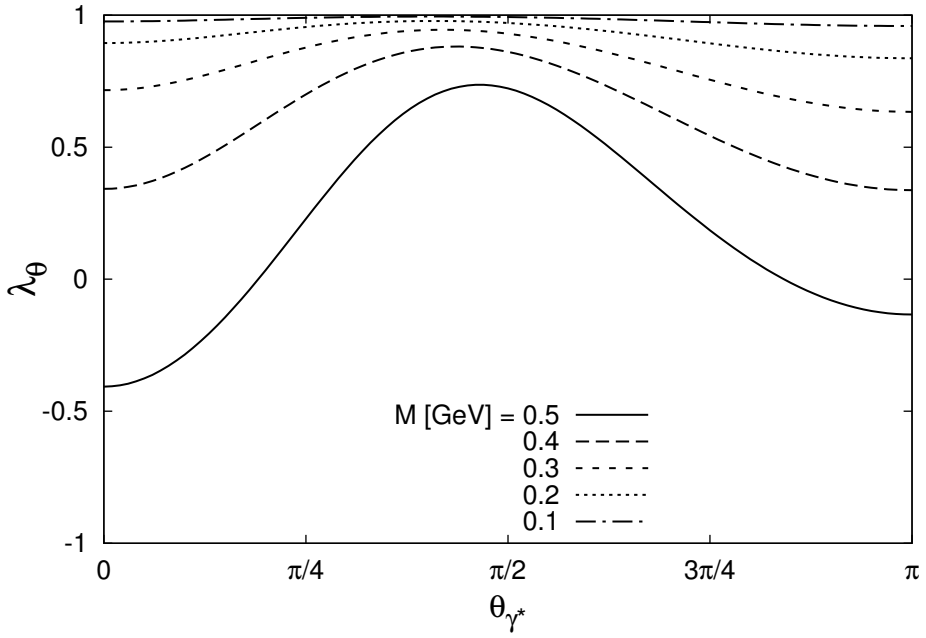

Figure 2.9.: The anisotropy coefficient λ_θ as a function of the virtual photon polar angle for various dilepton masses. The contributions of s- and u-channel diagrams of the two dominant resonances $N(1440)$ and $N(1520)$ and their interference term (with a positive relative phase) are included. The CM energy is $\sqrt{s} = 1.49$ GeV.

with a positive or negative relative sign to the case where the amplitude of the two resonances $N(1520)$ and $N(1440)$ are added with a positive relative sign. In Fig 2.11 we added the $N(1535)$ amplitude with a positive or negative relative sign to the case where the amplitude of the two resonances $N(1520)$ and $N(1440)$ are added with a negative relative sign. In Figs 2.12 and 2.13 we did the same considering, instead, the resonance $\Delta(1600)$. We note that the inclusion of the $N(1535)$ and $\Delta(1600)$ produces a small effect on the anisotropy coefficient λ_θ.

Dileptons with a low invariant mass originate from the decay of a virtual photon which is close to its mass shell. Such virtual photons must be predominantly transversely polarized. Consequently the λ_θ coefficient of the resulting dileptons is close to unity. This can be seen in Fig. 2.9, where we show the θ_{γ^*} dependence of the λ_θ coefficient for various values of the dilepton invariant mass. These results include the s- and u-channel diagrams of the dominant $N(1520)$ and $N(1440)$ resonances, assuming a positive relative sign between the amplitudes.

The anisotropy coefficient λ_θ can be determined experimentally by employing Eq. (1.78). Clearly this is very challenging, since such an analysis requires a triple-differential dilepton production cross section. For a fixed invariant mass M and scattering angle θ_{γ^*}, the λ_θ coefficient is obtained by extracting the dependence of the cross section on the electron angle $\cos^2\theta_e$. Nevertheless, the results shown in Fig. 2.9 suggest that a rough binning both in M and θ_{γ^*}, e.g. $M > 0.3$ GeV and three bins in θ_{γ^*}, would be sufficient for extracting interesting information on the polarization observable.

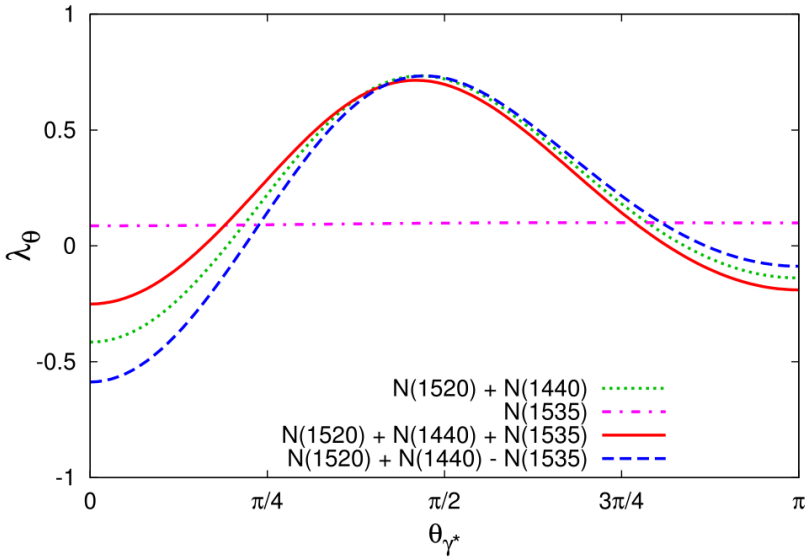

Figure 2.10.: The contribution of the $N(1535)$ to the anisotropy coefficient λ_θ at $\sqrt{s} = 1.49$ GeV CM energy. The amplitude of the $N(1535)$ is added with a positive and negative relative sign to the case where the $N(1520)$ and $N(1440)$ amplitudes are added with a positive relative sign. Both $s-$ and $u-$channel are included.

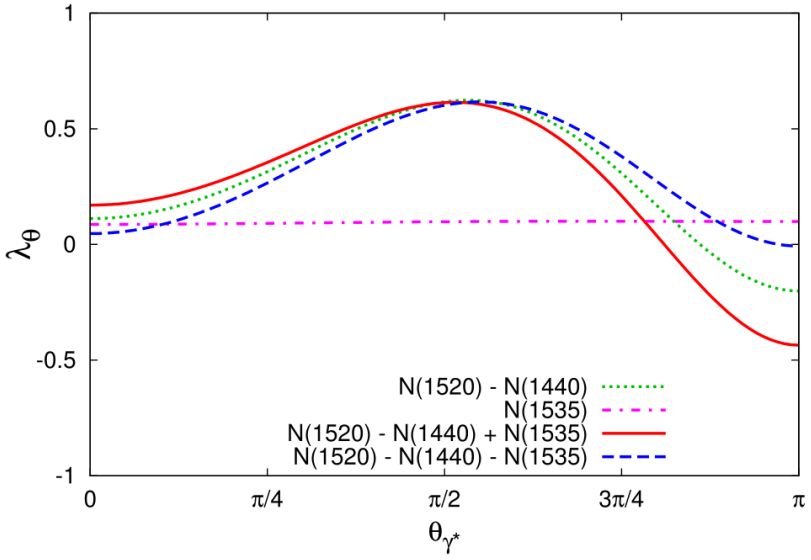

Figure 2.11.: The contribution of the $N(1535)$ to the anisotropy coefficient λ_θ at $\sqrt{s} = 1.49$ GeV CM energy. The amplitude of the $N(1535)$ is added with a positive and negative relative sign to the case where the $N(1520)$ and $N(1440)$ amplitudes are added with a negative relative sign. Both $s-$ and $u-$channel are included.

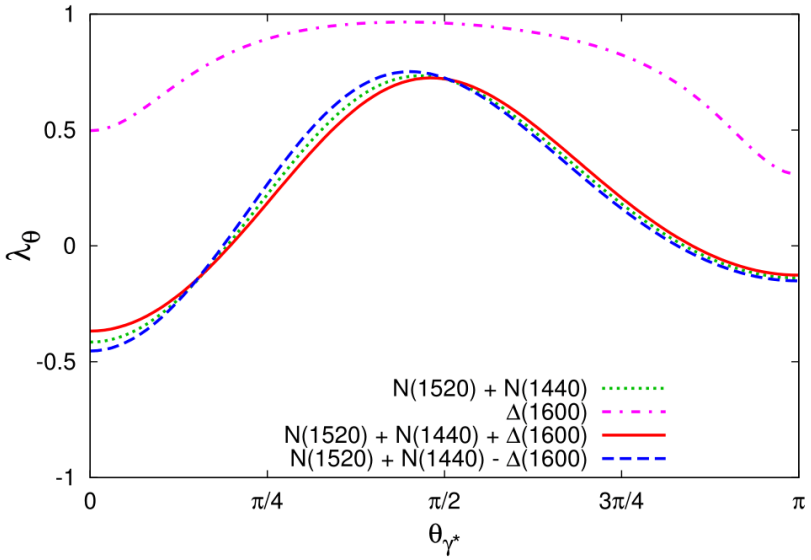

Figure 2.12.: The contribution of the $\Delta(1600)$ to the anisotropy coefficient λ_θ at $\sqrt{s} = 1.49$ GeV CM energy. The amplitude of the $\Delta(1600)$ is added with a positive and negative relative sign to the case where the $N(1520)$ and $N(1440)$ amplitudes are added with a positive relative sign. Both $s-$ and $u-$channel are included.

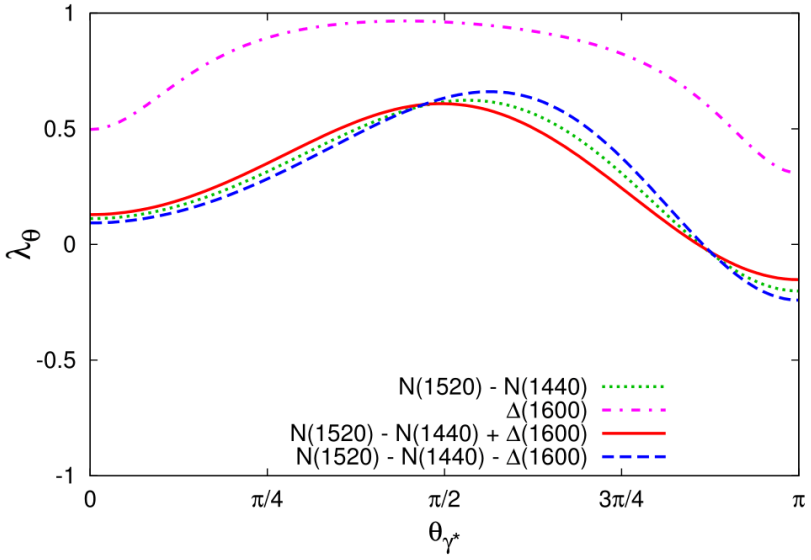

Figure 2.13.: The contribution of the $\Delta(1600)$ to the anisotropy coefficient λ_θ at $\sqrt{s} = 1.49$ GeV CM energy. The amplitude of the $\Delta(1600)$ is added with a positive and negative relative sign to the case where the $\Delta(1520)$ and $N(1440)$ amplitudes are added with a negative relative sign. Both $s-$ and $u-$channel are included.

Chapter 3

Dilepton rate at finite temperature

In this Chapter we illustrate some features of the two-point correlation function of operators (also called Green function) at finite temperature. Correlation functions are important tools in quantum field theory because they contain all the information needed to describe a many-body system. For example, in a medium certain collective excitations may occur. The propagation of collective phenomena in the medium can be described by correlation functions in a similar way as one describes particles in vacuum. Medium excitations appear as poles of the correlation function: the real part of the pole gives the dispersion relation and the imaginary part gives the damping of the excitation.

Correlation functions are also the key ingredients for calculating the thermal rate for particle production. In the next Section we will show that the production rate of weakly interacting particles produced from a thermalized medium reduces to the calculation of the two-point current-correlation function. More generally, correlation functions can also be used to calculate other real-time observables like e.g. shear viscosity.

In this Thesis we are interested in studying real-time correlation functions, i.e. we work with Minkowskian coordinates. The Minkowski space-time coordinates are denoted by $x = (t, \mathbf{x})$ and the momenta by $q = (q_0, \mathbf{q})$. For the sake of completeness, in this Section we will also briefly discuss correlation functions in Euclidean coordinates (or imaginary time) and we will discuss the connection between correlation functions in real and imaginary time. We denote the Euclidean coordinates by $\tilde{x} = (\tau, \mathbf{x})$. Passing from real to imaginary time means making the Wick rotation $\tau \to it$. We also adopt the convention $f(x) \equiv f(t, \mathbf{x})$, $f(q) \equiv f(q_0, \mathbf{q})$, with f any function or field operator. It will be clear from the context and the argument whether f is a function or an operator and whether it is defined in coordinate or momentum space. In Section 3.1, we consider for simplicity only a scalar bosonic field operator $\phi(x)$ that, in the Heisenberg picture, is defined by

$$\phi(t, \mathbf{x}) = e^{iHt}\phi(t, \mathbf{0})e^{-iHt}, \qquad \phi(\tau, \mathbf{x}) = e^{H\tau}\phi(t, \mathbf{0})e^{-H\tau}, \tag{3.1}$$

where H is the Hamiltonian of the system. The thermal average is denoted by $\langle \dots \rangle$, implying that

$$\langle \phi(x) \rangle = \frac{1}{Z}\mathrm{Tr}(e^{-\beta H}\phi(x)), \tag{3.2}$$

where $Z = \mathrm{Tr}(e^{-\beta H})$ is the partition function. All the definitions and results can be quite easily extended to the case of fermion and vector field operators. We will follow [85] for the conventions for correlation functions.

The structure of this Chapter is the following. In Section 3.1, basic concepts of thermal field theory are outlined. In Section 3.2 and Section 3.3, we present the derivation of the thermal rate for dileptons and emphasize the importance of the current correlation

function. In Section 3.4, a general form for the current correlation function is given. We conclude by analyzing the Drell-Yan process and the Boltzmann limit for the distribution functions in Section 3.5.

3.1 Basics of thermal field theory

We start by defining correlation functions in coordinate space. It is convenient to define

$$D^{>}(x) = \langle \phi(x)\phi(0)\rangle \tag{3.3}$$
$$D^{<}(x) = \langle \phi(0)\phi(x)\rangle, \tag{3.4}$$

Let us explicitly evaluate the trace of Eq. (3.3) and insert a complete set of eigenstates of the Hamiltonian and the momentum operator. By exploiting translation invariance, we find

$$D^{>}(x) = \frac{1}{Z}\sum_{m,n} e^{-\beta E_n} e^{i(p_n - p_m)x} |\langle n|\phi(0)|m\rangle|^2, \tag{3.5}$$

where E_n and p_n are the energy and 4-momentum of the state $|n\rangle$. An analogous derivation applies for $D^{<}(x)$. We can define the Feynman time-ordered correlation function as

$$\begin{aligned} iD^{F}(x) &= \langle T\phi(x)\phi(0)\rangle \\ &= \theta(t)D^{>}(x) + \theta(-t)D^{<}(x), \end{aligned} \tag{3.6}$$

where $\theta(t)$ is the step function. We would like to work in the momentum space, hence we take the Fourier transform

$$D^{>}(q) = \int d^4x\, e^{iqx}\langle \phi(x)\phi(0)\rangle. \tag{3.7}$$

Using the cyclic invariance of the trace, we obtain

$$D^{<}(q) = e^{-\beta q_0} D^{>}(q). \tag{3.8}$$

At this point we would like to define three correlation functions which are of crucial importance for the calculation of observables and we will emphasize the connections between them. The first one is the spectral function $\rho(q)$ defined as the thermal average of the commutator of the fields

$$\rho(q) = \frac{1}{2\pi}\int d^4x\, e^{iqx}\langle [\phi(x), \phi(0)]\rangle. \tag{3.9}$$

We note that

$$\rho(q) = \frac{1}{2\pi}(D^{>}(q) - D^{<}(q)) = \frac{1}{2\pi}(e^{\beta q_0} - 1)D^{<}(q). \tag{3.10}$$

With the help of Eq. (3.5), the spectral function can be more explicitly written as

$$\rho(q) = \frac{1}{Z}\sum_{m,n}(e^{-\beta E_n} - e^{-\beta E_m})(2\pi)^3\delta^{(4)}(q + p_n - p_m)|\langle n|\phi(0)|m\rangle|^2, \tag{3.11}$$

where p_m and p_n are the 4-momentum of the state $|m\rangle$ and $|n\rangle$, respectively. The other two are the "retarded" $D^R(q)$ and "advanced" $D^A(q)$ correlators defined as

$$D^R(q) = -i \int d^4x\, e^{iqx} \theta(t) \langle [\phi(x), \phi(0)] \rangle, \tag{3.12}$$

$$D^A(q) = i \int d^4x\, e^{iqx} \theta(-t) \langle [\phi(x), \phi(0)] \rangle. \tag{3.13}$$

Using the integral representation for the step function

$$\theta(t) = i \int_{-\infty}^{\infty} \frac{d\omega}{2\pi} \frac{e^{-i\omega t}}{\omega + i\epsilon} \tag{3.14}$$

and Eq. (3.10) we can write the retarded correlator Eq. (3.12) in terms of the spectral function, namely

$$D^R(q) = 2\pi \int dt \int \frac{d\omega}{2\pi} \int \frac{dp_0}{2\pi} \frac{e^{i(q_0 - p_0 - \omega)t}}{\omega + i\epsilon} \rho(p_0, \mathbf{q}). \tag{3.15}$$

Applying an analogous procedure to the advanced Green functions we arrive at the so-called Lehmann spectral representation

$$D^R(q) = -\int_{-\infty}^{\infty} d\omega \frac{\rho(\omega, \mathbf{q})}{\omega - q_0 - i\epsilon}, \tag{3.16}$$

$$D^A(q) = -\int_{-\infty}^{\infty} d\omega \frac{\rho(\omega, \mathbf{q})}{\omega - q_0 + i\epsilon}. \tag{3.17}$$

Making use of the formal relation

$$\frac{1}{\Delta \pm i\epsilon} = P\left(\frac{1}{\Delta}\right) \mp i\pi\delta(\Delta), \tag{3.18}$$

where P denotes the principal value, we can relate the real and imaginary parts of the retarded and advanced correlators with the spectra function, namely

$$\mathrm{Im}\, D^R(q) = -\mathrm{Im}\, D^A(q) = -\pi\rho(q) \tag{3.19}$$

and

$$\mathrm{Re}\, D^R(q) = \mathrm{Re}\, D^A(q). \tag{3.20}$$

We can also write the Fourier transform of the Feynman correlation function (3.6) and, using again Eq. (3.14), we can relate it to the spectral function, i.e.

$$D^F(q) = \int_{-\infty}^{\infty} d\omega \frac{\rho(\omega, \mathbf{q})}{q_0 - \omega + i\epsilon} - 2i\pi n_B(q_0)\rho(q), \tag{3.21}$$

where $n_B(q_0) = 1/(e^{\beta q_0} - 1)$ is the Bose distribution function.

Now we want to establish the connection between the previous real-time propagators with the Euclidean ones. We define the Euclidean propagator in position space as

$$D^E(\tau,\mathbf{x}) = \langle \phi(\tau,\mathbf{x})\phi(0)\rangle. \tag{3.22}$$

Using the cyclic invariance of the trace, we can show that the Euclidean correlation function is periodic in τ, i.e.

$$D^E(\tau-\beta) = D^E(\tau), \tag{3.23}$$

for $0 \leq \tau \leq \beta$. The Fourier transform of the Euclidean correlator is

$$D^E(\omega_n,\mathbf{q}) = \int_0^\beta d\tau \int d^3x\, e^{-i(\omega_n\tau+\mathbf{k}\cdot\mathbf{x})} D^E(\tau,\mathbf{x}), \tag{3.24}$$

where the inverse transformation is given by

$$D^E(\tau,\mathbf{x}) = T\sum_n e^{-i\omega_n\tau} \int \frac{d^3q}{(2\pi)^3}\, e^{i\mathbf{q}\cdot\mathbf{x}} D^E(\omega_n,\mathbf{q}). \tag{3.25}$$

Owing to the periodicity, the Fourier transform is taken over a finite interval $0 \leq \tau \leq \beta$. Consequently, the frequencies $\omega_n = 2\pi n/\beta$ take discrete values, the Matsubara frequencies. After some manipulation, we can write Eq. (3.24) in terms of the spectral function as

$$D^E(\omega_n,\mathbf{q}) = \int_{-\infty}^{\infty} d\omega\, \frac{\rho(\omega,\mathbf{q})}{\omega + i\omega_n}. \tag{3.26}$$

The connection between Euclidean (3.26) and real-time correlation functions (3.16) and (3.17) is made with the following analytic continuation

$$D^R(q) = -D^E(\omega_n \to iq_0 - \epsilon), \tag{3.27}$$

$$D^A(q) = -D^E(\omega_n \to iq_0 + \epsilon). \tag{3.28}$$

We finally note that the retarded (advanced) Green function is analytic in the upper (lower) half complex q_0 plane.

3.2 Derivation for the dilepton thermal rate

In this Section we briefly outline the derivation of the formula for the thermal dilepton production rate [85–90]. We consider a system consisting of strongly-interacting particles that are assumed to be in thermal equilibrium. The strongly interacting particles emit another species of particles which interact weakly with the medium and, therefore, can escape from the system without further interactions. In this Thesis, we consider the case in which virtual photons are produced in a thermalized strongly interacting medium produced in heavy-ion collisions (i.e. quark-gluon plasma). Since the photon interacts only electromagnetically, its mean free path is much larger than the size of the system. A similar situation occurs for neutrinos emitted from a neutron star.

As already mentioned, here we want to focus on the emission in heavy-ion collisions of virtual photons which subsequently decay into lepton pairs. Since neither the photon nor the leptons are scattered by the particles composing the medium, both retain their vacuum properties. The photon does not feel any rescattering with the particles composing the medium and, hence, both the photon and the lepton pair are treated as in vacuum. The Lagrangian describing the whole system is of the form

$$\mathcal{L} = \mathcal{L}_{\mathbf{bath}} + \mathcal{L}_{\gamma} + \mathcal{L}_{\mathrm{int}} + \mathcal{L}_{l^+l^-} + \mathcal{L}_{\mathrm{QED}}, \tag{3.29}$$

where $\mathcal{L}_{\mathbf{bath}}$ describes the thermalized degrees of freedom, while $\mathcal{L}_{\gamma}$ and $\mathcal{L}_{l^+l^-}$ is the free Lagrangian respectively for the photon and the lepton pair. Moreover, $\mathcal{L}_{\mathrm{int}}$ is the Lagrangian describing the interaction between the particles in the heat bath and the photon, namely

$$\mathcal{L}_{\mathrm{int}} = -J^{\mu}A_{\mu}, \tag{3.30}$$

where J_{μ} is the (hermitian) electromagnetic current operator and A^{μ} the photon field. Finally, $\mathcal{L}_{\mathrm{QED}}$ is the standard QED interaction responsible for the decay of the photon into the lepton pair.

$$\mathcal{L}_{QED} = -J^{\mu}_{\mathrm{QED}}A_{\mu}, \tag{3.31}$$

with $J_{\mathrm{QED}} = e\bar{\psi}\gamma^{\mu}\psi$, ψ being the lepton field and e the electron charge.

The total initial state $|I\rangle$ and final state $|F\rangle$ can be expressed as the tensor product of the initial $|i\rangle$ and final $|f\rangle$ state describing the heat bath and the state of the dilepton in vacuum, i.e.

$$|I\rangle = |i\rangle \otimes |0\rangle, \qquad |F\rangle = |f\rangle \otimes |l^+l^-\rangle. \tag{3.32}$$

The S matrix element for the transition $|I\rangle \to |F\rangle$ is then given by

$$S_{FI} = \langle F| \int d^4x d^4y J_{\mathrm{QED}\,\mu}(x) D_0^{\mu\nu}(x-y) J_{\nu}(y)|I\rangle, \tag{3.33}$$

where $D_0^{\mu\nu}(x-y)$ is the free photon propagator, which is given by

$$D_0^{\mu\nu}(x-y) = \int \frac{d^4q}{(2\pi)^4} e^{-iq(x-y)} D_0^{\mu\nu}(q). \tag{3.34}$$

The free propagator in momentum space reads

$$D_0^{\mu\nu}(q) = \frac{-g^{\mu\nu} + q^{\mu}q^{\nu}/q^2}{q^2}. \tag{3.35}$$

We now factorize the matrix element of Eq. (3.33) in the lepton and heat bath part and use current conservation. Hence, Eq. (3.33) becomes

$$S_{FI} = \frac{e}{q^2}(2\pi)^4 \int \frac{d^4q}{(2\pi)^4} \delta^{(4)}(q - l_- - l_+) \bar{u}(\mathbf{l}_-)\gamma^{\mu} v(\mathbf{l}_+) \int d^4x\, e^{iqx} \langle f|J_{\mu}(x)|i\rangle, \tag{3.36}$$

where the lepton (antilepton) 4-momentum is denoted by $l_-^{\mu} = (E_-, \mathbf{l}_-)$ ($l_+^{\mu} = (E_+, \mathbf{l}_+)$), while u and v are the Dirac spinors. In order to calculate the dilepton rate, we need to

consider that the system we are considering is thermalized, therefore one has to carry out an ensamble average over all the possible initial states weighted with a thermal factor. Furthermore, we sum over the final states. The particle production rate is then given by

$$d\Gamma \equiv \frac{dN}{d^4x} = \frac{1}{\Omega}\frac{1}{Z}\sum_{i,f}\sum_{\text{spins}} e^{-\beta E_i}|S_{FI}|^2 \frac{d^3l_-}{(2\pi)^3 2E_-}\frac{d^3l_+}{(2\pi)^3 2E_+}, \tag{3.37}$$

with $Z = \text{Tr}(e^{-\beta H_{\text{bath}}})$ the partition function of the heat bath, H_{bath} being the Hamiltonian of the thermalized system, $\beta = 1/T$ the inverse temperature and Ω the space time volume needed to define the rate. By squaring the matrix element (3.36), we obtain

$$\begin{aligned}|S_{FI}|^2 = e^2\bar{u}(\mathbf{l}_-)\gamma^\mu v(\mathbf{l}_+)\bar{v}(\mathbf{l}_+)\gamma^\nu u(\mathbf{l}_-)\int d^4q d^4q' \delta^{(4)}(q-l_--l_+)\frac{1}{q^2}\,\delta^{(4)}(q'-l_--l_+)\frac{1}{q'^2}\\ \times\int d^4x d^4x'\, e^{iqx}e^{-iq'x'}\langle f|J_\mu(x)|i\rangle\langle i|J_\nu(x')|f\rangle\end{aligned} \tag{3.38}$$

The integration of the two delta functions reduces to that of only one delta function. We now need to plug Eq. (3.38) into the expression for the rate in Eq. (3.37). The space-time integration involving the current expectation values can be simplified by making use of translational invariance in order to cancel the space-time volume Ω. The rate in function of the virtual photon 4-momentum is thus given by

$$\frac{d\Gamma}{d^4q} = \frac{e^2}{q^4}W^<_{\mu\nu}(q)L^{\mu\nu}(l_-,l_+)\delta^{(4)}(q-l_--l_+)\frac{d^3l_-}{(2\pi)^3 2E_-}\frac{d^3l_+}{(2\pi)^3 2E_+}. \tag{3.39}$$

In the equation above we have defined the electromagnetic current-current correlation function as

$$W^<_{\mu\nu}(q) = \int d^4x\, e^{iqx}\langle J^\mu(0)J^\nu(x)\rangle, \tag{3.40}$$

where here we have extended the definition of the correlation function in Eq. (3.4) for the electromagnetic current J_μ. The integrand in Eq. (3.40) can be interpreted as representing the interference between photon emission at the space-time point x and 0. The current-current correlator (3.40) is a very important object and in Chapter 5 we will see how it is related to the polarization observables in the angular distribution of the lepton pair. In Eq. (3.39) we have also introduced the lepton tensor Eq. (1.66)

$$\begin{aligned}L^{\mu\nu}(l_-,l_+) = \sum_{\text{spins}}|\bar{u}(\mathbf{l}_-)\gamma^\mu v(\mathbf{l}_+)|^2 &= 4[l_-^\mu l_+^\nu + l_-^\nu l_+^\mu - (l_-\cdot l_+ + m_l^2)]\\ &= 2(-q^2 g^{\mu\nu} + q^\mu q^\nu - \Delta l^\mu \Delta l^\nu),\end{aligned} \tag{3.41}$$

with $\Delta l^\mu = l_-^\mu - l_+^\mu$ and $q^\mu = l_-^\mu + l_+^\mu$. Using Eqs. (3.10) and (3.19), we can relate the current correlation functions in Eq. (3.40) with the retarded current correlation function which has the required analytic properties in a heat bath, namely

$$W^<_{\mu\nu}(q) = -2n_B(q_0)\text{Im}\,W^R_{\mu\nu}(q), \tag{3.42}$$

$n_B(q_0)$ being the Bose function, and (see Eq. (3.12))

$$W^R_{\mu\nu} = -i \int d^4x\, e^{iqx}\theta(t)\langle[J_\mu(x), J_\nu(0)]\rangle. \tag{3.43}$$

We define the *improper* (or *one particle reducible*) retarded in medium photon self-energy $P^R_{\mu\nu}$ through the relation

$$D^{R,\alpha\beta} = D_0^{R,\alpha\beta} + D_0^{R,\alpha\mu}\, P^R_{\mu\nu}\, D_0^{R,\nu\beta}, \tag{3.44}$$

where $D^{R,\alpha\beta}$ is the fully dressed retarded photon propagator and $D_0^{R,\alpha\beta}$ is the free photon propagator. By definition, $P^R_{\mu\nu}$ takes into account all the possible interactions, both strong and electromagnetic, at any order, and we also have

$$P^R_{\mu\nu} = W^R_{\mu\nu}. \tag{3.45}$$

Therefore, one can rewrite Eq. (3.39) using Eq. (3.42) and Eq. (3.45).

We can also express the dilepton rate in terms of the photon spectral function defined in analogy with Eq. (3.9) as

$$\rho_{\mu\nu}(q) = \frac{1}{2\pi}\int d^4x\, e^{iqx}\langle[A_\mu(x), A_\nu(0)]\rangle. \tag{3.46}$$

The quantity $A_\mu(x)$ is the interacting photon field which is related to the electromagnetic current through Maxwell's equation

$$\partial_\alpha\partial^\alpha A_\mu(x) - \zeta^{-1}(\zeta-1)\partial_\mu(\partial_\alpha A^\alpha(x)) = J_\mu(x), \tag{3.47}$$

where ζ is a parameter that fixes the gauge ($\zeta = 1$ is the Feynman gauge). By substituting Eq. (3.47) into Eq. (3.40), we obtain the connection between the current-current correlator and the spectra function, namely

$$\begin{aligned} W^<_{\mu\nu}(q) &= \left(q^2 g_{\mu\alpha} - \frac{\zeta-1}{\zeta}q_\mu q_\alpha\right) D^{<,\alpha\beta}(q)\left(q^2 g_{\beta\nu} - \frac{\zeta-1}{\zeta}q_\beta q_\nu\right) \\ &= 2\pi\left(q^2 g_{\mu\alpha} - \frac{\zeta-1}{\zeta}q_\mu q_\alpha\right)\rho^{\alpha\beta}(q)\left(q^2 g_{\beta\nu} - \frac{\zeta-1}{\zeta}q_\beta q_\nu\right) n_B(q_0). \end{aligned} \tag{3.48}$$

At this level, it is important to note that the analysis that brought us to derive the rates Eq. (3.39) is basically nonperturbative. If now we want to consider only the lowest order in the electromagnetic coupling $O(e^2)$, the improper retarded self-energy $P^R_{\mu\nu}$ can be approximated with the *proper* or *one particle irreducible* retarded self-energy $\Pi^R_{\mu\nu}$ defined as

$$D^{R,\alpha\beta} = D_0^{R,\alpha\beta} + D_0^{R,\alpha\mu}\,\Pi^R_{\mu\nu}\, D^{R,\nu\beta}. \tag{3.49}$$

We can also calculate the integrated dilepton rate. Using the relation

$$\int (2\pi)^4\delta^{(4)}(q-l_- -l_+)L^{\mu\nu}(l_-,l_+)\frac{d^3l_-}{(2\pi)^3 2E_-}\frac{d^3l_+}{(2\pi)^3 2E_+} = \frac{1}{6\pi}L(q^2)(q^\mu q^\nu - q^2 g^{\mu\nu}), \tag{3.50}$$

with

$$L(q^2) = \left(1 + \frac{2m_l^2}{q^2}\right)\sqrt{1 - \frac{4m_l^2}{q^2}}, \tag{3.51}$$

where m_l is the lepton mass ($L(q^2) = 1$ for massless leptons). Equation (3.39) yields

$$\frac{d\Gamma}{d^4q} = -\frac{\alpha}{24\pi^4 q^2} L(q^2) g^{\mu\nu} W^<_{\mu\nu}(q), \tag{3.52}$$

Equations (3.39) and (3.52) will be the expressions for the dilepton thermal rate that we will use in the following of this Thesis.

We conclude this Section by presenting the differential rate for real photon. From the dilepton rate one simply has to replace the information about the decay of the virtual photon into the lepton pair, namely the quantity $e^2 L^{\mu\nu}\delta^{(4)}(q - l_- - l_+)/q^4$, with the sum over the photon polarization $\sum_\lambda \epsilon_\mu^{(\lambda)}(\epsilon_\mu^{(\lambda)})^* = -g^{\mu\nu}$. Moreover, one has to replace the dilepton phase space $(d^3l_-/(2\pi)^3 2E_-)(d^3l_+/(2\pi)^3 2E_+)$ with the real photon phase space $d^3q/(2\pi)^3 2q_0$. From Eqs. (3.39), we obtain the corresponding rate for real photons

$$d\Gamma = -g^{\mu\nu} W^<_{\mu\nu}(q) \frac{d^3q}{(2\pi)^3 2q_0}, \tag{3.53}$$

which is valid at all orders of the electromagnetic and strong interaction.

3.3 The current correlation function and the dilepton rate

In the previous Section we showed that the calculation of the rate for dilepton production at finite temperature reduces to the calculation of the current correlation function in Eq. (3.40) or, equivalently, the imaginary part of the retarded in medium photon self energy defined in Eq. (3.49). In principle, the self energy contains all processes of the strong interaction at any order. In practice, one must approximate the self energy considering only terms up to a certain order in some perturbative expansion. Of course we have to make sure that perturbation theory can be applied. Otherwise one can use some effective interaction.

The imaginary part of the self energy has a precise physical meaning. The optical theorem relates the imaginary part of the self energy to the matrix element squared for all possible processes. The imaginary part of the self energy is obtained by cutting the diagram by means of the so-called cutting rules at finite temperature [89, 91]. In practice, one dresses the self energy with the loops describing the processes that one wants to take into account.

One can also prove that the formalism for the calculation of the decay rate for photons described in the previous Section is equivalent to relativistic kinetic theory [86, 92]. Consider a general dilepton emission process where the initial thermal state is composed by N particles and the final thermal state by M particles. The particles in the medium can be fermions or bosons. We express the initial and final thermal state of Eq. (3.32) as

$$|i\rangle = |p_1, \ldots, p_N\rangle, \qquad |f\rangle = |p'_1, \ldots, p'_M\rangle, \tag{3.54}$$

respectively. According to kinetic theory, the rate for dilepton production can be written as

$$\begin{aligned}\frac{d\Gamma}{d^4q} = e^2 &\frac{d^3p_1}{(2\pi)^3 2E_1}\cdots\frac{d^3p_N}{(2\pi)^3 2E_N}\frac{d^3p'_1}{(2\pi)^3 2E'_1}\cdots\frac{d^3p'_M}{(2\pi)^3 2E'_M}\frac{d^3l_-}{(2\pi)^3 2E'_-}\frac{d^3l_+}{(2\pi)^3 2E'_+}\\ &\times(2\pi)^4\delta\left(\sum_{i=1}^{N}p_i-\sum_{i=1}^{M}p'_i-l_+-l_-\right)\langle p_1,\ldots,p_N|J_\mu(0)|p'_1,\ldots,p'_M\rangle\\ &\times\langle p'_1,\ldots,p'_M|J_\nu(0)|p_1,\ldots,p_N\rangle\frac{1}{e^{\beta E_1}\pm 1}\cdots\frac{1}{e^{\beta E_N}\pm 1}\left(1\mp\frac{1}{e^{\beta E'_1}\pm 1}\right)\cdots\left(1\mp\frac{1}{e^{\beta E'_M}\pm 1}\right)\\ &\times\delta^{(4)}(q-l_--l_+)\frac{1}{q^4}L^{\mu\nu}. \end{aligned}\tag{3.55}$$

Here, J^μ is the electromagnetic current responsible for the interaction between the photon and the particles in the medium defined in Eq. (3.30). We also introduced the Fermi distribution $1/(e^{\beta E}+1)$ and the Bose distribution $1/(e^{\beta E}-1)$ for particles in the initial state and Pauli blocking $1-1/(e^{\beta E}+1)$ and Bose enhancement $1+1/(e^{\beta E}-1)$ factors for particles in the final state. In the last line of Eq. (3.55), $L^{\mu\nu}$ is the lepton tensor defined in Eq. (3.41). The energy in the distribution functions in Eq. (3.55) is that of the particle in the fluid rest frame.

We can define the tensor $W^<_{\mu\nu}$ as

$$\begin{aligned}W^<_{\mu\nu}(q) = &\frac{d^3p_1}{(2\pi)^3 2E_1}\cdots\frac{d^3p_N}{(2\pi)^3 2E_N}\frac{d^3p'_1}{(2\pi)^3 2E'_1}\cdots\frac{d^3p'_M}{(2\pi)^3 2E'_M}(2\pi)^4\delta\left(\sum_{i=1}^{N}p_i-\sum_{i=1}^{M}p'_i-l_+-l_-\right)\\ &\times\langle p_1,\ldots,p_N|J_\mu(0)|p'_1,\ldots,p'_M\rangle\langle p'_1,\ldots,p'_M|J_\nu(0)|p_1,\ldots,p_N\rangle\\ &\times\frac{1}{e^{\beta E_1}\pm 1}\cdots\frac{1}{e^{\beta E_N}\pm 1}\left(1\mp\frac{1}{e^{\beta E'_1}\pm 1}\right)\cdots\left(1\mp\frac{1}{e^{\beta E'_M}\pm 1}\right).\end{aligned}\tag{3.56}$$

One can prove that the tensor of Eq. (3.56) is the same as the current-current corelation function defined in Eq. (3.40). In the above definition for the tensor $W^<_{\mu\nu}$, spin degeneracy or color factors are suppressed. For practical calculations, in this Thesis it will be more convenient to use the expression for $W^<_{\mu\nu}$ given in Eq. (3.56).

3.4 General structure of the current correlation function

The current correlation function incorporates all processes in a thermal medium that yield a photon. Therefore, it also provides information on the medium 4-velocity. In the expression for the $W^<_{\mu\nu}$, we implicitly assumed that all the integrations over the initial and final particles are carried out in the local fluid rest frame. In general, if we want to express the integrations in an other frame, we should replace the energy E in the distribution functions with the scalar product $u\cdot p$, where u^μ is the 4-velocity of the fluid, such that

$$u^\mu = \gamma(1,\mathbf{v}),\tag{3.57}$$

where $\mathbf{v}$ is the fluid 3-velocity and γ the Lorentz factor. We note that $u^2=1$. In the local fluid rest frame we clearly have

$$u^\mu = (1,\mathbf{0}).\tag{3.58}$$

We can deduce a general model-independent form for the current correlation function by imposing basic conditions on the Lorentz structure. First of all, $W^{<,\mu\nu}$ can only be constructed with the metric tensor $g^{\mu\nu}$ and the only two vectors at our disposal after the integration over the momenta of the initial particles, namely the photon momentum q^μ and the medium velocity u^μ. Moreover, we require $W^{<,\mu\nu}$ to be a symmetric function of q^μ and u^μ, since we contract it with the symmetric tensor $L^{\mu\nu}$ in the dilepton rate. Clearly, $W^{<,\mu\nu}$ must be also current conserving, i.e. $q^\mu W^<_{\mu\nu} = 0$. Thus, the most general form is given by

$$W^{<,\mu\nu} = W_1(q^2, u\cdot q, T)\left(-g^{\mu\nu} + \frac{q^\mu q^\nu}{q^2}\right) + W_2(q^2, u\cdot q, T)\left(u^\mu - \frac{u\cdot q}{q^2}q^\mu\right)\left(u^\nu - \frac{u\cdot q}{q^2}q^\nu\right). \tag{3.59}$$

The structure functions W_1 and W_2 are Lorentz scalars and depend on all the scalar quantities we can construct from the two vectors at our disposal and the temperature of the medium T. Note that the second term proportional to W_2 is present because it describes the fact that in general the fluid rest frame and the rest frame of the photon do not coincide. If these two frames coincide, the second term vanishes. The general form for $W^{<,\mu\nu}$ in Eq. (3.59) is analogous to the hadronic tensor in deep-inelastic scattering. In that case, the second 4-vector which the hadronic tensor depends on, besides the photon momentum, is the momentum of the struck nucleon. Another difference compared to deep-inelastic scattering is that, in our current correlation function, the photon is time-like rather than space-like, allowing for the decay into a lepton pair. We finally point out that the structure of Eq. (3.59) is clearly valid both in a nonperturbative and perturbative analysis. So now the calculation of the current correlation function or, equivalently, the imaginary part of the retarded photon self energy boils down to calculating the two structure functions W_1 and W_2.

3.5 The Drell-Yan process and the Boltzmann limit

In this Section we calculate explicitly the structure functions W_1 and W_2 for a particularly simple case, the Drell-Yan process to lowest order in perturbation theory. In this process a quark and an antiquark in the quark-gluon plasma annihilate into dileptons through a virtual photon [86]. Using the QED current $J^\mu_{\mathrm{QED}} = e\bar\psi\gamma^\mu\psi$, the current correlation function Eq. (3.56) for this process takes the simple form

$$\begin{aligned} W^{<,\mu\nu} = e^2 \int \frac{d^3p_1}{(2\pi)^3 2E_1}\frac{d^3p_2}{(2\pi)^3 2E_2}\frac{1}{e^{\beta E_1}+1}\frac{1}{e^{\beta E_2}+1}(2\pi)^4\delta^{(4)}(q-p_1-p_2) \\ \times \mathrm{Tr}[(\not{p}_1 - m)\gamma^\mu(\not{p}_2 + m)\gamma^\nu], \end{aligned} \tag{3.60}$$

m being the quark mass. Again we suppressed the color factor. In the case of a quark-gluon plasma the energy is high enough to neglect the quark mass. Furthermore, we consider the case in which the photon momentum is much bigger than the temperature of the quark-gluon plasma

$$u\cdot q \gg T, \qquad q^2 \gg T^2. \tag{3.61}$$

Hence, we can approximate the Fermi distributions to Boltzmann distributions:

$$\frac{1}{e^{\beta E_1}+1}\frac{1}{e^{\beta E_2}+1} \sim e^{-\beta E_1}e^{-\beta E_2} = e^{-\beta q_0} = e^{-\beta u\cdot q}, \tag{3.62}$$

where, in the last step, we expressed the exponential in a covariant form. In this approximation we can pull the exponential outside the integral and Eq. (3.60) reduces formally to the same integral as in Eq. (3.50), namely

$$\begin{aligned} W^{<,\mu\nu} &\sim e^2 e^{-\beta u\cdot q}\int \frac{d^3p_1}{(2\pi)^3 2E_1}\frac{d^3p_2}{(2\pi)^3 2E_2}(2\pi)^4\delta^{(4)}(q-p_1-p_2)\mathrm{Tr}[\not{p}_1\gamma^\mu\not{p}_2\gamma^\nu] \\ &= e^{-\beta u\cdot q}\mathrm{Im}\,\Pi^{\mu\nu}_{\mathrm{vac}}(q) \\ &= e^{-\beta u\cdot q}\mathrm{Im}\,\Pi_{\mathrm{vac}}(-g^{\mu\nu}q^2+q^\mu q^\nu), \end{aligned} \tag{3.63}$$

where $\Pi^{\mu\nu}_{\mathrm{vac}}(q)$ is the vacuum photon self-energy, which is a constant, $\mathrm{Im}\,\Pi_{\mathrm{vac}} = e^2/6\pi$. By comparing with Eq. (3.59), we see that the structure functions are given by

$$W_1 = e^{-\beta u\cdot q}q^2\mathrm{Im}\,\Pi_{\mathrm{vac}} = \frac{e^2}{6\pi}e^{-\beta u\cdot q}q^2, \qquad W_2 = 0. \tag{3.64}$$

Equations (3.63) and (3.64) show that, under the approximations discussed above, we could factorize the medium and the vacuum information. All the medium information are contained only in the factor $e^{-\beta u\cdot q}$.

The result of Eq. (3.63) and (3.64) can be generalized under the same approximations to a wider class of Feynman diagrams at all orders of perturbation theory. Consider those processes in which we have a total of N quarks and gluons in the initial state in the plasma that are all annihilated into the virtual photon. Hence, there is only a lepton pair in the final state. The integral over the initial states in Eq. (3.56) involves the product of the Fermi and Bose distribution functions. Under the condition discussed above in Eq. (3.61), where the main contribution to the integral comes from hard particles, the Fermi and Bose distributions can all be approximated to Boltzmann factors. Thus, the product of the distribution functions will just be

$$e^{-\beta E_1}e^{-\beta E_2}\cdots e^{-\beta E_N} = e^{-\beta q_0} = e^{-\beta u\cdot q}. \tag{3.65}$$

Therefore, we can again factorize the medium from the vacuum contribution and we find

$$W^{<,\mu\nu} = e^{-\beta u\cdot q}\mathrm{Im}\,\Pi_{\mathrm{vac}}(q^2)(-g^{\mu\nu}q^2+q^\mu q^\nu), \tag{3.66}$$

where again $\Pi_{\mathrm{vac}}(q^2)$ is the vacuum-photon self energy describing the complicated thermal initial state. Thus the structure functions read

$$W_1 = e^{-\beta u\cdot q}q^2\mathrm{Im}\,\Pi_{\mathrm{vac}}(q^2), \qquad W_2 = 0. \tag{3.67}$$

If the photon momentum is not large compared to the plasma temperature, we cannot use the Boltzmann approximation for the distribution functions and the structure function W_2 does not vanish. In Chapter 5, we will show how the Boltzmann limit affects the polarization state of a virtual photon. In the rest of the Thesis, for the sake of simplicity we will omit the superscript $<$ in the notation for the current correlation function.

Chapter 4

Relativistic hydrodynamics

Relativistic hydrodynamics provides an extremely good description of the space-time evolution of the fireball created in ultrarelativistic heavy-ion collisions [10–15]. In this Chapter we review the basic aspect of relativistic hydrodynamics. The Chapter is structured as follows: in Section 4.1 we briefly outline some basic concepts of thermodynamics, in Section 4.2 we discuss the equations of motions for relativistic ideal hydrodynamics and in Section 4.3 those in case of dissipation. Finally, in Section 4.4 we describe the widely used Bjorken flow.

4.1 Basics of thermodynamics

A thermodynamic system can be described by the internal energy E, the entropy S, the volume V and the temperature T. When we combine quantum mechanics and relativity, the number of total particles is in general not conserved and the actual conserved quantity is the net baryon particle number. In this Thesis, however, we will not study non-zero net baryon number and, therefore, we will not introduce the baryon-chemical potential. The first law of thermodynamics expresses the principle of energy conservation. In the differential form we have

$$dE = TdS - PdV. \tag{4.1}$$

In the above equation the first two terms represent the heat and work transferred. From Eq. (4.1) we can define

$$\left.\frac{\partial S}{\partial E}\right|_V = \frac{1}{T}, \qquad \left.\frac{\partial S}{\partial V}\right|_E = \frac{P}{T}. \tag{4.2}$$

The entropy $S(E,V)$ is an extensive variable, this means that

$$S(\lambda E, \lambda V) = \lambda S(E,V). \tag{4.3}$$

The above expression is valid for arbitrary λ. We can differentiate the previous equation with respect to λ and set $\lambda = 1$. Furthermore, using Eq. (4.2), we obtain the Euler relation

$$E = -PV + TS. \tag{4.4}$$

Differentiating Eq. (4.4), we obtain the so-called Gibbs-Duhem relation

$$VdP = SdT, \tag{4.5}$$

for vanishing chemical potential. Instead of the total energy and entropy, it is useful to define the density of these quantities

$$\epsilon \equiv \frac{E}{V}, \qquad s \equiv \frac{S}{V}, \tag{4.6}$$

respectively, which are intensive variables. Thus, Eqs. (4.4) and (4.5) become

$$\epsilon = Ts - P, \tag{4.7}$$

$$dP = s\,dT. \tag{4.8}$$

Differentiating Eq. (4.7) and using Eq. (4.8), the first law of thermodynamics is expressed by

$$d\epsilon = T ds. \tag{4.9}$$

4.2 Relativistic ideal fluid dynamics

We can schematically picture a fluid as a system composed by many elements each of those moving with a certain velocity. Therefore, we can assign to each space-time point $x \equiv x^\mu$ a 4-velocity of the fluid

$$u^\mu(x) \equiv \frac{dx^\mu}{d\tau} = \gamma(x)(\mathbf{v}(x))(1, \mathbf{v}(x)), \tag{4.10}$$

where τ is the proper time, $\mathbf{v}(x) \equiv d\mathbf{x}/dt$, $\gamma(x) = 1/\sqrt{1-\mathbf{v}^2(x)}$. The fluid 4-velocity obeys the relation

$$u^2 \equiv u_\mu(x) u^\mu(x) = 1. \tag{4.11}$$

In the following, for the sake of simplicity, we will suppress the dependence of the velocity and the thermodynamic quantities on the space time. We define the local rest frame of the fluid that frame in which the fluid 4-velocity is just $u^\mu = (1, \mathbf{0})$. All the thermodynamic quantities that we will associate with the fluid are defined in the local rest frame of the fluid.

The total energy and momentum are locally conserved. Therefore we have four conservation laws that can be arranged in the so-called energy-momentum tensor $T^{\mu\nu}$. The energy momentum tensor is defined such that T^{00} is the energy density, T^{0j} is the density of the j^{th} component of the momentum, T^{i0} is the energy flux in the direction i, and T^{ij} is the flow of the j^{th} component of the momentum along the direction i. Energy and momentum conservation laws can be expressed covariantly in the form

$$\partial_\mu T^{\mu\nu} = 0. \tag{4.12}$$

The equations (4.12) are the hydrodynamic equations of motion.

An ideal (or inviscid) fluid is completely characterized by its energy density ϵ and pressure P as defined in the local rest frame. Ideal hydrodynamics is based on the assumption of local thermodynamic equilibrium, implying that the fluid element is isotropic in its rest

frame. This means that the energy-momentum tensor in the local fluid rest frame $T^{\mu\nu}_{(0)LRF}$ is diagonal (the subscript (0) indicates that we are referring to the ideal fluid), i.e.

$$T^{\mu\nu}_{(0)LRF} = \begin{pmatrix} \epsilon & 0 & 0 & 0 \\ 0 & P & 0 & 0 \\ 0 & 0 & P & 0 \\ 0 & 0 & 0 & P \end{pmatrix}, \tag{4.13}$$

and there is no entropy flow

$$S^{\mu}_{(0)LRF} = \begin{pmatrix} s \\ 0 \\ 0 \\ 0 \end{pmatrix}, \tag{4.14}$$

where $S^{\mu}_{(0)LRF}$ is the entropy 4-current. In the above equation, s is the entropy density in the local rest frame. To obtain the energy-momentum tensor Eq. (4.13) in a moving frame, we can consider for simplicity the approximation of small fluid velocity $\mathbf{v}$ [14]. The Lorentz transformation is given by

$$\Lambda^{\mu}_{\nu} = \begin{pmatrix} 1 & v_x & v_y & v_z \\ v_x & 1 & 0 & 0 \\ v_y & 0 & 1 & 0 \\ v_z & 0 & 0 & 1 \end{pmatrix} \tag{4.15}$$

and the Lorentz transformed energy-momentum tensor is given by

$$T^{\mu\nu} = \begin{pmatrix} \epsilon & (\epsilon+P)v_x & (\epsilon+P)v_y & (\epsilon+P)v_z \\ (\epsilon+P)v_x & P & 0 & 0 \\ (\epsilon+P)v_y & 0 & P & 0 \\ (\epsilon+P)v_z & 0 & 0 & P \end{pmatrix}. \tag{4.16}$$

Note that, since Lorentz transformations do not change the symmetry properties of tensors, $T^{\mu\nu}$ is a symmetric tensor in any frame and this implies that in a relativistic description of fluids, the momentum density and energy flux are equal.

The general covariant form for the tensors in Eq. (4.13) and (4.14) valid in any frame can be built out of the most general Lorentz structure at our disposal that respects the symmetry required. At this point we only have the metric tensor $g^{\mu\nu}$ and the fluid velocity u^{μ}. Therefore, we can write in any frame [93]

$$T^{\mu\nu}_{(0)} = c_1 u^{\mu} u^{\nu} + c_2 g^{\mu\nu}, \quad S^{\mu}_{(0)} = c_3 u^{\mu}. \tag{4.17}$$

The four scalar quantities c_1, c_2 and c_3 can be easily determined if we go to the fluid rest frame, namely

$$T^{\mu\nu}_{(0)LRF} = \begin{pmatrix} c_1+c_2 & 0 & 0 & 0 \\ 0 & -c_2 & 0 & 0 \\ 0 & 0 & -c_2 & 0 \\ 0 & 0 & 0 & -c_2 \end{pmatrix}, \quad S^{\mu}_{(0)LRF} = \begin{pmatrix} c_3 \\ 0 \\ 0 \\ 0 \end{pmatrix}. \tag{4.18}$$

By comparing Eq. (4.18) with Eq. (4.13), we obtain

$$c_1 = \epsilon + P, \quad c_2 = -P, \quad c_3 = s, \tag{4.19}$$

and Eq. (4.17) becomes

$$T^{\mu\nu}_{(0)} = (\epsilon + P)u^\mu u^\nu - P g^{\mu\nu} = \epsilon u^\mu u^\nu - P\Delta^{\mu\nu}, \quad S^\mu_{(0)} = s u^\mu, \tag{4.20}$$

where we have introduced the projection operator orthogonal to u^μ, $\Delta^{\mu\nu} = g^{\mu\nu} - u^\mu u^\nu$, such that

$$u_\mu \Delta^{\mu\nu} = \Delta^{\mu\nu} u_\nu = 0, \quad \Delta^\mu_\rho \Delta^{\rho\nu} = \Delta^{\mu\nu}, \quad \Delta^\mu_\mu = 3. \tag{4.21}$$

We can now define two differential operators

$$D \equiv u^\mu \partial_\mu, \qquad \nabla_\mu \equiv \Delta^{\mu\rho}\partial_\rho, \tag{4.22}$$

such that the partial derivative ∂_μ can be decomposed into a part parallel and a part transverse to u^μ

$$\partial_\mu = u_\mu D + \nabla_\mu. \tag{4.23}$$

Note that D reduces to the time derivative and ∇_μ to the spatial derivatives in the fluid rest frame. The equation of motion for ideal hydrodynamics are given by the projection along and transverse to u^μ of the energy-momentum conservation laws. The equations $u_\mu \partial_\nu T^{\mu\nu}_{(0)} = 0$ and $\Delta^\alpha_\mu \partial_\nu T^{\mu\nu}_{(0)} = 0$ give respectively

$$D\epsilon + (\epsilon + P)\partial_\mu u^\mu = 0, \tag{4.24}$$

$$(\epsilon + P)Du^\alpha - \nabla^\alpha P = 0. \tag{4.25}$$

These are the fundamental equations that govern ideal hydrodynamics. To understand their physical meaning, it is useful to calculate the non-relativistic limit, i.e. when the fluid 3-velocity $\mathbf{v}$ is small ($|\mathbf{v}| \ll 1$). Moreover, in order to obtain a meaningful non-relativistic reduction, we relax the condition that the baryon chemical potential is zero, and assume that the number of antiparticles is negligible. The differential operators defined in Eq. (4.22) reduce to

$$D \simeq \partial_t + \mathbf{v}\cdot\boldsymbol{\partial} + \mathcal{O}(|\mathbf{v}|^2), \qquad \nabla_\mu \simeq \partial^i + \mathcal{O}(|\mathbf{v}|). \tag{4.26}$$

Furthermore, if we assume that for a non relativistic system the pressure is much smaller than the energy density ($P \ll \epsilon$) and the energy can be approximated with the mass density $\rho \simeq \epsilon$, Eqs. (4.24)-(4.25) reduce to

$$\partial_t \rho + \rho\,\boldsymbol{\partial}\cdot\mathbf{v} + \mathbf{v}\cdot\boldsymbol{\partial}\rho = 0, \tag{4.27}$$

$$\partial_t \mathbf{v} + (\mathbf{v}\cdot\boldsymbol{\partial})\mathbf{v} + \frac{1}{\rho}\boldsymbol{\partial} P = 0, \tag{4.28}$$

respectively. The first of the above equations is the non-relativistic continuity equation and the second is the non relativistic Euler's equation saying that the fluid acceleration is due to the pressure gradient.

We end this Section by briefly giving a generalization to a covariant form of the equilibrium thermodynamic laws discussed in Section 4.1 [94, 95]. In order to do that, It is useful to define the quantities

$$\beta \equiv \frac{1}{T}, \quad \beta^{\mu} \equiv \frac{u^{\mu}}{T}. \tag{4.29}$$

We can write the covariant Euler's and Gibbs-Duhem relation in Eqs. (4.7) and (4.8) respectively as

$$S^{\mu}_{(0)} = P\beta^{\mu} + \beta_{\nu} T^{\mu\nu}_{(0)}, \tag{4.30}$$

$$d\left(P\beta^{\mu}\right) = -T^{\mu\nu}_{(0)} d\beta_{\nu}. \tag{4.31}$$

Consequently, Eq. (4.9) can be generalized as

$$dS^{\mu}_{(0)} = \beta_{\nu} dT^{\mu\nu}_{(0)}. \tag{4.32}$$

The second law of thermodynamics states that the entropy of an isolated system can only increase or remain constant over time. The entropy remains constant only if the system is in a thermodynamic equilibrium state or can go through a reversible process. For a state in equilibrium we can express the second law covariantly as

$$\partial_{\mu} S^{\mu}_{(0)} = 0. \tag{4.33}$$

In general we write

$$\partial_{\mu} S^{\mu} \geq 0. \tag{4.34}$$

4.3 Relativistic dissipative fluid dynamics

As already mentioned, an ideal fluid is characterized by the assumption of local equilibrium. However, quantum mechanics gives fundamental constraints on dissipation effects based on the uncertainty principle [96] implying that, in practice, in nature all fluids are dissipative. Therefore local equilibrium is a strong assumption for a realistic description of the fluid dynamics. Dissipation is caused by the presence of irreversible thermodynamic processes. A fluid, for example, can loose energy from the friction experienced by the movement of adjacent fluid layers. This leads to the fact that different layers of the fluid move with different velocities. This property is called shear viscosity. A fluid can also experience an internal friction called bulk viscosity due to the compression and expansion of the fluid.

The basic equations describing a dissipative fluid are still given by energy-momentum conservation and formally we have the same equations as in the ideal case

$$\partial_{\mu} T^{\mu\nu} = 0. \tag{4.35}$$

The difference is that now, since we do not assume local thermodynamic equilibrium, the energy-momentum tensor $T^{\mu\nu}$ is not diagonal anymore in the fluid rest frame and the system in no longer isotropic. A dissipative fluid dynamic framework can be applied if the

dissipative effects are small. We introduce the dissipation tensor $\Pi^{\mu\nu}$ that will correct the ideal fluid energy-momentum tensor in the form

$$T^{\mu\nu} = T^{\mu\nu}_{(0)} + \Pi^{\mu\nu}. \tag{4.36}$$

We can decompose the dissipation tensor in the following way

$$\Pi^{\mu\nu} = \pi^{\mu\nu} + \Delta^{\mu\nu}\Pi\,, \tag{4.37}$$

where the first term is traceless ($\pi^{\mu}_{\mu} = 0$) and Π is a scalar quantity. Using Eq. (4.20), we find

$$T^{\mu\nu} = \epsilon u^{\mu}u^{\nu} - (P+\Pi)\Delta^{\mu\nu} + \pi^{\mu\nu}. \tag{4.38}$$

In order to find the equation of motion for a dissipative fluid, we proceed as in the ideal case. We project the conservation laws (4.35) parallel and and orthogonal to u^{μ}, using the form for the energy-momentum tensor in (4.38). The projections $u_{\mu}\partial_{\nu}T^{\mu\nu} = 0$ and $\Delta^{\alpha}_{\mu}\partial_{\nu}T^{\mu\nu} = 0$ yield respectively

$$D\epsilon + (\epsilon + P + \Pi)\partial_{\mu}u^{\mu} - \pi^{\mu\nu}\sigma_{\mu\nu} = 0, \tag{4.39}$$

$$(\epsilon + P + \Pi)Du^{\alpha} - \nabla^{\alpha}(P+\Pi) + \Delta^{\alpha}_{\mu}\partial_{\nu}\pi^{\mu\nu} = 0, \tag{4.40}$$

with $\sigma^{\mu\nu} \equiv \nabla^{(\mu}u^{\nu)}$. Here the brackets denote the symmetrization of the indices (i.e. $A^{(\mu}B^{\nu)} = \frac{1}{2}(A^{\mu}B^{\nu} + A^{\nu}B^{\mu})$). Equations (4.39) and (4.40) are the fundamental equations for relativistic viscous hydrodynamics.

In order to find the explicit form for $\pi^{\mu\nu}$ and Π, we exploit the second law of thermodynamics stating that the entropy never decreseaes, $\partial_{\mu}S^{\mu} \geq 0$, introduced in the previous Section. We assume that the dissipation effects are small so that we can extend the Euler relation in Eq. (4.30) valid for ideal fluids to the case of dissipative fluids [97, 98]. In practice, even though there is no local equilibrium anymore, we assume that the thermodynamic relations are satisfied as if in equilibrium. Therefore, from Eq. (4.30), we now have

$$S^{\mu} = P\beta^{\mu} + \beta_{\nu}T^{\mu\nu}. \tag{4.41}$$

After taking the divergence of the previous equation and substituting the viscous equations of motion (4.39)-(4.40), we get

$$\partial_{\mu}S^{\mu} = -\beta\,\Pi\partial_{\mu}u^{\mu} + \beta\,\pi^{\mu\nu}\sigma_{\mu\nu}. \tag{4.42}$$

In order to satisfy the second law of thermodynamics we must impose that the change of entropy above is greater or equal than zero. A sufficient condition is to assume

$$\Pi = -\zeta\,\partial_{\mu}u^{\mu}, \tag{4.43}$$

$$\pi^{\mu\nu} = 2\eta\sigma^{\mu\nu}, \tag{4.44}$$

so that

$$\partial_{\mu}S^{\mu} = \frac{\beta}{\zeta}\Pi^2 + \frac{\beta}{2\eta}\pi_{\mu\nu}\pi^{\mu\nu}. \tag{4.45}$$

The trace of the square of a symmetric matrix is positive and hence we have $\pi_{\mu\nu}\pi^{\mu\nu} \geq 0$. We can conclude that the right-hand side of Eq. (4.45) is a positive sum of squares. The equations (4.43) are the relativistic Navier-Stokes equations.

4.4 Bjorken flow

In high-energy heavy-ion collisions the two nuclei pass through each other in a time which is of the order of 0.15 fm. This time is much smaller than the transverse size of the colliding nuclei. Therefore, it makes sense to assume that the longitudinal momentum of the particles is much bigger than their transverse momentum and the matter expansion is predominantly along the beam axis z. After the collision, all the particles are created in a short space-time interval around $z = 0$ and time $t = 0$. Normally, the basic assumption is that around the space-time origin, the motion of particles along the beam axis is uniform, meaning that the velocity of the particles is given by

$$v_z = \frac{z}{t}. \tag{4.46}$$

In a hydrodynamical picture, we can indentify in this case the velocity of the particles with the velocity of the fluid. It can be shown using the hydrodynamic equations that Eq. (4.46) is also a solution at later times. This is called the Bjorken picture [99]. The Bjorken picture was developed and extended in [96, 100, 101]. The Bjorken prescription is boost-invariant in the sense that if we make a Lorentz boost along the beam axis, the relation $v_z = z/t$ still holds in the new frame, even though the quantities z, t and v_z change. It is convenient to change the (t, z) variables into the proper time τ and the space-time rapidity η thorough the relation

$$\tau = \sqrt{t^2 - z^2}, \tag{4.47a}$$

$$\eta = \frac{1}{2}\log\left(\frac{t+z}{t-z}\right) = \operatorname{artanh}\left(\frac{z}{t}\right). \tag{4.47b}$$

Hence, we have $t = \tau\cosh\eta$ and $z = \tau\sinh\eta$. The non-zero components of the fluid 4-velocity are $u^0 = t/\tau$ and $u^z = z/\tau$. Therefore, the fluid 4-velocity can also be expressed as

$$u^\mu = (\cosh\eta, 0, 0, \sinh\eta). \tag{4.48}$$

We can also derive the energy density evolution for an ideal Bjorken expansion. In this case, Eq. (4.24) can be written as

$$\frac{\partial\epsilon}{\partial\tau} + \frac{\epsilon + P}{\tau} = 0. \tag{4.49}$$

If we assume a conformal equation of state $\epsilon = 3P \propto T^4$, we obtain the temperature as a function of the proper time

$$T(\tau) = T_0\left(\frac{\tau_0}{\tau}\right)^{1/3}, \tag{4.50}$$

where τ_0 is the proper time of the initial stage of heavy-ion collisions we are considering, and T_0 the corresponding temperature. For a conformal equation of state, the entropy density is given by $s \propto T^3$. Hence, Eq. (4.50) implies that $s\tau$ is constant and the entropy of the unit cell is conserved.

Chapter 5

Virtual photon polarization and dilepton anisotropy in heavy-ion collisions

In this Chapter we study the effect of a thermalized medium on the anisotropy coefficients. We will specifically consider a medium formed in heavy-ion collisions. In Section 5.1, a simple expression for the structure function is derived, and a general form for the current-correlation function is given in presence of an additional anisotropy vector. In Section 5.2 we study the connection between the anisotropy coefficient and the velocity profile characterizing the medium. The explicit form for the current-correlation function for Drell-Yan and pion annihilation process are given In Section 5.3. Furthermore, in Section 5.4 we illustrate three velocity profiles: a static uniform medium, a longitudinal Bjorken expansion, and a Bjorken expansion combined with a radial expansion, transverse to the beam axis. Finally, numerical results are presented in Section 5.5.

5.1 Dilepton production rate

Let us consider a process of the type $X_1X_2 \to \gamma^* \to e^+e^-$, where X_1 and X_2 are two particles in a thermalized medium, γ^* is the virtual photon which decays into an electron and a positron. The rate per unit volume at finite temperature for this process is given by Eq. (3.39)

$$\frac{d\Gamma}{d^4q} = \frac{e^2}{q^4}\int \frac{d^3l_+}{(2\pi)^3 2E_+}\frac{d^3l_-}{(2\pi)^3 2E_-}\delta^{(4)}(q-l_+-l_-)W^{\mu\nu}L_{\mu\nu}, \tag{5.1}$$

where $E_\pm = \sqrt{|\mathbf{l}_\pm|^2 + m^2}$, e the electron charge and $L_{\mu\nu}$ the lepton tensor

$$L^{\mu\nu} = 2(-q^2 g^{\mu\nu} + q^\mu q^\nu - \Delta l^\mu \Delta l^\nu). \tag{5.2}$$

In the above equation, $q^\mu = l_+^\mu + l_-^\mu$ is the virtual photon momentum, and l_+ and l_- are the positron and electron momenta, respectively, while $\Delta l^\mu = l_+^\mu - l_-^\mu$. The tensor $W^{\mu\nu}$ is the electromagnetic current correlation function discussed in Chapter 3, which can be written as

$$W^{\mu\nu} = \langle w^{\mu\nu}\rangle, \tag{5.3}$$

where $w^{\mu\nu}$ is given below and we have introduced the notation

$$\langle A\rangle = \int \frac{d^3p_1}{(2\pi)^3 2E_1}\frac{d^3p_2}{(2\pi)^3 2E_2}(2\pi)^4\delta^{(4)}(q-p_1-p_2)\frac{1}{e^{(u\cdot p_1)/T}\pm 1}\frac{1}{e^{(u\cdot p_2)/T}\pm 1}A. \tag{5.4}$$

Here p_1, p_2 are the momenta of X_1 and X_2, respectively, $E_{1,2} = \sqrt{|\mathbf{p}_{1,2}|^2 + m^2}$ and T is the temperature. The plus and minus sign in the distribution functions apply for fermions and bosons, respectively. In the above equation, u^μ is the 4-velocity of the medium

$$u^\mu = (\gamma, \gamma\mathbf{v}), \tag{5.5}$$

with $\mathbf{v}$ the 3-velocity and $\gamma = 1/\sqrt{1-|\mathbf{v}|^2}$ the Lorentz factor. Moreover $u^\mu u_\mu = 1$. The tensor $w^{\mu\nu}$ in Eq. (5.3) is given in terms of the corresponding vacuum matrix element of the electromagnetic-current operator J_μ,

$$w_{\mu\nu} = \sum_{\text{pol}} w_\mu w_\nu^*, \tag{5.6}$$

where

$$w_\mu = \langle 0|J_\mu|X_1X_2\rangle. \tag{5.7}$$

The general structure for $W^{\mu\nu}$ is discussed in Section 3.4. We rewrite it here for convenience:

$$W^{\mu\nu} = W_1\left(g^{\mu\nu} - \frac{q^\mu q^\nu}{q^2}\right) + W_2\left(u^\mu - \frac{u\cdot q}{q^2}q^\mu\right)\left(u^\nu - \frac{u\cdot q}{q^2}q^\nu\right), \tag{5.8}$$

W_1 and W_2 are Lorentz invariant functions that depend on q^2, $u\cdot q$ and the temperature T. In terms of the scalar contractions of $W^{\mu\nu}$, we obtain

$$W_1 = \frac{\alpha a - \beta}{2a}, \qquad W_2 = \frac{3\beta - \alpha a}{2a^2}, \tag{5.9}$$

where

$$\alpha \equiv g_{\mu\nu}W^{\mu\nu}, \quad \beta \equiv u_\mu u_\nu W^{\mu\nu}, \quad a \equiv 1 - \frac{(u\cdot q)^2}{q^2}. \tag{5.10}$$

In the following, we will relate the anisotropy coefficients of the dilepton angular distribution to the structure functions W_1 and W_2.

5.1.1 General structure in presence of an additional anisotropy vector

The form of the current correlation function in Eq. (5.8) presents a richer tensor structure in presence of additional anisotropy vectors describing the system. In general, one can consider other anisotropies besides those induced by the medium profile. In heavy-ion collisions, for example, one can think of anisotropies of the quarks and gluons distribution functions [102], meaning that the distributions functions are not spherically symmetric in the fluid rest frame. An other kind of anisotropy one can encounter in heavy-ion collisions is the presence of a magnetic field. Hence, in order to generalize Eq. (5.8), we need to introduce an other 4-vector in the problem, we call it n^μ, which defines the anisotropic direction. We assume that n^μ is a space-like vector and, in the fluid rest frame, can be written as

$$n^\mu = (0, \mathbf{n}), \tag{5.11}$$

with $|\mathbf{n}|^2 = 1$. Following the arguments given in Section 3.4, we construct the most general tensor structure such that $W^{\mu\nu}$ is current conserving and symmetric. One can show that $W^{\mu\nu}$ in Eq. (5.8) is extended by adding two further structures. In total we will thus have four different structures. One can write

$$W^{\mu\nu} = \sum_{i=1}^{4} W_i P_i^{\mu\nu}, \tag{5.12}$$

where

$$P_1^{\mu\nu} = g^{\mu\nu} - \frac{q^\mu q^\nu}{q^2}, \tag{5.13a}$$

$$P_2^{\mu\nu} = \left(u^\mu - \frac{u\cdot q}{q^2} q^\mu\right)\left(u^\nu - \frac{u\cdot q}{q^2} q^\nu\right), \tag{5.13b}$$

$$P_3^{\mu\nu} = \left(n^\mu - \frac{n\cdot q}{q^2} q^\mu\right)\left(n^\nu - \frac{n\cdot q}{q^2} q^\nu\right), \tag{5.13c}$$

$$P_4^{\mu\nu} = \left(n^\mu - \frac{n\cdot q}{q^2} q^\mu\right)\left(u^\nu - \frac{u\cdot q}{q^2} q^\nu\right) + \left(n^\nu - \frac{n\cdot q}{q^2} q^\nu\right)\left(u^\mu - \frac{u\cdot q}{q^2} q^\mu\right). \tag{5.13d}$$

5.2 Dilepton angular distribution

Starting from Eq. (5.1), we can write the angular distribution of the dilepton expressing the lepton phase space in the photon rest frame as

$$\frac{d\Gamma}{d^4q\, d\Omega_e} \propto \frac{1}{q^4} W_{\mu\nu} L^{\mu\nu}. \tag{5.14}$$

Using Eq. (5.2) and Eq. (5.8), the angular distributions becomes:

$$\frac{d\Gamma}{d^4q\, d\Omega_e} \propto \frac{1}{q^4}(-3q^2 - \Delta l^2) W_1 + \frac{1}{q^4}\left[-q^2 + (u\cdot q)^2 - (u\cdot \Delta l)^2\right] W_2. \tag{5.15}$$

We want to express the angular distribution in the rest frame of the virtual photon, in particular we choose the helicity frame. In this frame, the fluid 4-velocity and the difference of the lepton 4-momenta can in general be written as

$$u^\mu = \gamma(1, |\mathbf{v}|\sin\theta_v\cos\phi_v, |\mathbf{v}|\sin\theta_v\sin\phi_v, |\mathbf{v}|\cos\theta_v), \tag{5.16}$$

$$\Delta l^\mu = (0, 2|\mathbf{l}|\sin\theta_e\cos\phi_e, 2|\mathbf{l}|\sin\theta_e\sin\phi_e, 2|\mathbf{l}|\cos\theta_e), \tag{5.17}$$

where θ_e and ϕ_e are respectively the polar and azimuthal angles of the negative lepton, while θ_v and ϕ_v the polar and azimuthal angles of the fluid 3-velocity, see Figure 5.1. The polar angles are measured with respect to the direction of the photon 3-momentum which defines the helicity frame[1]. The azimuthal angle is measured with respect to the production plane, i.e. the plane formed by the 3-momenta of the two initial ion beams and the photon. We note that in Eq. (5.15) the dependence on the angles of the leptons is only present in the term $(u\cdot\Delta l)^2$. Using Eqs. (5.16) and (5.17), we obtain

[1] The direction of the photon defined in the photon rest frame has the usual meaning, i.e. it is the direction that the photon had before boosting to go to its rest frame.

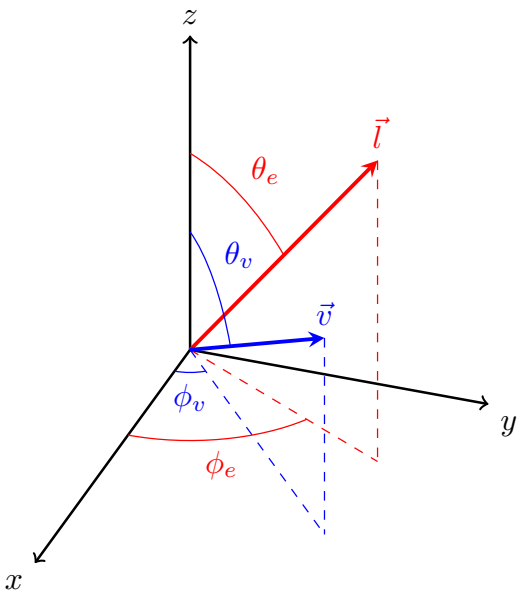

Figure 5.1.: Polar coordinates of the lepton 3-momentum and the fluid 3-velocity in the helicity frame. The z axis is the direction of the photon 3-momentum and the xz-plane is the production plane.

$$(u\cdot\Delta l)^2 = 4\gamma^2|\mathbf{v}|^2|\mathbf{l}|^2(\lambda_0' + \lambda_\theta' \cos^2\theta_e + \lambda_\phi' \sin^2\theta_e \cos 2\phi_e + \lambda_{\theta\phi}' \sin 2\theta_e \cos\phi_e + \lambda_\phi^{\perp\prime} \sin^2\theta_e \sin 2\phi_e + \lambda_{\theta\phi}^{\perp\prime} \sin 2\theta_e \sin\phi_e). \tag{5.18}$$

We note that Eq. (5.18) has the same angular dependence as the general expression for the angular distribution Eq. (1.72), where the anisotropy coefficients are given by

$$\lambda_0' = \frac{1}{2}\sin^2\theta_v, \tag{5.19a}$$
$$\lambda_\theta' = \frac{1}{2}(3\cos^2\theta_v - 1), \tag{5.19b}$$
$$\lambda_\phi' = \frac{1}{2}\sin^2\theta_v \cos 2\phi_v, \tag{5.19c}$$
$$\lambda_{\theta\phi}' = \frac{1}{2}\sin 2\theta_v \cos\phi_v, \tag{5.19d}$$
$$\lambda_\phi^{\perp\prime} = \frac{1}{2}\sin^2\theta_v \sin 2\phi_v, \tag{5.19e}$$
$$\lambda_{\theta\phi}^{\perp\prime} = \frac{1}{2}\sin 2\theta_v \sin\phi_v. \tag{5.19f}$$

After plugging Eq. (5.18) into Eq. (5.15), we obtain the general expression for the angular distribution

$$\frac{d\sigma}{d\Omega_e} \propto \mathcal{N}(1 + \lambda_\theta \cos^2\theta_e + \lambda_\phi \sin^2\theta_e \cos 2\phi_e + \lambda_{\theta\phi} \sin 2\theta_e \cos\phi_e + \lambda_\phi^\perp \sin^2\theta_e \sin 2\phi_e + \lambda_{\theta\phi}^\perp \sin 2\theta_e \sin\phi_e), \tag{5.20}$$

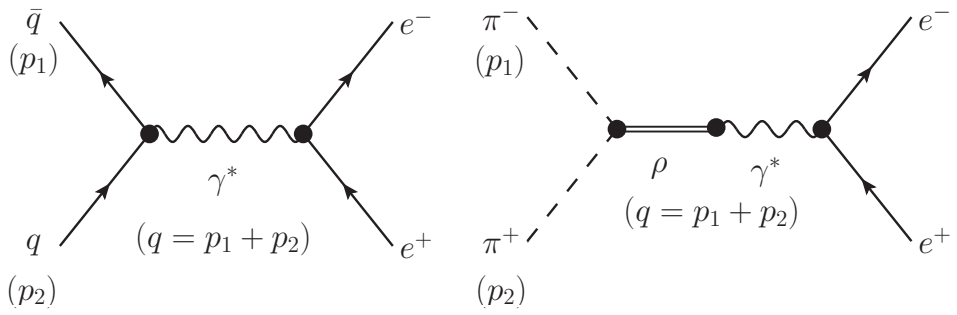

Figure 5.2.: Feynman diagrams for the Drell-Yan and pion annihilation processes

with the anisotropy coefficients and normalization defined as

$$\lambda_i = -W_2 4\gamma^2 |\mathbf{v}|^2 |\mathbf{l}|^2 \lambda_i', \tag{5.21}$$

$$\mathcal{N} = (-3q^2 - \Delta l^2) W_1 + [-u^2 q^2 + (u\cdot q)^2 - 4\gamma^2 |\mathbf{v}|^2 |\mathbf{l}|^2 \lambda_0'] W_2, \tag{5.22}$$

where $\lambda_i = \lambda_\theta, \lambda_\phi, \lambda_{\theta\phi}, \lambda_\phi^\perp, \lambda_{\theta\phi}^\perp$ and $\lambda_i' = \lambda_\theta', \lambda_\phi', \lambda_{\theta\phi}', \lambda_\phi^{\perp\prime}, \lambda_{\theta\phi}^{\perp\prime}$.

Equations (5.19), (5.21) and (5.22) clearly show that the anisotropy coefficients of dileptons originating from a thermal medium do not depend only on the process producing the virtual photon, but also on the shape of the velocity profile of the fluid. In particular, the value of the anisotropy coefficients depend on the shape of the velocity profile as seen in the photon rest frame. From Eqs. (5.19) and Figure 5.1 we see that, if the velocity distribution in the photon rest frame lies in the production plane, i.e. the xz-plane, in general the only non-vanishing coefficients will be λ_θ, λ_ϕ and $\lambda_{\theta\phi}$ because $\phi_v = 0$ (or $\phi_v = \pi$). If, instead, $|\mathbf{v}|$ has non-vanishing components out of the production plane, then in general also $\lambda_\phi^\perp$ and $\lambda_{\theta\phi}^\perp$ will be different from zero. In the next Section we will see how these arguments apply to the velocity distribution in the case of a static medium, a longitudinal Bjorken expansion and the case where we also have a radial expansion transverse to the beam axis.

In order to compute the angular distribution of the lepton pair originating from the medium, we can alternatively use the spin density matrix formalism. The definition of the spin density for the production and the decay of the virtual photon are discussed in Section 1.4. The tensor $W^{\mu\nu}$ describing the production of the virtual photon in the definition of the spin density matrix Eq. (1.57) is now given by Eq. (5.8).

5.3 Drell-Yan and pion annihilation

For the Drell-Yan process (i.e. quark-antiquark annihilation $q\bar{q} \to e^+e^-$) the expression for the $w^{\mu\nu}$ tensor of Eq. (5.6) is formally the same as the lepton tensor:

$$w^{\mu\nu} = 2(-q^2 g^{\mu\nu} + q^\mu q^\nu - \Delta p^\mu \Delta p^\nu), \tag{5.23}$$

where $\Delta p^\mu = p_1^\mu - p_2^\mu$, p_1 and p_2 being the momenta of the initial particles. The scalar contractions $\alpha \equiv g_{\mu\nu} W^{\mu\nu}$ and $\beta \equiv u_\mu u_\nu W^{\mu\nu}$ are given by

$$\alpha = 2(-3q^2 - \Delta p^2)\langle 1 \rangle, \tag{5.24}$$

$$\beta = 2((u\cdot q)^2 - u^2q^2)\langle 1\rangle - 2\langle (u\cdot\Delta p)^2\rangle, \tag{5.25}$$

where we used the notation introduced in Eq. (5.4). In the case of pion annihilation (i.e. $\pi^+\pi^- \to e^+e^-$), the vertex that couples pions to the electromagnetic radiation is proportional to the difference of the momenta of the two pions (cf. Eq. (2.10)). Therefore, we simply have

$$w^{\mu\nu} = \Delta p^\mu \Delta p^\nu, \tag{5.26}$$

which leads to

$$\alpha = \Delta p^2\langle 1\rangle, \quad \beta = \langle (u\cdot\Delta p)^2\rangle. \tag{5.27}$$

As shown in Figure 5.2, the two pions annihilate into a ρ meson which converts into a photon through vector meson dominance. Strictly speaking, in the calculation of the anisotropy coefficients, one should also take into account the ρ propagator. However, in the analysis done in this Chapter, we will always consider the dilepton invariant mass to be fixed. As a consequence the Breit-Wigner function in the ρ propagator yields a multiplicative factor, which cancels in the computation of polarization observables.

5.4 Medium and flow

We can now study how different velocity profiles of the medium affect the anisotropy coefficients. We consider three cases: (i) a static medium with uniform temperature, (ii) a longitudinally expanding system with Bjorken flow and (iii) a longitudinal Bjorken flow plus a radial expansion transverse to the beam axis.

5.4.1 Static uniform medium

Let us consider a non-expanding medium of uniform energy density. In the helicity frame (HX), the fluid velocity is given by

$$u^\mu_{HX} = \gamma_z(1,\ 0,\ 0,\ v_z), \quad v_z = -\frac{|\mathbf{q}|}{E_\gamma}, \tag{5.28}$$

where $\gamma_z \equiv 1/\sqrt{1-v_z^2}$, $E_\gamma = q^0$ and $\mathbf{q}$ are the energy and momentum of the virtual photon, respectively, in the fluid frame. It is clear from geometrical arguments that the velocity of the medium seen in the photon rest frame is exactly along the same axis as the photon momentum in the photon rest frame, but in the opposite direction. This means that the polar angles of the velocity in Eqs. (5.19) are $\theta_v = \pi$ and $\phi_v = 0$, implying that, in the HX, only the anisotropy coefficients λ_θ contributes to the dilepton angular distribution. Hence, for a static uniform medium, the dilepton angular distribution in the helicity frame cannot exhibit a dependence on the azimuthal angle. In other words, the photon 3-momentum breaks the spherical symmetry of the static medium, but the azimuthal symmetry around the photon momentum is preserved. Therefore, Eq. (5.15) simplifies to the following form

$$\frac{d\Gamma}{d^4q\,d\Omega_e} \propto -2W_1 + W_2\frac{|\mathbf{q}|^2}{M^2} - W_2\frac{|\mathbf{q}|^2}{M^2}\cos^2\theta_e. \tag{5.29}$$

To obtain the above equation, we made use of the relation $\gamma_z v_z = |\mathbf{q}|/M$, with M the invariant mass of the lepton pair, and we assumed massless leptons. The anisotropy coefficient is thus given by

$$\lambda_\theta = -\frac{W_2 \frac{|\mathbf{q}|^2}{M^2}}{-2W_1 + W_2 \frac{|\mathbf{q}|^2}{M^2}}. \tag{5.30}$$

We can also compute the spin density matrix in the helicity frame using the tensor (5.8), the polarization vectors (1.17) and the fluid velocity boosted to the photon rest frame (5.28). One obtains

$$\rho^{\text{prod}}_{\lambda',\lambda} = \begin{pmatrix} -W_1 & 0 & 0 \\ 0 & -W_1 + W_2 \frac{|\mathbf{q}|^2}{M^2} & 0 \\ 0 & 0 & -W_1 \end{pmatrix}, \tag{5.31}$$

which clearly leads to the same anisotropy λ_θ in (5.30) through Eq. (1.73a). The photon has no vector polarization, but rather it is tensor polarized along the direction defined by its momentum, compare Eqs. (5.31) and (1.50).

In Section 3.5, we saw that, in the Boltzmann limit, W_2 vanishes. This implies that the anisotropy Eq. (5.30) also vanishes. Hence, Boltzmann statistics gives rise to unpolarized photons [86]. Thus, we conclude that photon polarization is an effect due to quantum statistics.

In the photon rest frame, it is simple to perform the phase-space integrals in Eq. (5.3) to obtain W_1 and W_2 from Eq. (5.9). The average defined in Eq. (5.4) reduces to

$$\langle A \rangle = \frac{1}{8\pi} \int_{-1}^{1} d(\cos\theta_p)\, \chi\, \frac{1}{e^{(u\cdot p_1)/T} \pm 1}\, \frac{1}{e^{(u\cdot p_2)/T} \pm 1} A, \tag{5.32}$$

where $\chi \equiv \sqrt{1 - 4m^2/M^2}$, M is the invariant mass of the virtual photon, m the mass of the initial particles, θ_p is the angle between the initial particle 3-momentum and the fluid 3-velocity, and

$$u \cdot p_1 = \frac{E_\gamma}{2} + \frac{|\mathbf{q}|}{2}\, \chi\, \cos\theta_p, \tag{5.33}$$

$$u \cdot p_2 = \frac{E_\gamma}{2} - \frac{|\mathbf{q}|}{2}\, \chi\, \cos\theta_p. \tag{5.34}$$

For a static and uniform medium, the integration over space-time yields just a constant factor (the volume of the system times the emission duration), which cancels in the evaluation of the anisotropy coefficients.

For the sake of completeness, we compute the spin density matrix elements in the case where we also have an additional anisotropy vector n^μ. The general form for $W^{\mu\nu}$ is given by Eqs. (5.12) and (5.13). In order to calculate the elements of the spin density matrix explicitly, we need to give an expression for n^μ in the photon rest frame. The vector n^μ has only space components in the local rest frame. Let us define the angle θ_{qn} as the angle between $\mathbf{q}$ and $\mathbf{n}$ in the fluid rest frame, and the xz-plane the plane containing $\mathbf{q}$ and $\mathbf{n}$. Thus, in the helicity frame, the anisotropy vector takes the form

$$n^\mu_{HX} = \left(-\frac{|\mathbf{q}|}{M} \cos\theta_{qn},\, -\sin\theta_{qn},\, 0,\, \frac{E_\gamma}{M} \cos\theta_{qn} \right). \tag{5.35}$$

Using again the polarization vectors (1.17) and the tensors (5.13), we find

$$(\epsilon_\mu(-1))^* P_3^{\mu\nu} \epsilon_\mu(-1) = (\epsilon_\mu(+1))^* P_3^{\mu\nu} \epsilon_\mu(+1) = \frac{\sin^2\theta_{qn}}{2}, \tag{5.36}$$

$$(\epsilon_\mu(0))^* P_3^{\mu\nu} \epsilon_\mu(0) = \frac{E_\gamma^2}{M^2}\cos^2\theta_{qn}, \tag{5.37}$$

$$(\epsilon_\mu(-1))^* P_3^{\mu\nu} \epsilon_\mu(0) = -(\epsilon_\mu(0))^* P_3^{\mu\nu} \epsilon_\mu(+1) = -\frac{E_\gamma}{M}\frac{\sin 2\theta_{qn}}{2\sqrt{2}}, \tag{5.38}$$

$$(\epsilon_\mu(-1))^* P_3^{\mu\nu} \epsilon_\mu(+1) = -\frac{\sin^2\theta_{qn}}{2}, \tag{5.39}$$

and

$$(\epsilon_\mu(0))^* P_4^{\mu\nu} \epsilon_\mu(0) = -\frac{2|\mathbf{q}|E_\gamma}{M^2}\cos\theta_{qn}, \tag{5.40}$$

$$(\epsilon_\mu(-1))^* P_4^{\mu\nu} \epsilon_\mu(0) = -(\epsilon_\mu(0))^* P_4^{\mu\nu} \epsilon_\mu(+1) = \frac{|\mathbf{q}|}{M}\frac{\sin\theta_{qn}}{\sqrt{2}}. \tag{5.41}$$

Hence, the elements of the production spin density matrix are given by

$$\rho^{\text{prod}}_{-1-1} = \rho^{\text{prod}}_{+1+1} = -W_1 + \frac{W_3}{2}\sin^2\theta_{qn}, \tag{5.42}$$

$$\rho^{\text{prod}}_{00} = -W_1 + W_2\frac{|\mathbf{q}|^2}{M^2} + W_3\frac{E_\gamma^2}{M^2}\cos^2\theta_{qn}, \tag{5.43}$$

$$\rho^{\text{prod}}_{-10} = -\rho^{\text{prod}}_{0+1} = -\frac{W_3}{2\sqrt{2}}\frac{E_\gamma}{M}\sin 2\theta_{qn} + \frac{W_4}{\sqrt{2}}\frac{|\mathbf{q}|}{M}\sin\theta_{qn}, \tag{5.44}$$

$$\rho^{\text{prod}}_{-1+1} = -\frac{W_3}{2}\sin^2\theta_{qn}. \tag{5.45}$$

We can now compute the anisotropy coefficients using Eqs. (1.73):

$$\lambda_\theta = \frac{1}{\mathcal{N}}\left[-W_2\frac{|\mathbf{q}|^2}{M^2} + \frac{W_3}{2}\left(\sin^2\theta_{qn} - 2\frac{E_\gamma^2}{M^2}\cos^2\theta_{qn}\right)\right], \tag{5.46a}$$

$$\lambda_\phi = -\frac{1}{\mathcal{N}}\frac{W_3}{2}\sin^2\theta_{qn}, \tag{5.46b}$$

$$\lambda_{\theta\phi} = \frac{1}{\mathcal{N}}\left(W_3\frac{E_\gamma}{2M}\sin 2\theta_{qn} - W_4\frac{|\mathbf{q}|}{M}\sin\theta_{qn}\right), \tag{5.46c}$$

with the normalization factor

$$\mathcal{N} = -2W_1 + W_2\frac{|\mathbf{q}|^2}{M^2} + \frac{W_3}{2}\left(\sin^2\theta_{qn} - 2\frac{E_\gamma^2}{M^2}\cos^2\theta_{qn}\right). \tag{5.47}$$

In presence of an anisotropy vector the azimuthal symmetry around the photon momentum is broken and we see from Eqs. (5.46) that, in general, the coefficients λ_ϕ and $\lambda_{\theta\phi}$ in the helicity frame are also non vanishing. In the particular case where $\mathbf{n}$ and $\mathbf{q}$ are parallel or antiparallel, λ_ϕ and $\lambda_{\theta\phi}$ vanish because clearly the anisotropic direction and the photon momentum are not independent anymore and therefore the azimuthal symmetry atound the photon momentum has to be restored. In the rest of the discussion of this Chapter, in order to isolate the effect of the fluid velocity profile, we will not consider any additional anisotropic vector n^μ, and we will deal only with the structure functions W_1 and W_2.

5.4.2 Longitudinal Bjorken flow

In the case of transversely homogeneous and purely-longitudinal boost-invariant expansion [99], all scalar functions of space and time depend only on the longitudinal proper time $\tau \equiv \sqrt{t^2 - z^2}$. As discussed in Section 4.4, the fluid four-velocity in the lab frame can be written as

$$u^{\mu}_{LAB} = (\cosh\eta,\ 0,\ 0,\ \sinh\eta), \tag{5.48}$$

where $\eta \equiv \text{artanh}(z/t)$ is the space-time rapidity. In the absence of viscosity, the temperature evolution of the system is governed by the Bjorken's scaling solution, $T \propto \tau^{-1/3}$.

The photon momentum in the lab frame can be written as

$$q^{\mu}_{LAB} = \left(M_T \cosh y,\ q_T \cos\phi_y,\ q_T \sin\phi_y,\ M_T \sinh y\right), \tag{5.49}$$

where y is the longitudinal rapidity of the photon, q_T is its transverse momentum, $M_T \equiv \sqrt{M^2 + q_T^2}$, and ϕ_y its azimuthal angle. In this case, it is more convenient to carry out the initial particle integration (5.4) in the local rest frame.

In contrast to the static medium case, in the longitudinal Bjorken expansion, there are three non-vanishing anisotropy coefficients in Eq. (1.72) in the helicity (HX) frame, namely λ_θ, λ_ϕ and $\lambda_{\theta\phi}$. To understand this, we note that in the local fluid rest frame we have only the anisotropy due to the photon momentum. As already discussed in the previous Section, this leads to an angular distribution where there is only a dependence on the polar angle, where the polar angle is measured with respect to the direction of the photon momentum as seen in the fluid rest frame. Let us call this frame HX'. In other words, each of the local fluid rest frames behaves as a static medium. However, the helicity frame is properly defined by the direction of the photon momentum as seen in the lab frame. Therefore, starting from the angular distribution calculated in HX', we need to perform an additional rotation in the photon rest frame to get to HX. This rotation depends on η and y in a non-boost-invariant combination. The effect of this additional rotation is to render the coefficients λ_ϕ and $\lambda_{\theta\phi}$ different from zero (cf. Section 1.8). A schematic picture of the problem is shown in Figure 5.3, for the situation where the photon is emitted perpendicularly to the beam axis in the lab frame ($y = 0$). In the local rest frame of a fluid cell moving with velocity $v_z > 0$ ($\eta > 0$), the photon momentum is $\mathbf{q}_{LRF}$ and it defines the direction along which the photon is tensor polarized. In order to go to the HX, one has to perform a rotation of an angle δ in the production plane in the photon rest frame. This is called a Wick helicity rotation.

The appearance of the azimuthal anisotropy in the case of the Bjorken expansion can be also understood using the geometrical argument given in Section 5.2. In the HX frame, the velocity and the direction of the photon momentum are always both in the same plane which corresponds to the production plane. This means that the azimuthal angle of the velocity is $\phi_v = 0$, but θ_v is not necessarily antiparallel to the photon momentum. The result is that $\lambda^{\perp}_{\phi}$ and $\lambda^{\perp}_{\theta\phi}$ vanish, but λ_ϕ and $\lambda_{\theta\phi}$ are in general different from zero. Let us denote by $\lambda_\theta^{HX'}$ the anisotropy coefficient in the HX' frame. The explicit expression of $\lambda_\theta^{HX'}$ is formally given by Eq. (5.30), but now $|\mathbf{q}|$ has to be replaced by the photon momentum in the local rest frame $|\mathbf{q}_{LRF}|$. For the explicit form of the Lorentz transformation needed and the derivation of the expressions of the anisotropy coefficients in the HX' and HX frame, we refer the reader to Appendix C.

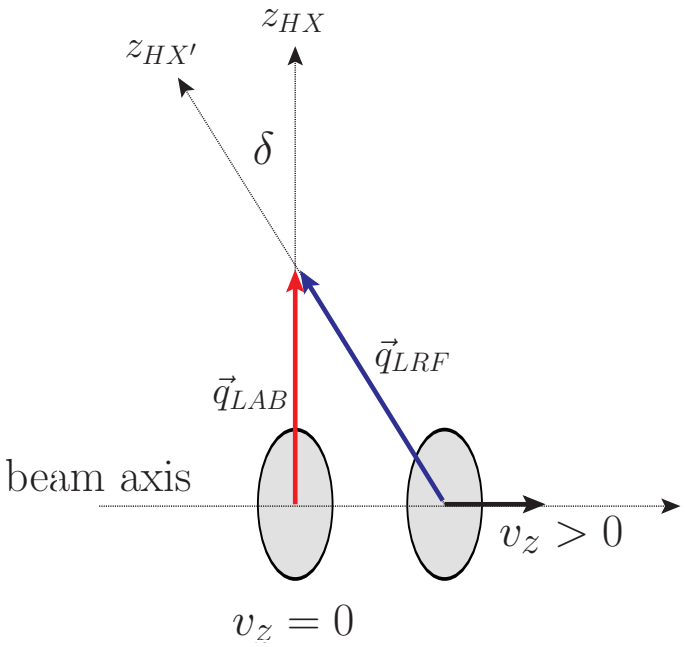

Figure 5.3.: Schematic representation of the HX and HX' frame. The vectors $\vec{q}_{LAB}$ and $\vec{q}_{LRF}$ are the photon 3-momoenta in the lab and local rest frame, respectively. Here it is depicted the case $y = 0$.

It is interesting to note that, while the anisotropy coefficients are not in general boost-invariant, the rate per unit volume $d\Gamma/d^4q$ after integrating over the lepton solid angle Ω_e in Eq. (1.72) must be boost invariant and frame invariant. This amounts to the fact that the combination $\mathcal{N}(1+\lambda_\theta/3)$ must be boost invariant. Indeed, within our calculations, we find it to be true. Moreover, we found that the combination $\mathcal{N}(\lambda_\theta + 3\lambda_\phi)$ is frame invariant and hence we have

$$\lambda_\theta^{HX'} = \frac{\mathcal{N}^{HX}}{\mathcal{N}^{HX'}}(\lambda_\theta^{HX} + 3\lambda_\phi^{HX}), \tag{5.50}$$

where the superscripts of the anisotropy coefficients denote the frame in which they are calculated. The above relation is also valid if, instead of calculating the anisotropy coefficient in HX in the right-hand side, one computes them in the Collins-Soper frame (see Section 1.8.1). We conclude that $\lambda_\theta^{HX'}$ is larger in magnitude than in any other frame. This is a consequence of the transformations Eqs. (1.112). Since in the HX' the only non vanishing coefficient is $\lambda_\theta^{HX'}$, in any other frame the anisotropy coefficients cannot be larger in magnitude than $\lambda_\theta^{HX'}$. We also point out that the combination above is frame invariant only in the case of the Bjorken expansion.

We now want to compute the effect of the space-time evolution on the anisotropy coefficient. The integration of the dilepton rate over the space-time evolution of the system is obtained from

$$\frac{dN}{d^2q_T dM^2 dy} = \pi R_A^2 \int_{\tau_i}^{\tau_f} d\tau\, \tau \int_{-\infty}^{\infty} d\eta \left(\frac{1}{2}\frac{dN}{d^4x d^4q}\right), \tag{5.51}$$

where τ_i and τ_f are initial and final proper time of the specific phase we are considering, $R_A = 1.2A^{1/3}$ is the nuclear radius, A being the nucleon number of the initial ion. The integrand in the right-hand side of Eq. (5.51) depends on T as well as the two Lorentz invariant quantities q^2 and $u\cdot q$. The dependence on the space-time variables is subsumed in $u\cdot q$ and T. When we integrate over the space-time rapidity, we include the contributions to the anisotropy coefficients emanating from all local rest frames. As already discussed, the direction specifying the HX frame is always the same for each local rest frame, but in general it differs from HX'.

5.4.3 Radial transverse expansion

In addition to the Bjorken longitudinal expansion, in this Section we also consider a radial expansion transverse to the beam-axis. The fluid four-velocity in the lab frame is given by

$$u^{\mu}_{LAB} = \gamma_r(\cosh\eta,\ v_r\cos\phi_r,\ v_r\sin\phi_r,\ \sinh\eta), \tag{5.52}$$

where $\gamma_r \equiv 1/\sqrt{1-v_r^2}$ is the transverse Lorentz factor. We consider a Hubble-like transverse expansion

$$v_r = v_0\frac{r}{R_0}, \tag{5.53}$$

where r is the radial coordinate in the transverse plane, v_0 is the maximum transverse flow velocity and R_0 is the transverse size of the medium. As in the case of pure Bjorken expansion, we perform the integration over the initial particle momenta (5.4) in the local rest frame.

From the geometrical arguments of Section 5.2, we can see that, unlike the case with only longitudinal expansion, the 3-velocity of the fluid in the rest frame of the photon has non-vanishing components out of the production plane. This means that ϕ_v is different from zero and thus, from Eq. (5.19), it is clear that the coefficients $\lambda^{\perp}_{\phi}$ and $\lambda^{\perp}_{\theta\phi}$ in general do not vanish. In other words, the difference compared to the pure Bjorken case is that now, in order to go from the HX frame to the HX', we need to perform a rotation which is not in the production plane. We find, however, that $\lambda^{\perp}_{\phi}$ and $\lambda^{\perp}_{\theta\phi}$ vanish after the space-time integration. Similarly to the pure longitudinal expansion, we can also define the HX' frame from the local rest frame and its corresponding anisotropy coefficient $\lambda_{\theta}^{HX'}$. The expression of $\lambda_{\theta}^{HX'}$ is again formally the same as in the static case Eq. (5.30), where $|\mathbf{q}|$ is replaced with the photon momentum in the local rest frame $|\mathbf{q}_{LRF}|$. For the expression of the anisotropy coefficients, see Appendix C.

5.5 Numerical results

In this Section we present the numerical results for the anisotropy coefficient λ_θ for Drell-Yan and pion annihilation process. We calculate λ_θ for a static uniform medium, a medium with longitudinal Bjorken expansion, and a medium with longitudinal Bjorken and radial transverse expansion. In the case of a pure longitudinal Bjorken expansion, we evolve the system from the initial temperature, $T_i = 500$ MeV to the final one $T_f = 160$ MeV for the Drell-Yan process and from $T_i = 160$ MeV to $T_f = 120$ MeV for pion

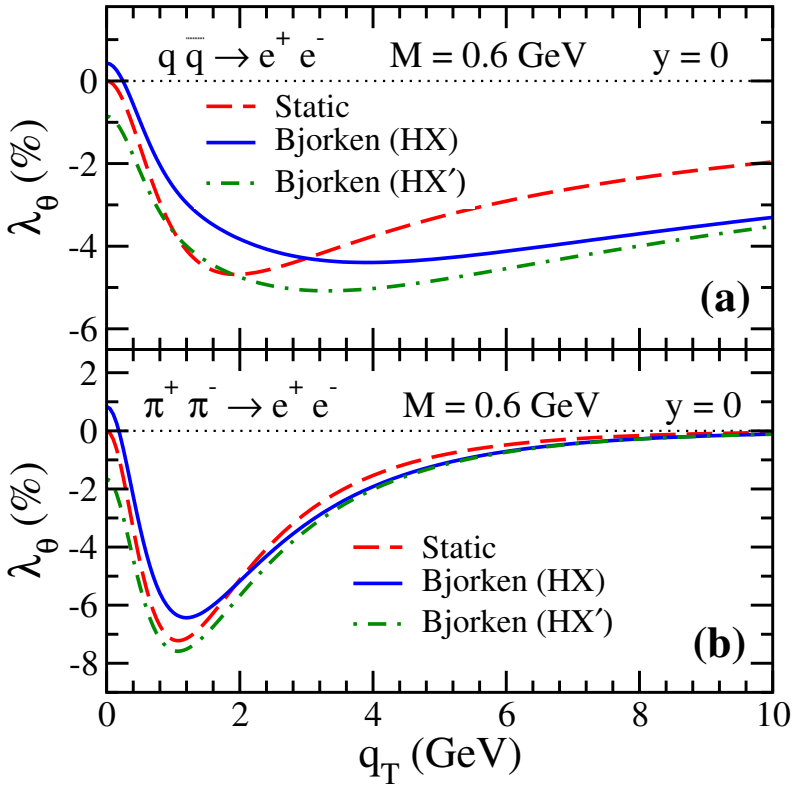

Figure 5.4.: The anisotropy coefficient λ_θ as a function of the virtual photon transverse momentum at invariant mass $M = 0.6$ GeV and photon rapidity $y = 0$ for: (a) Drell-Yan process, and (b) pion annihilation. The red dashed lines refer to the case of static uniform medium, the blue solid lines to the longitudinal Bjorken expansion in the HX frame, and the green dot dashed lines to the longitudinal Bjorken expansion in the HX' frame.

annihilation process. In the case of a uniform static medium and a longitudinal plus transverse expansion, we use the average temperature

$$T_{\rm av} = \frac{3}{2}\, T_i\, T_f \left(\frac{T_i + T_f}{T_i^2 + T_i\, T_f + T_f^2} \right), \tag{5.54}$$

obtained using Bjorken evolution, Eq. (4.50).

In Figure 5.4, we plot the anisotropy coefficient λ_θ against the photon transverse momentum at invariant mass $M = 0.6$ GeV. We show the coefficient for Drell-Yan and pion annihilation process in two velocity profiles describing a static and uniform medium, and a longitudinal Bjorken expansion. For the Bjorken case, we plot the coefficients both in the HX and HX' frame. We observe that, in the static case, the anisotropy coefficient tend to zero for small values of the photon transverse momentum and it vanishes at exactly $q_T = 0$ GeV, both for Drell-Yan and pion annihilation. The reason is that, in this limit, the photon is at rest with the medium and, therefore, the distribution functions of the initial states in Eq. (5.4) are spherically symmetric leading to zero anisotropy. In other words, the contribution in Eq. (5.8) proportional to W_2 vanishes. For large values of

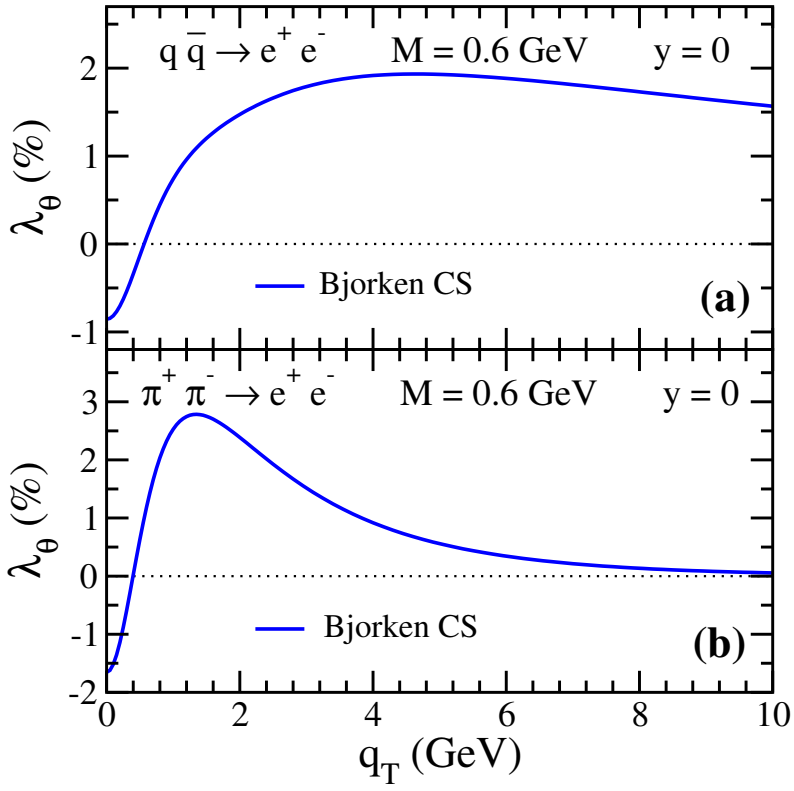

Figure 5.5.: The anisotropy coefficient λ_θ calculated in the CS frame as a function of the virtual photon transverse momentum at invariant mass $M = 0.6$ GeV and photon rapidity $y = 0$ in the case of a Bjorken longitudinal expansion for: (a) Drell-Yan process, and (b) pion annihilation.

q_T, the anisotropy coefficient again approaches zero because the momentum distribution functions approach the Boltzmann limit leading to a vanishing W_2. We stress again that photon polarization in a thermal medium is an effect due to quantum statistics.

In the case of the Bjorken expansion, (Figure. 5.4), we find that both the anisotropy coefficients for HX and HX' do not vanish in the limit of $q_T \to 0$. This is attributed to the fact that in the local rest frame, the photon has finite momentum even if $q_T = 0$ and $y = 0$ because of the space-time rapidity of the fluid elements. Similar to the static case, we also observe that for large momenta the anisotropy coefficient approaches zero because the momentum distribution function again approaches the Boltzmann limit. It is also clear from Figure 5.4 that the coefficient in the Bjorken expansion in HX' is always larger in magnitude than that in HX, accordingly to the discussions of the previous Sections. Moreover, we note that the magnitude of the coefficient takes on the largest values between $q_T = 2$ GeV and $q_T = 4$ GeV for Drell-Yan and at about $q_T \simeq 1$ GeV for pion annihilation.

In Figure 5.5, it is shown the anisotropy coefficient in the Collins-Soper (CS) frame for the Bjorken expansion. The numerical values of the parameters are the same as in Figure 5.4. We note that the coefficient changes sign for large q_T in the CS frame. In Figure 5.6 it is shown the anisotropy coefficient as a function of the virtual photon invari-

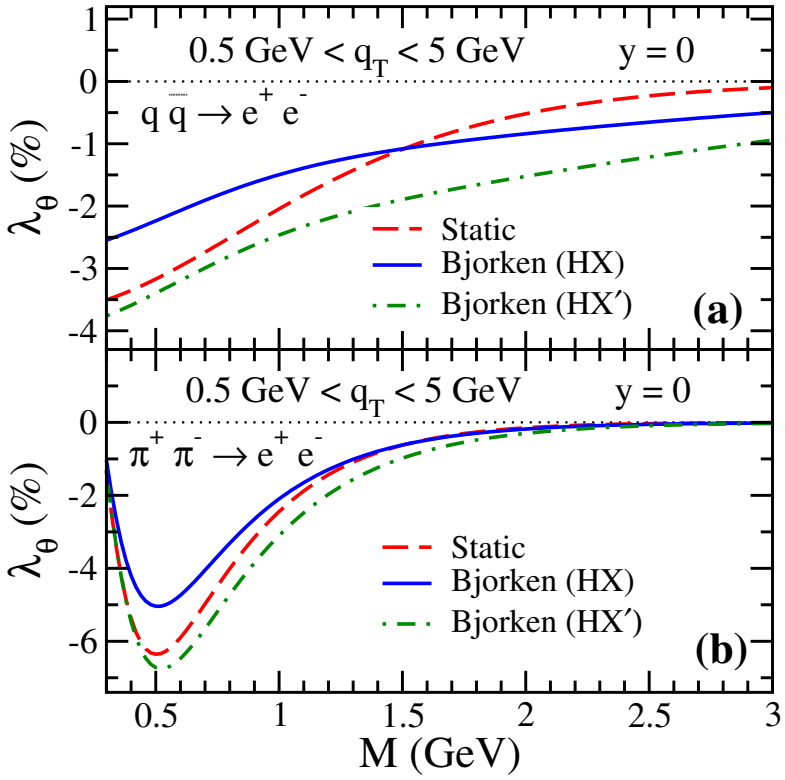

Figure 5.6.: The anisotropy coefficient λ_θ as a function of the virtual photon invariant mass integrated over a transverse momentum range between 0.5 GeV and 5 GeV for: (a) Drell-Yan process, and (b) pion annihilation. The red dashed lines refer to the case of static uniform medium, the blue solid lines to the longitudinal Bjorken expansion in the HX frame, and the green dot dashed lines to the longitudinal Bjorken expansion in the HX' frame.

ant mass integrated over q_T between 0.5 GeV and 5 GeV in the case of static and Bjorken expanding medium.

It is important to note that, in the limit of vanishing fluid space-time rapidity, $\eta \to 0$, we recover the results of static uniform medium. This is an important check because while the computation of the angular distribution given in Eq. (5.15) in the static case is done in the photon rest frame, in the longitudinal case, we compute it in the local fluid rest frame.

The last case studied is the longitudinal Bjorken expansion combined with a radial expansion transverse to the beam axis. Here there is an additional parameter, i.e. v_0 introduced in Eq. (5.53). Clearly, the larger v_0, the faster the transverse expansion. Figure 5.7 shows the anisotropy coefficient λ_θ as a function of q_T in the HX and HX' frame for different values of v_0, where the photon rapidity y and the azimuthal angle ϕ_y are taken to be zero. The effect of the increase of v_0 is to shift the minimum of the anisotropy coefficient toward larger q_T. Moreover, the higher v_0, the slower the coefficient approaches zero for large q_T.

Finally, in order to make a comparison with the experimental results obtained by the NA60 Collaboration in [31], we perform also an integration over the invariant mass in

the interval 0.4 GeV $< M <$ 0.9 GeV and over the photon rapidity window $0.3 < y < 1.3$. We do it in the HX and in the CS frame. We use $T_i = 250$ MeV for the initial QGP temperature. It is found that $\lambda_\theta^{HX} \simeq -0.01$ both for Drell-Yan and pion annihilation, Furthermore, $\lambda_\theta^{CS} \simeq 0.002$ for Drell-Yan and $\lambda_\theta^{CS} \simeq 0.007$ for pion-annihilation. These values are compatible with the measurements presented in [31].

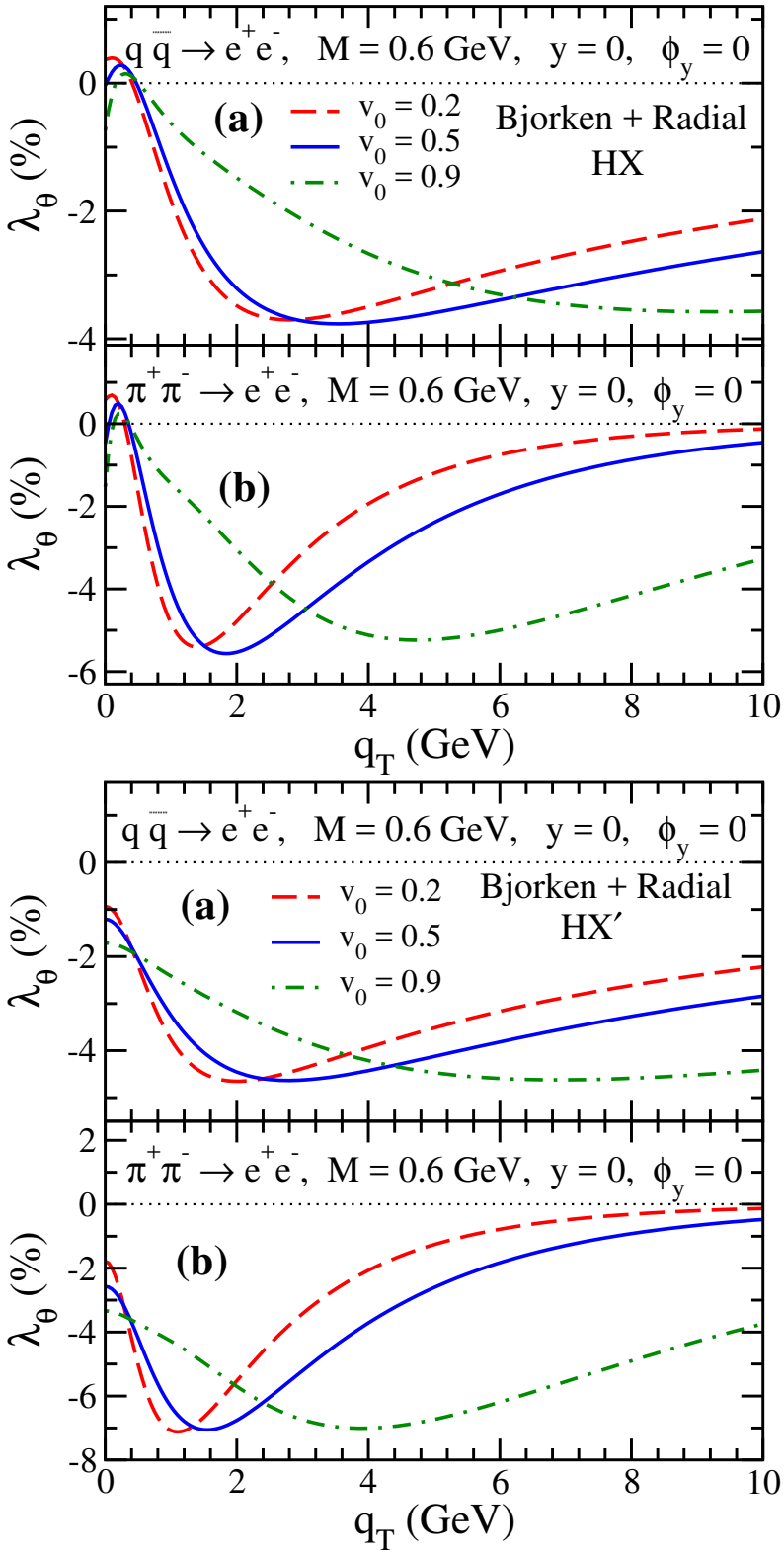

Figure 5.7.: The anisotropy coefficient λ_θ as a function of q_T for a Bjorken longitudinal expansion combined with a transverse expansion for different values of the parameter v_0 for: (a) Drell-Yan process, and (b) pion annihilation. The upper panel shows the HX frame, the lower panel the HX' frame.

Summary and outlook

In this Thesis we studied virtual photon polarization in hadronic and heavy-ion collisions. We computed the anisotropy coefficients of the angular distribution of dileptons originating from the decay of virtual photons. These coefficients carry information on the polarization state of the virtual photon and, hence, on the emission process. We showed that the anisotropy coefficients contain key information for understanding elementary reactions and medium properties.

We first studied the angular distribution of dileptons originating from the process $\pi N \to N e^+ e^-$ and presented numerical results for the anisotropy coefficient λ_θ based on the assumption that the process is dominated by intermediate baryon resonances. We employed effective Lagrangians to describe the interactions of baryon resonances with pions and photons. The coupling of the electromagnetic field to the baryon resonances is based on the vector meson dominance model. The coupling constants of the model have been determined using information given by the Particle Data Group [82]. Since the decay parameters of some of the baryon resonances are not very well known, our model contains uncertainties. However, the differential cross sections obtained using our model are in reasonable agreement with preliminary HADES data on dilepton production, and results on the neutral ρ contribution extracted from a partial wave analysis of pion pair production. The shape of the anisotropy coefficient λ_θ as a function of the scattering angle is determined mainly by the $N(1520)$ resonance and hence it depends only weakly on the uncertainties of the model.

The anisotropy coefficient can in principle be determined in experiments by the HADES Collaboration at GSI. To this end, at least a rough binning of the triple-differential dilepton production cross section is needed. This requires high statistics, which is not easily achieved for such a rare probe. On the other hand, as we argued in this Chapter, the angular distributions provide valuable additional information, which can help disentangle the various contributions to the dilepton production cross section and thus also provide novel information on the properties of baryon resonances. Consequently, high statistics data on pion induced dilepton production would provide important constraints on the elementary dilepton production mechanism as well as on the structure of baryons.

The calculation presented here is clearly exploratory. In future studies, several aspects of the model should be improved. First of all the model dependence of the predictions needs to be addressed. This can be done e.g. by repeating the calculation with different effective Lagrangians. A complementary approach, formulated in terms of helicity amplitudes or partial wave amplitudes, could provide a systematic framework for exploring the various contributions to the scattering amplitude. A previous study suggests that at the CM energy of the HADES experiment a major part of the pion photoproduction cross section is probably due to non-resonant Born contributions [71]. Consequently, these Born terms may significantly influence also the angular distributions of dilepton production and the anisotropy coefficient in pion-nucleon collisions. Thus, their contribution to λ_θ should be assessed. It is also known that the standard vector meson dominance model does not provide a satisfactory description of the electromagnetic interaction of baryon

resonances. This can be improved e.g. by relaxing the universal coupling assumption [74] for the photon coupling to baryons, as discussed e.g. in Ref. [71].

Additional constraints on the model are provided by pion-nucleon collisions with other final states. In particular the one-pion and two-pion final states are measured at HADES with much better statistics than for the dilepton final state. Investigation of these final states in the framework of the same model would provide an independent check and a possibility to put tighter constraints on some of the parameters of the model. Two-pion production can also proceed via an intermediate ρ meson, which makes this process particularly interesting in the present context.

After the analysis of elementary reactions, we studied how the anisotropy coefficients change when the virtual photon is emitted from a thermalized medium. We presented a general framework for studying the angular anisotropies of dileptons produced from virtual photons in high energy heavy-ion collisions. We saw how in general the velocity and temperature profile describing the evolution of the medium are reflected in the shape of the anisotropy coefficients. Two basic processes were considered: quark-antiquark annihilation in the QGP, and pion annihilation in the hadronic phase. Moreover, we specifically studied medium effects on the dilepton anisotropies in the case of a static uniform medium, a medium with a Bjorken expansion along the beam axis, and a medium with a Bjorken expansion combined with a symmetric expansion transverse to the beam axis. Our results show that virtual photons originating from a medium are in general polarized. Interestingly, we found that this polarization is an effect due to quantum statistics since, in the Boltzmann limit for the distribution function of the initial particles, the polarization vanishes. However, the overall effect is small and it seems to be consistent with the NA60 Collaboration data [31]. In the future, a better statistics could help measuring virtual photon polarization effects in heavy-ion collisions.

Looking forward, another medium anisotropy that can be studied with the formalism presented here is fluid viscosity, which plays an important role in the description of the collective flow in nuclear collisions. Moreover, the anisotropy coefficients clearly depend on the elementary process. Therefore, it would be interesting to compute the effect due to different type of reactions like, e.g., the gluon Compton scattering in the QGP.

Recently, there has been an intense experimental and theoretical activity on the study of vorticity in noncentral heavy-ion collisions. It has been shown by the STAR Collaboration at RHIC that Lambda baryons created in noncentral collisions exhibit a significant polarization [7]. It has been argued that the fluid vorticity of the QCD matter may induce such a polarization [5–7, 103, 104]. Measurements suggest that the state of matter produced is by far the most vortical system ever observed [7]. Moreover, a strong magnetic field is also expected to be formed in noncentral collisions due to the spectator nucleons [105]. This should also induce strong medium anisotropies which can lead to particle polarization. It has also been argued that, besides Lambda baryon decay, other hadronic decays, like the rho meson decay, can give information on the vorticity and magnetic field [106]. Furthermore, the combination of a non-trivial fluid velocity profile involving, e.g., vorticity and a strong magnetic field can produce novel physical phenomena like the chiral-magnetic effect and the chiral-vortical effect [107]. Although there is strong activity on the forefront research on polarization in heavy-ion physics, there is a lack in the literature of studies of effects of vorticity and magnetic field on virtual photon polarization. It is natural to ask also how these effects are reflected in the polarization state of virtual photons. The formalism presented in this Thesis is also suitable for studies of photon polarization in the

case of additional anisotropy axes. This makes it suitable for investigating vorticity and magnetic field effects. More generally, the present framework can be easily implemented in a realistic hydrodynamic simulation of relativistic heavy-ion collisions in order to study the effect of non-trivial medium properties on dilepton anisotropy.

Appendix A

Conventions and Notations

Throughout the Thesis we used the natural units, i.e.

$$\hbar = c = k_B = 1, \tag{A.1}$$

where c is the speed of light and k_B the Boltzmann constant.

We used the Einstein convention for the scalar products, i.e. given two 4-vectors $a^\mu = (a^0, a^1, a^2, a^3)$ and $b^\mu = (b^0, b^1, b^2, b^3)$, we have

$$a_\mu b^\mu = \sum_{\mu,\nu} g_{\mu\nu} a^\mu b^\nu, \tag{A.2}$$

where the metric tensor is given by

$$g_{\mu\nu} = \begin{pmatrix} 1 & 0 & 0 & 0 \\ 0 & -1 & 0 & 0 \\ 0 & 0 & -1 & 0 \\ 0 & 0 & 0 & -1 \end{pmatrix}. \tag{A.3}$$

For the gamma matrices γ^μ, we use the Dirac representation, i.e.

$$\gamma^0 = \begin{pmatrix} I_2 & 0 \\ 0 & -I_2 \end{pmatrix}, \qquad \gamma^i = \begin{pmatrix} 0 & \sigma^i \\ -\sigma^i & 0 \end{pmatrix}, \tag{A.4}$$

where $i = 1, 2, 3$, σ^i are the Pauli matrices, and I_2 is the unit matrix in two dimensions. The matrix γ_5 is defined as

$$\gamma_5 = i\gamma^0\gamma^1\gamma^2\gamma^3 = \begin{pmatrix} 0 & I_2 \\ I_2 & 0 \end{pmatrix}. \tag{A.5}$$

Appendix B

Feynman rules

In this Appendix we list the Feynman rules used for the calculations in Chapter 2. We used the same conventions as [108]. From the Lagrangians of Eqs. (2.13), (2.19), (2.20), (2.27), (2.28), (2.29), (2.30), we obtain the following Feynman rules.

$$-i\frac{eq^2}{g_\rho}\,g^{\mu\nu} \tag{B.1}$$

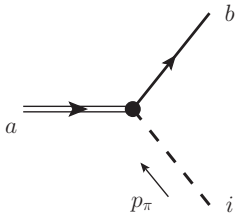

$$-\frac{g_{RN\pi}}{m_\pi}\Gamma\,(A^i)_{ab}\not{p}_\pi \tag{B.2}$$

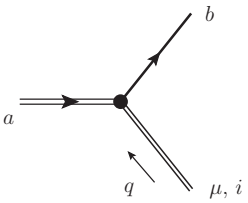

$$\frac{g_{RN\rho}}{m_N}\tilde{\Gamma}\sigma^{\alpha\mu}q_\alpha\,(A^i)_{ab} \tag{B.3}$$

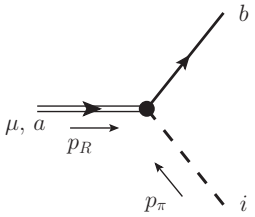

$$-i\frac{g_{RN\pi}}{m_\pi^2}\left(\gamma^\mu(p_R\cdot p_\pi)-p_\pi^\mu\not{p}_R\right)\Gamma\,(A^i)_{ab} \tag{B.4}$$

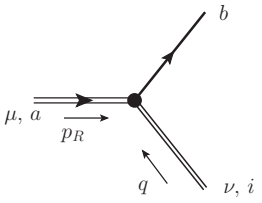

$$i\frac{g_{RN\rho}}{4m_\rho^2}(q^\alpha\gamma^\nu-g^{\alpha\nu}\not{q})(p_{R\alpha}\gamma_\mu-g_{\alpha\mu}\not{p}_R)\tilde{\Gamma}\,(A^i)_{ab} \tag{B.5}$$

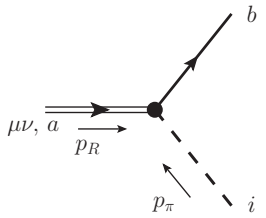

$$\frac{g_{RN\pi}}{m_\pi^4}\Gamma\, p_{\pi\alpha} p_{\pi\beta}\, O_{5/2}^{(\alpha\beta)\mu\nu}(-ip_R)\,(A^i)_{ab} \tag{B.6}$$

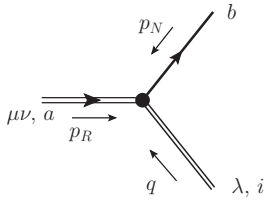

$$-i\frac{g_{RN\rho}}{(2m_\rho)^4}\tilde{\Gamma}(\gamma_\lambda q_\beta - g_{\lambda\beta}\not{q})p_{N\alpha} O_{5/2}^{(\alpha\beta)\mu\nu}(-ip_R)\,(A^i)_{ab} \tag{B.7}$$

In the Feynman rules, the solid line represents a nucleon, the double dashed line with arrow a baryon resonance, the double line without arrow a rho meson, the dashed line a pion, and the wavy line a photon. In coordinate space, the function $O_{5/2}^{(\alpha\beta)\mu\nu}(\partial)$ is defined as

$$O_{5/2}^{(\alpha\beta)\mu\nu}(\partial) = \gamma_\lambda\gamma_\rho O_{5/2}^{(\alpha\beta,\lambda\rho)\mu\nu}(\partial), \tag{B.8}$$

where

$$\begin{aligned} O_{5/2}^{(\alpha\beta,\lambda\rho)\mu\nu}(\partial) = &-\frac{1}{2}\partial^\alpha\partial^\beta\left(g^{\lambda\mu}g^{\rho\nu}+g^{\lambda\nu}g^{\rho\mu}\right)-\frac{1}{2}\partial^\lambda\partial^\rho\left(g^{\alpha\mu}g^{\beta\nu}+g^{\alpha\nu}g^{\beta\mu}\right)\\ &+\frac{1}{4}\partial^\alpha\partial^\lambda\left(g^{\beta\mu}g^{\rho\nu}+g^{\beta\nu}g^{\rho\mu}\right)+\frac{1}{4}\partial^\alpha\partial^\rho\left(g^{\beta\mu}g^{\lambda\nu}+g^{\beta\nu}g^{\lambda\mu}\right)\\ &+\frac{1}{4}\partial^\beta\partial^\lambda\left(g^{\alpha\mu}g^{\rho\nu}+g^{\alpha\nu}g^{\rho\mu}\right)+\frac{1}{4}\partial^\beta\partial^\rho\left(g^{\alpha\mu}g^{\lambda\nu}+g^{\alpha\nu}g^{\lambda\mu}\right). \end{aligned} \tag{B.9}$$

In the Feynman rules, we have $\Gamma = \gamma_5$ for $J^P = 1/2^+$, $3/2^-$ and $5/2^+$ resonances and $\Gamma = 1$ otherwise, and $\tilde{\Gamma} = \gamma_5\Gamma$. The isospin factor $(A^i)_{ab} = (\tau^i)_{ab}$, where τ^i is the i-th Pauli matrix if the baryon resonance is a N^* (i.e. total isospin equal to $1/2$). If the baryon resonance is a Δ (total isospin equal to $3/2$), then $(A^i)_{ab} = (T^i)_{ab}$, where T^i is the i-th isospin transition matrix from isospin $3/2$ to $1/2$. We now give the expression for the propagators for baryon resonances. The propagator of spin-1/2 baryon resonances is given by

$$G_{R_{1/2}}^{\mu\nu}(p_R) = \frac{i}{p_R^2 - m_R^2 + i\sqrt{p_R^2}\Gamma_R(p_R^2)}. \tag{B.10}$$

The propagator of spin-3/2 baryon resonances is given by

$$G_{R_{3/2}}^{\mu\nu}(p_R) = \frac{i}{p_R^2 - m_R^2 + i\sqrt{p_R^2}\Gamma_R(p_R^2)} P_{3/2}^{\mu\nu}(p_R, m_R), \tag{B.11}$$

where

$$P_{3/2}^{\mu\nu}(p_R, m_R) = -(\not{p}_R + m_R)\left(g^{\mu\nu} - \frac{\gamma^\mu\gamma^\nu}{3} - \frac{2}{3}\frac{p_R^\mu p_R^\nu}{m_R^2} + \frac{p_R^\mu\gamma^\nu - p_R^\nu\gamma^\mu}{3m_R}\right). \tag{B.12}$$

The propagator of spin-5/2 baryon resonances is given by

$$G^{\mu\nu,\rho\sigma}_{R_{5/2}}(p_R) = \frac{i}{p_R^2 - m_R^2 + i\sqrt{p_R^2}\Gamma_R(p_R^2)} P^{\mu\nu,\rho\sigma}_{5/2}(p_R, m_R), \tag{B.13}$$

where

$$\begin{aligned} P^{\mu\nu,\rho\sigma}_{5/2}(p_R, m_R) = (\not{p}_R + m_R)\Big(\frac{3}{10}(G^{\mu\rho}G^{\nu\sigma} + G^{\mu\sigma}G^{\nu\rho}) - \frac{1}{5}G^{\mu\nu}G^{\rho\sigma} \\ - \frac{1}{10}(T^{\mu\rho}G^{\nu\sigma} + T^{\nu\sigma}G^{\mu\rho} + T^{\mu\sigma}G^{\nu\rho} + T^{\nu\rho}G^{\mu\sigma})\Big), \end{aligned} \tag{B.14}$$

with

$$G^{\mu\nu} = -g^{\mu\nu} + \frac{p_R^\mu p_R^\nu}{m_R^2}, \tag{B.15}$$

and

$$T^{\mu\nu} = -\frac{1}{2}(\gamma^\mu\gamma^\nu - \gamma^\nu\gamma^\mu) + \frac{p_R^\mu\left(\not{p}_R\gamma^\nu - \gamma^\nu\not{p}_R\right)}{2m_R^2} - \frac{p_R^\nu\left(\not{p}_R\gamma^\mu - \gamma^\mu\not{p}_R\right)}{2m_R^2}. \tag{B.16}$$

We conclude by noting that the Lagrangians discussed in Subsection 2.2.3 imply that the vertices are transverse to the momentum of the resonance p_R^μ.

Appendix C

Lorentz transformations and anisotropy coefficients

In this Appendix we give the explicit expressions of the Lorentz transformation matrices and the anisotropy coefficients discussed in Chapter 5.

C.1 Longitudinal Bjorken expansion

The 4-vectors that we need to consider are the photon momentum in the lab frame q^μ_{LAB}, the fluid velocity in the lab frame u^μ_{LAB}, and the difference between the lepton momenta in the HX' frame $\Delta l^\mu_{HX'}$:

$$q^\mu_{LAB} = (M_T \cosh y, q_T, 0, M_T \sinh y), \tag{C.1}$$
$$u^\mu_{LAB} = (\cosh \eta, 0, 0, \sinh \eta), \tag{C.2}$$
$$\Delta l^\mu_{HX'} = 2|\mathbf{l}|(0, \sin\theta_e \cos\phi_e, \sin\theta_e \sin\phi_e, \cos\theta_e), \tag{C.3}$$

where $M_T = \sqrt{q_T^2 + M^2}$, q_T is the photon transverse momentum, y its rapidity, $|\mathbf{l}| = M/2$, θ_e and ϕ_e are the polar angles corresponding to the chosen quantization axis. We can freely choose the coordinates such that q_T is along the x axis. In order to calculate the scalar product $u \cdot \Delta l$ in the dilepton angular distribution Eq. (5.15), we need of course to write the two vectors in the same reference frame. We transform q^μ_{LAB}, $\Delta l^\mu_{HX'}$ and u^μ_{LAB} in the local fluid rest frame defined as $u^\mu_{LRF} = (1,0,0,0)$. To transform q^μ_{LAB} to the local fluid rest frame, we apply the Lorentz boost

$$(B_\eta)^\mu_\nu = \begin{pmatrix} \cosh\eta & 0 & 0 & -\sinh\eta \\ 0 & 1 & 0 & 0 \\ 0 & 0 & 1 & 0 \\ -\sinh\eta & 0 & 0 & \cosh\eta \end{pmatrix}, \tag{C.4}$$

$$q^\mu_{LRF} = (B_\eta)^\mu_\nu q^\nu_{LAB} = \begin{pmatrix} M_T \cosh(y-\eta) \\ q_T \\ 0 \\ M_T \sinh(y-\eta) \end{pmatrix}, \tag{C.5}$$

and celarly

$$u^\mu_{LRF} = (B_\eta)^\mu_\nu u^\nu_{LAB} = \begin{pmatrix} 1 \\ 0 \\ 0 \\ 0 \end{pmatrix}. \tag{C.6}$$

To transform $\Delta l^{\mu}_{HX'}$ to the local fluid rest frame, we first boost along the direction of the photon momentum, namely along the z direction with the matrix

$$(B_q)^{\mu}_{\nu} = \begin{pmatrix} \gamma_q & 0 & 0 & \gamma_q v_q \\ 0 & 1 & 0 & 0 \\ 0 & 0 & 1 & 0 \\ \gamma_q v_q & 0 & 0 & \gamma_q \end{pmatrix}, \tag{C.7}$$

where

$$v_q = \frac{|\mathbf{q}_{LRF}|}{E_{\gamma\, LRF}}, \tag{C.8}$$

$|\mathbf{q}_{LRF}| = \sqrt{q_T^2 + M_T^2 \sinh^2(y-\eta)}$ being the modulus of the photon momentum in the local fluid rest frame, $E_{\gamma\, LRF} = \sqrt{M^2 + |\mathbf{q}_{LRF}|^2}$ and $\gamma_q = 1/\sqrt{1-v_q^2}$. Secondly, we want to make a rotation in order to align the axis defined by the photon momentum and that defined by the beam. Hence, we want to rotate the coordinate system in the xz-plane in the clockwise direction or, equivalently, in the counterclockwise direction the 4-vector. The counterclockwise rotation around the y axis of an angle θ_γ to apply to the 4-vector is given by

$$(R_{\theta_\gamma})^{\mu}_{\nu} = \begin{pmatrix} 1 & 0 & 0 & 0 \\ 0 & \cos\theta_\gamma & 0 & \sin\theta_\gamma \\ 0 & 0 & 1 & 0 \\ 0 & -\sin\theta_\gamma & 0 & \cos\theta_\gamma \end{pmatrix}, \tag{C.9}$$

where θ_γ is the angle between the photon momentum and the beam axis in the local fluid rest frame, i.e.

$$\theta_\gamma = \arccos\left(\frac{M_T \sinh(y-\eta)}{|\mathbf{q}_{LRF}|}\right). \tag{C.10}$$

Thus, the Lorentz transformation to go from the HX' to the local fluid rest frame is given by

$$(\Lambda_{HX'\to LRF})^{\mu}_{\nu} = (R_{\theta_\gamma})^{\mu}_{\alpha}(B_q)^{\alpha}_{\nu} = \begin{pmatrix} \gamma_q & 0 & 0 & \gamma_q v_q \\ \gamma_q v_q \sin\theta_\gamma & \cos\theta_\gamma & 0 & \gamma \sin\theta_\gamma \\ 0 & 0 & 1 & 0 \\ \gamma_q v_q \cos\theta_\gamma & -\sin\theta_\gamma & 0 & \gamma_q \cos\theta_\gamma \end{pmatrix}, \tag{C.11}$$

and the difference of the lepton 3-momenta in the fluid rest frame is given by

$$\Delta l^{\mu}_{LRF} = (\Lambda_{HX'\to LRF})^{\mu}_{\nu}\Delta l^{\nu}_{HX'} = 2|\mathbf{l}| \begin{pmatrix} \gamma_q v_q \cos\theta_e \\ \cos\theta_\gamma \sin\theta_e \cos\phi_e + \gamma_q \sin\theta_\gamma \cos\theta_e \\ \sin\theta_e \sin\phi_e \\ \gamma_q \cos\theta_\gamma \cos\theta_e - \sin\theta_\gamma \sin\theta_e \cos\phi_e \end{pmatrix}. \tag{C.12}$$

Hence, we get

$$(u \cdot \Delta l)^2 = 4|\mathbf{l}|^2 \gamma_q^2 v_q^2 \cos^2\theta_e. \tag{C.13}$$

If the difference of the lepton momenta (C.3) is expressed in the HX frame, i.e. Δl^{μ}_{HX}, meaning now that the angles θ_e and ϕ_e are measured with respect to the direction of the

photon lab momentum as seen in the photon rest frame, we need to perform an additional rotation. The rotation is of course again around the y axis and it is counterclockwise if we apply it to the 4-momenta (clockwise if we consider a rotation of the coordinate system). This is a rotation that transforms a 4-vector defined in HX to a 4-vector defined in HX', namely

$$(R_{HX\to HX'})^{\mu}_{\nu} = \begin{pmatrix} 1 & 0 & 0 & 0 \\ 0 & \cos(\theta_\gamma - \theta_y) & 0 & \sin(\theta_\gamma - \theta_y) \\ 0 & 0 & 1 & 0 \\ 0 & -\sin(\theta_\gamma - \theta_y) & 0 & \cos(\theta_\gamma - \theta_y) \end{pmatrix}, \tag{C.14}$$

where we defined the angle between the beam axis and the photon momentum in the lab frame as

$$\theta_y = \arccos\left(\frac{M_T \sinh y}{|\mathbf{q}_{LAB}|}\right), \tag{C.15}$$

where the modulus of the photon momentum in the lab frame is given by $|\mathbf{q}_{LAB}| = \sqrt{q_T^2 + M_T^2 \sinh^2 y}$. One can find that

$$\cos(\theta_\gamma - \theta_y) = \frac{q_T^2 + M_T^2 \sinh y \, \sinh(y-\eta)}{\sqrt{[q_T^2 + M_T^2 \sinh^2 y][q_T^2 + M_T^2 \sinh^2(y-\eta)]}}, \tag{C.16}$$

$$\sin(\theta_\gamma - \theta_y) = \frac{q_T M_T [\sinh y - \sinh(y-\eta)]}{\sqrt{[q_T^2 + M_T^2 \sinh^2 y][q_T^2 + M_T^2 \sinh^2(y-\eta)]}}. \tag{C.17}$$

Note that for $\eta = 0$, $\cos(\theta_\gamma - \theta_y) = 1$ and $\sin(\theta_\gamma - \theta_y) = 1$. The complete Lorentz transformation from HX' to the local rest frame is given by

$$\begin{aligned}(\Lambda_{HX\to LRF})^{\mu}_{\nu} &= (R_{\theta_\gamma})^{\mu}_{\alpha} (B_q)^{\alpha}_{\beta} (R_{HX\to HX'})^{\beta}_{\nu} \\ &= \begin{pmatrix} \gamma_q & -\gamma_q v_q s & 0 & \gamma_q v_q c \\ \gamma_q v_q \sin\theta_\gamma & c\,\cos\theta_\gamma - s\,\gamma_q \sin\theta_\gamma & 0 & s\,\cos\theta_\gamma + c\,\gamma_q \sin\theta_\gamma \\ 0 & 0 & 1 & 0 \\ \gamma_q v_q \cos\theta_\gamma & -s\,\gamma_q \cos\theta_\gamma - c\,\sin\theta_\gamma & 0 & c\,\gamma_q \cos\theta_\gamma - s\,\sin\theta_\gamma \end{pmatrix},\end{aligned} \tag{C.18}$$

where we used the abbreviation $c = \cos(\theta_\gamma - \theta_y)$ and $s = \sin(\theta_\gamma - \theta_y)$. Consequently, the difference of the lepton momenta transforms as

$$\begin{aligned}\Delta l^{\mu}_{LRF} &= (\Lambda_{HX\to LRF})^{\mu}_{\nu} \Delta l^{\nu}_{HX} \\ &= 2|\mathbf{l}| \begin{pmatrix} \gamma_q v_q (c\,\cos\theta_e - s \sin\theta_e \cos\theta_e) \\ \cos\theta_e (s\,\cos\theta_\gamma + \gamma_q c\,\sin\theta_\gamma) + \sin\theta_e \cos\phi_e (c\,\cos\theta_\gamma - \gamma_q s\,\sin\theta_\gamma) \\ \sin\theta_e \sin\phi_e \\ -\sin\theta_e \cos\phi_e (\gamma_q s\,\cos\theta_\gamma + c\,\sin\theta_\gamma) + \cos\theta_e (\gamma_q c\,\cos\theta_\gamma - s\,\sin\theta_\gamma) \end{pmatrix}.\end{aligned} \tag{C.19}$$

Thus we have

$$\begin{aligned}(u\cdot\Delta l)^2 = 2|\mathbf{l}|^2 \gamma_q^2 v_q^2 s^2 [1 &+ (2\cot^2(\theta_\gamma - \theta_y) - 1)\cos^2\theta_e + \sin^2\theta_e \cos 2\phi_e \\ &- 2\cot(\theta_\gamma - \theta_y)\sin 2\theta_e \cos\phi_e]\end{aligned} \tag{C.20}$$

and the primed anisotropy coefficients defined in Eqs. (5.18) and (5.19) are given by

$$\lambda_\theta'^{HX} = 2|\mathbf{l}|^2\gamma_q^2 v_q^2 s^2(2-3s^2), \tag{C.21}$$

$$\lambda_\phi'^{HX} = 2|\mathbf{l}|^2\gamma_q^2 v_q^2 s^2 \tag{C.22}$$

$$\lambda_{\theta\phi}'^{HX} = -4|\mathbf{l}|^2\gamma_q^2 v_q^2 s\, c \tag{C.23}$$

C.2 Longitudinal Bjorken expansion combined with a radial transverse expansion

The 4-velocity in the lab frame in the case where we have a Bjorken longitudinal expansion and a transverse expansion is given by

$$u^\mu_{LAB} = \gamma_r \begin{pmatrix} \cosh\eta \\ v_r\cos\phi_r \\ v_r\sin\phi_r \\ \sinh\eta \end{pmatrix}, \tag{C.24}$$

where the transverse Lorentz factor is $\gamma_r = 1/\sqrt{1-v_r^2}$. The transverse velocity being $v_r = v_0 r/R_0$ and ϕ_r is the azimuthal angle of the velocity. Similarly to Eq. (C.1) we write the photon 4-momentum in the lab frame as

$$q^\mu_{LAB} = \begin{pmatrix} M_T\cosh y \\ q_T\cos\phi_y \\ q_T\sin\phi_y \\ M_T\sinh y \end{pmatrix}. \tag{C.25}$$

To transform q^μ_{LAB} to the fluid rest frame, we now need to do first a boost along the beam axis using Eq. (C.4), then a a boost along the transverse velocity $\mathbf{v}_r$. In order to carry out a general boost along $\mathbf{v}_r$, one can make a rotation of an angle ϕ_r to align the x axis with the transverse velocity $\mathbf{v}_r$ using the matrix

$$(R_{\phi_r})^\mu_\nu = \begin{pmatrix} 1 & 0 & 0 & 0 \\ 0 & \cos\phi_r & \sin\phi_r & 0 \\ 0 & -\sin\phi_r & \cos\phi_r & 0 \\ 0 & 0 & 0 & 1 \end{pmatrix}, \tag{C.26}$$

then boost along x with velocity magnitude v_r with the matrix

$$(B_r)^\mu_\nu = \begin{pmatrix} \gamma_r & -\gamma_r v_r & 0 & 0 \\ -\gamma_r v_r & \gamma_r & 0 & 0 \\ 0 & 0 & 1 & 0 \\ 0 & 0 & 0 & 1 \end{pmatrix}, \tag{C.27}$$

and eventually rotate back with $(R^{-1}_{\phi_r})^\mu_\nu$. Hence we have

$$(\Lambda_{LAB\to LRF})^\mu_\nu = (R^{-1}_{\phi_r})^\mu_\alpha (B_r)^\alpha_\beta (R_{\phi_r})^\beta_\delta (B_\eta)^\delta_\nu$$

$$= \begin{pmatrix} \gamma_r \cosh\eta & -\gamma_r v_r \cos\phi_r & -\gamma_r v_r \sin\phi_r & -\gamma_r \sinh\eta \\ -\gamma_r v_r \cos\phi_r \cosh\eta & \gamma_r \cos^2\phi_r + \sin^2\phi_r & (\gamma_r - 1)\cos\phi_r \sin\phi_r & \gamma_r v_r \cos\phi_r \sinh\eta \\ -\gamma_r v_r \sin\phi_r \cosh\eta & (\gamma_r - 1)\cos\phi_r \sin\phi_r & \cos^2\phi_r + \gamma_r \sin^2\phi_r & \gamma_r v_r \sin\phi_r \sinh\eta \\ -\sinh\eta & 0 & 0 & \cosh\eta \end{pmatrix}. \tag{C.28}$$

By applying the Lorentz transformation $(\Lambda_{LAB\to LRF})^{\mu}_{\nu}$ in the previous equation to q^{μ}_{LAB}, one obtains the 4-momentum of the photon in the fluid rest frame. Its components are given by

$$\begin{aligned} q^0_{LRF} = & -q_T\gamma_r v_r \cos\phi_r \cos\phi_y + M_T\gamma_r \cosh y \cosh\eta - q_T\gamma_r v_r \sin\phi_r \sin\phi_y \\ & - M_T\gamma_r \sinh y \sinh\eta, \end{aligned} \tag{C.29}$$

$$\begin{aligned} q^1_{LRF} = & -M_T\gamma_r v_r \cos\phi_r \cosh y \cosh\eta + q_T \cos\phi_y(\gamma_r \cos^2\phi_r + \sin^2\phi_r) \\ & + q_T(-\cos\phi_r \sin\phi_r + \gamma_r \cos\phi_r \sin\phi_r)\sin\phi_y + M_T\gamma_r v_r \cos\phi_r \sinh y \sinh\eta, \end{aligned} \tag{C.30}$$

$$\begin{aligned} q^2_{LRF} = & -M_T\gamma_r v_r \sin\phi_r \cosh y \cosh\eta + q_T \cos\phi_y(-\cos\phi_r \sin\phi_r + \gamma_r \cos\phi_r \sin\phi_r) \\ & + q_T(\cos^2\phi_r + \gamma_r \sin^2\phi_r)\sin\phi_y + M_T\gamma_r v_r \sin\phi_r \sinh y \sinh\eta, \end{aligned} \tag{C.31}$$

$$q^3_{LRF} = M_T \cosh\eta \sinh y - M_T \cosh y \sinh\eta. \tag{C.32}$$

As in the previous Section, we want to transform the difference of the lepton momenta Eq. (C.3) from the HX frame to the local rest frame. First, we need to make a rotation from the direction HX to that of HX'. In presence of transverse expansion, we cannot simply perform a rotation in the xz-plane as in Eq. (C.14). The reason is that now the HX' and the HX axes do not lie in the production plane (the xz-plane). In order to perform this rotation, we use the so-called Rodrigues' rotation formula. Given two vectors $\mathbf{a}$ and $\mathbf{b}$, the rotation from the axis defined by the unit vector $\hat{\mathbf{a}}$ to that defined by $\hat{\mathbf{b}}$ is given by

$$R_R = I + (\sin\delta)K + (1 - \cos\delta)K^2, \tag{C.33}$$

where I is the identity matrix in three dimension and

$$\delta = \arccos\left(\frac{\mathbf{a}\cdot\mathbf{b}}{|\mathbf{a}||\mathbf{b}|}\right). \tag{C.34}$$

The matrix K in Eq. (C.33) is defined by

$$K = \begin{pmatrix} 0 & -k_3 & k_2 \\ k_3 & 0 & -k_1 \\ -k_2 & k_1 & 0 \end{pmatrix}, \tag{C.35}$$

and the vector $\mathbf{k} = (k_1, k_2, k_3)$ is given by

$$\mathbf{k} = \frac{\mathbf{a}\times\mathbf{b}}{|\mathbf{a}||\mathbf{b}|\sin\delta}. \tag{C.36}$$

Equation (C.33) is the Rodrigues' rotation formula. The corresponding Lorentz transformation is given by

$$(R_R)^{\mu}_{\nu} = \begin{pmatrix} 1 & 0 \\ 0 & R_R \end{pmatrix}. \tag{C.37}$$

In our case, $\mathbf{a}$ is replaced by $\mathbf{q}_{LAB}$ (the spacial components of Eq. (C.25)), and $\mathbf{b}$ by $\mathbf{q}_{LRF}$ (Eqs. (C.30), (C.31) and (C.32)). With this replacement, $(R_R)^{\mu}_{\nu}$ becomes the rotation between the HX and HX', $(R_{HX\to HX'})^{\mu}_{\nu}$. The explicit expression of Eq. (C.33) is rather lengthy and will not be quoted here. However, it is possible to show that, if $\mathbf{q}_{LAB}$ and $\mathbf{q}_{LRF}$ lie in the xz-plane, $(R_{HX\to HX'})^{\mu}_{\nu}$ reduces to Eq. (C.14).

Bibliography

[1] C. Bourrely, J. Soffer, and E. Leader, "Polarization Phenomena in Hadronic Reactions," Phys. Rept. **59**, 95 (1980).

[2] E. Leader, *Spin in Particle Physics* (Cambridge University Press, 2001).

[3] X. Artru, M. Elchikh, J.-M. Richard, J. Soffer, and O. V. Teryaev, "Spin observables and spin structure functions: inequalities and dynamics," Phys. Rept. **470**, 1 (2009), arXiv:0802.0164 [hep-ph].

[4] H. E. Haber, "Spin formalism and applications to new physics searches," in *Spin structure in high-energy processes: Proceedings, 21st SLAC Summer Institute on Particle Physics, 26 Jul - 6 Aug 1993, Stanford, CA* (1994) pp. 231–272, arXiv:hep-ph/9405376 [hep-ph].

[5] Z.-T. Liang and X.-N. Wang, "Globally polarized quark-gluon plasma in non-central A+A collisions," Phys. Rev. Lett. **94**, 102301 (2005), [Erratum: Phys. Rev. Lett.96,039901(2006)], arXiv:nucl-th/0410079 [nucl-th].

[6] F. Becattini, F. Piccinini, and J. Rizzo, "Angular momentum conservation in heavy ion collisions at very high energy," Phys. Rev. **C77**, 024906 (2008), arXiv:0711.1253 [nucl-th].

[7] L. Adamczyk *et al.* (STAR), "Global Λ hyperon polarization in nuclear collisions: evidence for the most vortical fluid," (2017), arXiv:1701.06657 [nucl-ex].

[8] D. H. Rischke, "The Quark gluon plasma in equilibrium," Prog. Part. Nucl. Phys. **52**, 197 (2004), arXiv:nucl-th/0305030 [nucl-th].

[9] M. J. Tannenbaum, "Recent results in relativistic heavy ion collisions: From 'a new state of matter' to 'the perfect fluid'," Rept. Prog. Phys. **69**, 2005 (2006), arXiv:nucl-ex/0603003 [nucl-ex].

[10] K. H. Ackermann *et al.* (STAR), "Elliptic flow in Au + Au collisions at (S(NN))**(1/2) = 130 GeV," Phys. Rev. Lett. **86**, 402 (2001), arXiv:nucl-ex/0009011 [nucl-ex].

[11] K. Aamodt *et al.* (ALICE), "Elliptic flow of charged particles in Pb-Pb collisions at 2.76 TeV," Phys. Rev. Lett. **105**, 252302 (2010), arXiv:1011.3914 [nucl-ex].

[12] G. Baym, B. L. Friman, J. P. Blaizot, M. Soyeur, and W. Czyz, "Hydrodynamics of Ultrarelativistic Heavy Ion Collisions," *Nucl. Phys. A407 (1983) 541-570, In *Odenthal-altenberg 1983, Proceedings, Recent Progress In Many-body Theories*, 60-67*, Nucl. Phys. **A407**, 541 (1983).

[13] D. Teaney, "Lecture notes on shear viscosity in heavy ion collisions," *Heavy-ion collisions from the Coulomb barrier to the quark-gluon plasma. Proceedings, International Workshop on Nuclear Physics, 30th Course, Erice, Italy, September 16-24, 2008*, Prog. Part. Nucl. Phys. **62**, 451 (2009).

[14] J.-Y. Ollitrault, "Relativistic hydrodynamics for heavy-ion collisions," *Advanced School on Quark-Gluon Plasma Mumbai, India, July 3-13, 2007*, Eur. J. Phys. **29**, 275 (2008), arXiv:0708.2433 [nucl-th].

[15] P. Romatschke, "New Developments in Relativistic Viscous Hydrodynamics," Int. J. Mod. Phys. **E19**, 1 (2010), arXiv:0902.3663 [hep-ph].

[16] M. G. Alford, K. Rajagopal, and F. Wilczek, "QCD at finite baryon density: Nucleon droplets and color superconductivity," Phys. Lett. **B422**, 247 (1998), arXiv:hep-ph/9711395 [hep-ph].

[17] E. L. Feinberg, "Direct Production of Photons and Dileptons in Thermodynamical Models of Multiple Hadron Production," Nuovo Cim. **A34**, 391 (1976).

[18] E. V. Shuryak, "Quark-Gluon Plasma and Hadronic Production of Leptons, Photons and Psions," Phys. Lett. **B78**, 150 (1978), [Yad. Fiz.28,796(1978)].

[19] E. V. Shuryak, "Quantum Chromodynamics and the Theory of Superdense Matter," Phys. Rept. **61**, 71 (1980).

[20] K. Kajantie, J. I. Kapusta, L. D. McLerran, and A. Mekjian, "Dilepton Emission and the QCD Phase Transition in Ultrarelativistic Nuclear Collisions," Phys. Rev. **D34**, 2746 (1986).

[21] R. Rapp and J. Wambach, "Chiral symmetry restoration and dileptons in relativistic heavy ion collisions," Adv. Nucl. Phys. **25**, 1 (2000), arXiv:hep-ph/9909229 [hep-ph].

[22] H. van Hees and R. Rapp, "Comprehensive interpretation of thermal dileptons at the SPS," Phys. Rev. Lett. **97**, 102301 (2006), arXiv:hep-ph/0603084 [hep-ph].

[23] H. van Hees and R. Rapp, "Dilepton Radiation at the CERN Super Proton Synchrotron," Nucl. Phys. **A806**, 339 (2008), arXiv:0711.3444 [hep-ph].

[24] R. Rapp, J. Wambach, and H. van Hees, "The Chiral Restoration Transition of QCD and Low Mass Dileptons," Landolt-Bornstein **23**, 134 (2010), arXiv:0901.3289 [hep-ph].

[25] R. Rapp and H. van Hees, "Thermal Dileptons as Fireball Thermometer and Chronometer," Phys. Lett. **B753**, 586 (2016), arXiv:1411.4612 [hep-ph].

[26] P. Hoyer, "Particle Polarization as a Signal of Plasma Formation," Phys. Lett. **B187**, 162 (1987).

[27] E. L. Bratkovskaya, O. V. Teryaev, and V. D. Toneev, "Anisotropy of dilepton emission from nuclear collisions," Phys. Lett. **B348**, 283 (1995).

[28] E. Shuryak, "Monitoring parton equilibration in heavy ion collisions via dilepton polarization," (2012), arXiv:1203.1012 [nucl-th].

[29] G. Baym and T. Hatsuda, "Polarization of Direct Photons from Gluon Anisotropy in Ultrarelativistic Heavy Ion Collisions," PTEP **2015**, 031D01 (2015), arXiv:1405.1376 [nucl-th].

[30] G. Baym, T. Hatsuda, and M. Strickland, "Virtual photon polarization in ultrarelativistic heavy-ion collisions," Phys. Rev. **C95**, 044907 (2017), arXiv:1702.05906 [nucl-th].

[31] R. Arnaldi *et al.* (NA60), "First results on angular distributions of thermal dileptons in nuclear collisions," Phys. Rev. Lett. **102**, 222301 (2009), arXiv:0812.3100 [nucl-ex].

[32] G. Agakishiev *et al.* (HADES), "Dielectron production in Ar+KCl collisions at 1.76A GeV," Phys. Rev. **C84**, 014902 (2011), arXiv:1103.0876 [nucl-ex].

[33] G. E. Brown and M. Rho, "Scaling effective Lagrangians in a dense medium," Phys. Rev. Lett. **66**, 2720 (1991).

[34] R. D. Pisarski, "Where does the rho go? Chirally symmetric vector mesons in the quark - gluon plasma," Phys. Rev. **D52**, R3773 (1995), arXiv:hep-ph/9503328 [hep-ph].

[35] M. Harada and K. Yamawaki, "Hidden local symmetry at loop: A New perspective of composite gauge boson and chiral phase transition," Phys. Rept. **381**, 1 (2003), arXiv:hep-ph/0302103 [hep-ph].

[36] P. M. Hohler and R. Rapp, "Is ρ-Meson Melting Compatible with Chiral Restoration?" Phys. Lett. **B731**, 103 (2014), arXiv:1311.2921 [hep-ph].

[37] R. Aaij *et al.* (LHCb), "Determination of the X(3872) meson quantum numbers," Phys. Rev. Lett. **110**, 222001 (2013), arXiv:1302.6269 [hep-ex].

[38] P. Salabura, J. Stroth, and L. Fabbietti (HADES), "The HADES Pion Beam Facility," Nucl. Phys. News **25**, 22 (2015).

[39] W. Przygoda, "JPS Conf. Proc. **10** (2016) 010013, Proceedings of the 10th International Workshop on the Physics of Excited Nucleons, NSTAR2015, May 25-28, Osaka, Japan; W. Przygoda (HADES Collaboration), talk presented at NSTAR2015," (2015).

[40] W. Przygoda, "talk presented at the International Conference on the Structure of Baryons, Baryons 2016, May 16-20, Tallahassee, Florida, USA." (2016).

[41] W. Przygoda, "Production and decay of baryonic resonances in pion induced reactions," *Proceedings, 14th International Workshop on Meson Production, Properties and Interaction (MESON 2016): Cracow, Poland, June 2-7, 2016*, EPJ Web Conf. **130**, 01021 (2016).

[42] F. Scozzi, "Resonance production and decay in pion induced collisions with HADES," *Proceedings, 12th Conference on Quark Confinement and the Hadron Spectrum (Confinement XII): Thessaloniki, Greece*, EPJ Web Conf. **137**, 05023 (2017).

[43] G. Agakishiev *et al.* (HADES), "The High-Acceptance Dielectron Spectrometer HADES," Eur. Phys. J. **A41**, 243 (2009), arXiv:0902.3478 [nucl-ex].

[44] K. Blum, *Density Matrix Theory and Applications* (Springer-Verlag Berlin Heidleberg, 2012).

[45] U. Fano, "Description of States in Quantum Mechanics by Density Matrix and Operator Techniques," Rev. Mod. Phys. **29**, 74 (1957).

[46] C. J. Mullin, J. M. Keller, C. L. Hammer, and R. H. Good Jr., Ann. Phys. (N.Y.) **37**, 55 (1966).

[47] S. Y. Choi, T. Lee, and H. S. Song, "Density Matrix for Polarization of High Spin Particles," Phys. Rev. **D40**, 2477 (1989).

[48] M. Jacob and G. C. Wick, "On the general theory of collisions for particles with spin," Annals Phys. **7**, 404 (1959), [Annals Phys.281,774(2000)].

[49] S. U. Chung, "Spin Formalisms," CERN Yellow Report **71-8 (1971)** (1971).

[50] J. D. Richman, "An Experimenter's Guide to the Helicity Formalism," Caltech Preprint CALT-68-1148, (1986) (1984).

[51] D. M. Brink and G. R. Satchler, *Angular Momentum, 3rd edn.* (Clarendon Press, Oxford, 1993).

[52] P. Faccioli, C. Lourenço, J. Seixas, and H. Woehri, "Minimal physical constraints on the angular distributions of two-body boson decays," Phys. Rev. **D88**, 031901 (2013), arXiv:1307.7121 [hep-ph].

[53] P. Faccioli, C. Lourenço, J. Seixas, and H. K. Wohri, "Rotation-invariant observables in parity-violating decays of vector particles to fermion pairs," Phys. Rev. **D82**, 096002 (2010), arXiv:1010.1552 [hep-ph].

[54] J. C. Collins and D. E. Soper, "Angular Distribution of Dileptons in High-Energy Hadron Collisions," Phys. Rev. **D16**, 2219 (1977).

[55] K. Gottfried and J. D. Jackson, "On the Connection between production mechanism and decay of resonances at high-energies," Nuovo Cim. **33**, 309 (1964).

[56] P. Faccioli, C. Lourenço, J. Seixas, and H. K. Wohri, "Towards the experimental clarification of quarkonium polarization," Eur. Phys. J. **C69**, 657 (2010), arXiv:1006.2738 [hep-ph].

[57] E. N. Argyres and C. S. Lam, "Constraints on Angular Distributions of Dileptons in Different Frames," Phys. Rev. **D26**, 114 (1982).

[58] P. Faccioli, C. Lourenço, and J. Seixas, "Rotation-invariant relations in vector meson decays into fermion pairs," Phys. Rev. Lett. **105**, 061601 (2010), arXiv:1005.2601 [hep-ph].

[59] S. D. Drell and T.-M. Yan, "Massive Lepton Pair Production in Hadron-Hadron Collisions at High-Energies," Phys. Rev. Lett. **25**, 316 (1970), [Erratum: Phys. Rev. Lett.25,902(1970)].

[60] C. S. Lam and W.-K. Tung, "A Systematic Approach to Inclusive Lepton Pair Production in Hadronic Collisions," Phys. Rev. **D18**, 2447 (1978).

[61] C. S. Lam and W.-K. Tung, "A Parton Model Relation Sans QCD Modifications in Lepton Pair Productions," Phys. Rev. **D21**, 2712 (1980).

[62] J.-C. Peng, W.-C. Chang, R. E. McClellan, and O. Teryaev, "Interpretation of Angular Distributions of Z-boson Production at Colliders," Phys. Lett. **B758**, 384 (2016), arXiv:1511.08932 [hep-ph].

[63] S. Falciano *et al.* (NA10), "Angular Distributions of Muon Pairs Produced by 194-GeV/c Negative Pions," Z. Phys. **C31**, 513 (1986).

[64] M. Guanziroli *et al.* (NA10), "Angular Distributions of Muon Pairs Produced by Negative Pions on Deuterium and Tungsten," Z. Phys. **C37**, 545 (1988).

[65] J. S. Conway *et al.*, "Experimental Study of Muon Pairs Produced by 252-GeV Pions on Tungsten," Phys. Rev. **D39**, 92 (1989).

[66] J. G. Heinrich *et al.*, "Higher twist effects in the reaction pi- N —> mu+ mu- X at 253-GeV/c," Phys. Rev. **D44**, 1909 (1991).

[67] L. Y. Zhu *et al.* (NuSea), "Measurement of Angular Distributions of Drell-Yan Dimuons in p + d Interaction at 800-GeV/c," Phys. Rev. Lett. **99**, 082301 (2007), arXiv:hep-ex/0609005 [hep-ex].

[68] L. Y. Zhu *et al.* (NuSea), "Measurement of Angular Distributions of Drell-Yan Dimuons in p + p Interactions at 800-GeV/c," Phys. Rev. Lett. **102**, 182001 (2009), arXiv:0811.4589 [nucl-ex].

[69] T. Aaltonen *et al.* (CDF), "First Measurement of the Angular Coefficients of Drell-Yan e^+e^- pairs in the Z Mass Region from $p\bar{p}$ Collisions at $\sqrt{s} = 1.96$ TeV," Phys. Rev. Lett. **106**, 241801 (2011), arXiv:1103.5699 [hep-ex].

[70] E. Speranza, M. Zetenyi, and B. Friman, "Polarization and dilepton anisotropy in pion-nucleon collisions," Phys. Lett. **B764**, 282 (2017), arXiv:1605.04954 [hep-ph].

[71] M. Zétényi and G. Wolf, "Dilepton production in pion–nucleon collisions in an effective field theory approach," Phys. Rev. **C86**, 065209 (2012), arXiv:1208.5671 [nucl-th].

[72] J. J. Sakurai, "Theory of strong interactions," Annals Phys. **11**, 1 (1960).

[73] J. J. Sakurai, *Currents and Mesons, University of Chicago Press, 1969*.

[74] N. M. Kroll, T. D. Lee, and B. Zumino, "Neutral Vector Mesons and the Hadronic Electromagnetic Current," Phys. Rev. **157**, 1376 (1967), [,39(1967)].

[75] H. B. O'Connell, B. C. Pearce, A. W. Thomas, and A. G. Williams, "$\rho - \omega$ mixing, vector meson dominance and the pion form-factor," Prog. Part. Nucl. Phys. **39**, 201 (1997), arXiv:hep-ph/9501251 [hep-ph].

[76] C.-N. Yang and R. L. Mills, "Conservation of Isotopic Spin and Isotopic Gauge Invariance," Phys. Rev. **96**, 191 (1954).

[77] W. Rarita and J. Schwinger, "On a theory of particles with half integral spin," Phys. Rev. **60**, 61 (1941).

[78] V. Pascalutsa, "Quantization of an interacting spin-3/2 field and the Delta isobar," Phys. Rev. **D58**, 096002 (1998), arXiv:hep-ph/9802288 [hep-ph].

[79] V. Pascalutsa and R. Timmermans, "Field theory of nucleon to higher spin baryon transitions," Phys. Rev. **C60**, 042201 (1999), arXiv:nucl-th/9905065 [nucl-th].

[80] V. Pascalutsa, "Correspondence of consistent and inconsistent spin - 3/2 couplings via the equivalence theorem," Phys. Lett. **B503**, 85 (2001), arXiv:hep-ph/0008026 [hep-ph].

[81] T. Vrancx, L. De Cruz, J. Ryckebusch, and P. Vancraeyveld, "Consistent interactions for high-spin fermion fields," Phys. Rev. **C84**, 045201 (2011), arXiv:1105.2688 [nucl-th].

[82] K. A. Olive *et al.* (Particle Data Group), "Review of Particle Physics," Chin. Phys. **C38**, 090001 (2014).

[83] B. Friman and H. J. Pirner, "P wave polarization of the rho meson and the dilepton spectrum in dense matter," Nucl. Phys. **A617**, 496 (1997), arXiv:nucl-th/9701016 [nucl-th].

[84] M. F. M. Lutz, G. Wolf, and B. Friman, "Scattering of vector mesons off nucleons," Nucl. Phys. **A706**, 431 (2002), [Erratum: Nucl. Phys. A765, 495 (2006)], arXiv:nucl-th/0112052 [nucl-th].

[85] J. Alam, S. Sarkar, P. Roy, T. Hatsuda, and B. Sinha, "Thermal photons and lepton pairs from quark gluon plasma and hot hadronic matter," Annals Phys. **286**, 159 (2001), arXiv:hep-ph/9909267 [hep-ph].

[86] L. D. McLerran and T. Toimela, "Photon and Dilepton Emission from the Quark - Gluon Plasma: Some General Considerations," Phys. Rev. **D31**, 545 (1985).

[87] H. A. Weldon, "Reformulation of finite temperature dilepton production," Phys. Rev. **D42**, 2384 (1990).

[88] C. Gale and J. I. Kapusta, "Vector dominance model at finite temperature," Nucl. Phys. **B357**, 65 (1991).

[89] M. Le Bellac, *Thermal Field Theory* (Cambridge University Press, 2011).

[90] J. I. Kapusta and C. Gale, *Finite-temperature field theory: Principles and applications* (Cambridge University Press, 2011).

[91] R. L. Kobes and G. W. Semenoff, "Discontinuities of Green Functions in Field Theory at Finite Temperature and Density," Nucl. Phys. **B260**, 714 (1985).

[92] C. Gale and J. I. Kapusta, "Dilepton radiation from high temperature nuclear matter," Phys. Rev. **C35**, 2107 (1987).

[93] A. Jaiswal and V. Roy, "Relativistic hydrodynamics in heavy-ion collisions: general aspects and recent developments," Adv. High Energy Phys. **2016**, 9623034 (2016), arXiv:1605.08694 [nucl-th].

[94] W. Israel and J. M. Stewart, "Transient relativistic thermodynamics and kinetic theory," Annals Phys. **118**, 341 (1979).

[95] W. Israel, "Nonstationary irreversible thermodynamics: A Causal relativistic theory," Annals Phys. **100**, 310 (1976).

[96] P. Danielewicz and M. Gyulassy, "Dissipative Phenomena in Quark Gluon Plasmas," Phys. Rev. **D31**, 53 (1985).

[97] C. Eckart, "The Thermodynamics of Irreversible Processes. 1. The Simple Fluid," Phys. Rev. **58**, 267 (1940).

[98] L. D. Landau and E. M. Lifshitz, "Fluid Mechanics," (Butterworth-Heinemann, Oxford, 1987) (1987).

[99] J. D. Bjorken, "Highly Relativistic Nucleus-Nucleus Collisions: The Central Rapidity Region," Phys. Rev. **D27**, 140 (1983).

[100] G. Baym, "Thernal Equilibration in Ultrarelativistic Heavy Ion Collisions," Phys. Lett. **B138**, 18 (1984).

[101] M. Gyulassy, Y. Pang, and B. Zhang, "Transverse energy evolution as a test of parton cascade models," Nucl. Phys. **A626**, 999 (1997), arXiv:nucl-th/9709025 [nucl-th].

[102] P. Romatschke and M. Strickland, "Collective modes of an anisotropic quark gluon plasma," Phys. Rev. **D68**, 036004 (2003), arXiv:hep-ph/0304092 [hep-ph].

[103] F. Becattini, I. Karpenko, M. Lisa, I. Upsal, and S. Voloshin, "Global hyperon polarization at local thermodynamic equilibrium with vorticity, magnetic field and feed-down," Phys. Rev. **C95**, 054902 (2017), arXiv:1610.02506 [nucl-th].

[104] W. Florkowski, B. Friman, A. Jaiswal, and E. Speranza, "Relativistic fluid dynamics with spin," (2017), arXiv:1705.00587 [nucl-th].

[105] V. Skokov, A. Yu. Illarionov, and V. Toneev, "Estimate of the magnetic field strength in heavy-ion collisions," Int. J. Mod. Phys. **A24**, 5925 (2009), arXiv:0907.1396 [nucl-th].

[106] E. Shuryak, "Comment on measurement of the rotaion frequency and the magnetic field at the freezeout of heavy ion collisions," (2016), arXiv:1606.02915 [hep-ph].

[107] D. E. Kharzeev, J. Liao, S. A. Voloshin, and G. Wang, "Chiral magnetic and vortical effects in high-energy nuclear collisions—A status report," Prog. Part. Nucl. Phys. **88**, 1 (2016), arXiv:1511.04050 [hep-ph].

[108] C. Itzykson and J. B. Zuber, *Quantum Field Theory*, International Series In Pure and Applied Physics (McGraw-Hill, New York, 1980).

Acknowledgments

First of all, I would like to express my deepest gratitude towards my supervisor Bengt Friman. He has constantly guided and taken care of me with patience and kindness, and he conveyed his passion for physics to me. He has been always open for discussions about physics and not only. Among many things I wanted to learn from him, I think that the most precious one is trying to understand as much as possible just with simple calculations using only a sheet of paper and a pen. I hope I can continue my career in physics following his way of doing research.

I would like to deeply thank Tetyana Galatyuk for financing my position and being part of my PhD committee. I liked a lot working on topics relevant for her and the HADES group. I feel that having constant and close connections with an experimentalist has helped me in gaining a thorough understanding of the physics I have been working on.

I would never find the proper words to express my gratitude to Miklós Zétényi. He has always helped me since the first year of my PhD. I could ask him anything I wanted, and working and chatting with him has been a lot of fun. Thank you Miklós!

I am profoundly grateful to Amaresh Jaiswal. Unfortunately we started to work together late, but after we have begun to collaborate, my productivity has increased exponentially! I wish we could have started much earlier. I enjoyed a lot staying with him and it is a pity that now he went back to India.

I would also like to thank Dirk Rischke for being part of my PhD committee meeting and for interesting and useful discussions.

Moreover, I am indebted to Wojtek Florkowski, the time spent with him has been very nice and super productive.

I am also grateful to GSI for the support provided and to HGS-HIRe for the graduate program.

I would particularly like to thank Xiaoyu Guo for the very nice time together and for helping me with anything. He always knows how to lift me up when I am in a bad mood. I want to thank Gábor Almási for the fun times we had together and for being always reliable anytime I was in need. I would also like to thank Sofija Antic and all the members of the theory group at GSI.

I wish to give special thanks to the Italians for sharing great times: Samuel Giuliani, Marta Rovituso, Daria Boscolo, Francesco Tommasino and Giorgia Ciliberti.

Finally, I would like to thank my family, in particular my sister Maria Caterina who always kept encouraging me.

Curriculum vitae

Enrico Speranza

Date of Birth: November 11, 1987
Place of Birth: Foligno, Italy
Nationality: Italian

Education

- Sept. 2013 - Present: **Ph.D. in Physics**, Technical University of Darmstadt, Germany
  Affiliated with GSI Helmholtz Center for Heavy Ion Research, Darmstadt, Germany
- Oct. 2010 - Oct. 2012: **M.Sc. in Physics**, Sapienza University of Rome, Italy
- Oct. 2006 - July 2010: **B.Sc. in Physics**, University of Perugia, Italy